NBSIR 74-382

A STUDY OF THE MEASUREMENT OF G/T USING CASSIOPEIA A

D.F. Wait
W.C. Daywitt
M. Kanda
C.K.S. Miller

Electromagnetics Division
Institute for Basic Standards
National Bureau of Standards
Boulder, Colorado 80302

June 1974

Prepared for
Advanced Concepts Office
United States Army Communications Command
Fort Huachuca, Arizona 85613

NBSIR 74-382

A STUDY OF THE MEASUREMENT OF G/T USING CASSIOPEIA A

D.F. Wait
W.C. Daywitt
M. Kanda
C.K.S. Miller

Electromagnetics Division
Institute for Basic Standards
National Bureau of Standards
Boulder, Colorado 80302

June 1974

Prepared for
Advanced Concepts Office
United States Army Communications Command
Fort Huachuca, Arizona 85613

U.S. DEPARTMENT OF COMMERCE, Frederick B. Dent, Secretary

NATIONAL BUREAU OF STANDARDS, Richard W. Roberts, Director

FOREWORD

An important element of the mission of the Advanced Concepts Office of Headquarters, U.S. Army Communications Command, is to conduct studies whereby scientific knowledge can be utilized in the solution of current or foreseen problems affecting USACC's operational capabilities. This report investigates the problem of expeditiously measuring the G/T parameter of a satellite communications earth terminal as a check on the possible antenna-receiver degradation of portable ground stations after transfer from one site to another, and to provide an overall performance test for the acceptance of new ground stations.

This study was conducted by the Noise and Interference Section of the Electromagnetics Division of the National Bureau of Standards, Boulder, Colorado, under ACOM Project Order SCC-411-73.

Mr. D.D. Taylor of USA-ACC-POA was the project monitor supervising this study.

CONTENTS

		Page
1.	INTRODUCTION	1
	1.1 The Concept of, and a Working Definition for G/T	4
	1.2 The Relationship of G/T to C/n and ERP	7
	1.3 The Measurement of G/T -- Advantages and Disadvantages of Using Radio Stars	9
	1.4 A Brief Outline of the Radio Star Method of Measuring G/T	11
	1.5 A Brief Description of Some Important Radio Stars	12
2.	REVIEW OF THE PROPERTIES OF CAS A FROM THE LITERATURE	16
	2.1 Early Measurements	16
	2.2 The Location of Cas A	16
	2.2.1 The Equatorial and Galactic Coordinate System	16
	2.2.2 The Precession of the Earth's Axis	20
	2.2.3 Cas A	20
	2.3 Flux Density and Spectral Index	22
	2.3.1 Brightness, Brightness Temperature, and Flux Density	22
	2.3.2 Flux Density and Spectral Index of Cas A	26
	2.4 Secular Decay	29
	2.4.1 Decay Rate	29
	2.4.2 Some Measured Values of R	34
	2.5 Polarization	35
	2.5.1 Polarization and Faraday Rotation	35
	2.5.2 Measured Polarization of Cas A	37
	2.6 High Resolution Maps	39
	2.7 Cosmic Background Radiation	46
	2.7.1 Nature of the Cosmic Radio Background	47
	2.7.2 Cosmic Background Contribution to the System Noise Temperature	53

CONTENTS (Continued)

		Page
3.	THE ATMOSPHERIC EFFECTS IN VIEWING CAS A----------	61
4.	THE MEASUREMENT OF POWER GAIN OF A LARGE GROUND ANTENNA FOR CALIBRATING COSMIC RADIO STARS----------	65
	4.1 Introduction----------	65
	4.2 Calibration of the Standard Gain Antenna by Use of the Generalized Three-Antenna Extrapolation Technique----------	67
	4.2.1 Introduction----------	67
	4.2.2 Antenna Scattering Matrix Analysis------	68
	4.2.3 Generalized Three Antenna Measurement Technique----------	72
	4.2.4 Extrapolation Technique----------	78
	4.2.5 Accuracy Consideration----------	80
	A. Error in Mismatch Factors----------	82
	B. Attenuator Error----------	83
	C. Receiver Nonlinearity and Gain Instability----------	83
	D. Atmospheric Loss Uncertainty--------	84
	E. Range Misalignment----------	84
	F. Distance Inaccuracy----------	88
	4.2.6 Summary and Concluding Remarks----------	88
	4.3 The Calibration of a Large Ground Antenna by the Gain Comparison Method----------	97
	4.3.1 Introduction----------	97
	4.3.2 Theory----------	98
	4.3.3 Accuracy Consideration----------	103
	A. The Power Gain of a Standard Antenna	103
	B. Frequency Instability----------	103
	C. Effective Radiated Power (ERP)------	104
	D. Path Loss----------	104
	E. Polarization Mismatch----------	105
	F. Tracking Accuracy----------	106

CONTENTS (Continued)

		Page
	G. Waveguide Feed Loss Uncertainty-----	108
	H. Uncertainty in Power Ratio Measurement----------	111
	I. Uncertainty Due to Receiver Gain Instability and Nonlinearity----------	111
	J. Uncertainty in Antenna System Noise Temperature----------	116
	K. Error Due to Change in Effective Input Noise Temperature, Bandwidth and Ambient Temperature----------	117
4.3.4	Results and Concluding Remarks----------	118
4.4	Summary and Conclusions----------	126
5.	THE ACCURACY OF MEASURING THE FLUX DENSITY OF CAS A-	134
6.	THE ACCURACY OF MEASURING G/T----------	138
6.1	The Measurement of G/T Using Cas A----------	138
6.2	Cas A Method of Measuring G/T Compared to the Gain/Noise Temperature Method----------	138
7.	G/T MEASUREMENT REPEATABILITY----------	146
8.	CONCLUSIONS----------	149
8.1	The Accuracy of Measuring G/T----------	149
8.2	The Accuracy of the Cas A Flux Densities Cited in the Literature----------	151
8.3	Proposed Future Efforts----------	152
8.3.1	Evaluation of the Literature----------	152
8.3.2	Stars Other than Cas A for G/T Measurements----------	152
8.3.3	Independent Methods for Measurement of G/T----------	153
8.3.4	Definitions of and Alternatives to G/T--	153
8.3.5	Uncertainties in Antenna Gain Measurements----------	153
8.3.6	Radio Star Method of Measuring G and T--	154
REFERENCES----------		155

CONTENTS (Continued)

	Page
APPENDIX A: COMMENTS ON THE INTRODUCTORY SECTIONS--	162
APPENDIX B: COMPUTER PRINTOUT AND PROGRAMS---------	164
B.1 A Printout for the Practicable Accuracy of G/T----------	165
B.2 The BASIC Program for the Computation of the Errors in the Measurement of G/T Using Cas A----------	177
APPENDIX C: DETERMINATION OF ANTENNA AND RECEIVER PARAMETERS BY NOISE-ADDING TECHNIQUES--	183
C.1 The Measurement of Antenna Parameters-----	185
C.2 The Measurement of System Noise Temperature and G/T----------	186

LIST OF ILLUSTRATIONS

Figure		Page
1-1	Pictorial diagram of the system as defined for the purpose of this report	5
1-2	Pictorial diagram for defining the carrier-to-noise density ratio	8
1-3	The flux density spectrum of several radio stars	14
2-1	The equatorial and galactic coordinate systems superimposed onto the celestial sphere	18
2-2	The position of the radio source Cas A relative to the visible stars in the constellation of Cassiopeia	21
2-3	An artist's sketch of the position of the sun, and the directions to Cas A, Tau A, and Cyg A relative to the Milky Way Galaxy	23
2-4	Brightness B of an elemental radiating surface dA	24
2-5	Elemental radiating surface dA on the celestial surface	24
2-6	The flux density of Cas A around 7 GHz	28
2-7	Decay curve of the Cas A flux density as calculated from the shell model	30
2-8	Decay curve of the Cas A flux density showing the relation between the differential and average decay ratio	32
2-9	Hypothetical position angle curve for the linearly polarized flux from Cas A	38
2-10	Brightness temperature contour map of Cas A (Epoch AD 1950.0, 5.0 GHz). (Courtesy of Monthly Notices of the Royal Astronomical Society, Vol. 151, No. 1, p. 112, 1970)	40
2-11	Brightness temperature contour map of Cas A (Epoch 1968.4, 1.4 GHz) showing the variation of the spectral index across the source. (After Monthly Notices of the Royal Astronomical Society, Vol. 151, No. 1, p. 114, 1970)	42

LIST OF ILLUSTRATIONS (Continued)

Figure		Page
2-12	Brightness temperature contour map of Cas A (Epoch AD 1966.8, 19.4 GHz) showing (a) the brightness temperature, (b) the linearly polarized component of (a) amplified 20 times. (Courtesy of Astrophysical Journal, Vol. 151, p. 56, 1968; C.H. Mayer and I.P. Hollinger; University of Chicago Press)	43
2-13	Brightness temperature contour map of Cas A (Epoch 1950.0, 5.0 GHz) showing the distribution of polarized emission across the source with the average position angle of the electric vectors superimposed. (After Monthly Notices of the Royal Astronomical Society, Vol. 151, No. 1, p. 116, 1970)	44
2-14	Mean brightness temperatue profile from the center of Cas A outward (Epoch AD 1950.0, 5.0 GHz). (After Monthly Notices of the Royal Astronomical Society, Vol. 151, No. 1, p. 118, 1970)	45
2-15	The cosmic radio sky at 250 MHz. (After Sky and Telescope, Vol. 16, p. 160, 1957)	48
2-16	Brightness spectrum of the continuous cosmic radiation as deduced from the literature	52
2-17	Cosmic radio background at 400 MHz. (After Monthly Notices of the Royal Astronomical Society, Vol. 124, No. 1, p. 74A, 1962)	54
2-18	Cosmic radio background at 960 MHz. (After Publications of the Astronomical Society of the Pacific, Vol. 72, No. 428, p. 336, 1960)	55
2-19	Cosmic radio background at 1.4 GHz. (After Publications of the National Radio Astronomy Observatory, Vol. 1, No. 3, p. 55, 1961)	56
2-20	Cosmic radio background at 3.2 GHz. (After Monthly Notices of the Royal Astronomical Society, Vol. 129, No. 2, p. 166, 1965)	57
2-21	Hypothetical cosmic radio background at 1.4 GHz with effect of Cas A removed	59

LIST OF ILLUSTRATIONS (Continued)

Figure		Page
4-1	Antenna in the measurement coordinate system------	69
4-2	Schematic of two antennas oriented for measurement	74
4-3	Measured data, 5-term polynominal fit, and residuals for x-band standard horn (frequency = 7.25 GHz, antenna power gain 23 dB, major aperture dimension of antenna = 23.5 cm)----------	81
4-4	Error in the measured antenna power gain due to receiver non-linearity (frequency = 7.25 GHz)-----	85
4-5	Atmospheric attenuation versus frequency (courtesy of Bean and Dutton)----------	86
4-6	Error in the measured antenna power gain due to atmospheric loss uncertainty (frequency = 7.25 GHz)----------	87
4-7	Error in the measured antenna power gain due to range misalignment (frequency = 7.25 GHz)---------	89
4-8	Error in the measured antenna power gain due to distance uncertainty (frequency = 5 to 10 GHz, antenna power gain = 20 to 50 dB, major aperture dimension of antenna = 0.5 to 10 m)----------	90
4-9	Accumulated error in the measured power gain of the generalized three-antenna extrapolation method (frequency = 7.25 GHz)----------	92
4-10	Linear error accumulation for the measured power gain of the standard antenna using the generalized three-antenna extrapolation method (major aperture dimension of antenna = 23.5 cm)----------	93
4-11	Quadrature error accumulation for the measured power gain of the standard antenna using the generalized three-antenna extrapolation method (frequency = 7.25 GHz)----------	95
4-12	Quadrature error accumulation for the measured power gain of the standard antenna using the generalized three-antenna extrapolation method (major aperture dimension of antenna = 23.5 cm)---	96

LIST OF ILLUSTRATIONS (Continued)

Figure		Page
4-13	Schematic for experimental gain comparison method-	99
4-14	Average power gain loss as a function of ratio of tracking error to half power bandwidth----------	109
4-15	Error in the antenna power gain due to tracking inaccuracy (frequency = 7.25 GHz, tracking inaccuracy = 5 seconds of arc, rms)----------	110
4-16	Error in the antenna power gain due to uncertainty in $Y = P_1/P_3$----------	112
4-17	Error in the antenna power gain due to uncertainty in $Z = P_2/P_4$----------	113
4-18	Error in the antenna power gain due to uncertainty in g_2----------	114
4-19	Error in the antenna power gain due to uncertainty in g_4----------	115
4-20	Linear error accumulation for the power gain of a large microwave antenna using the gain comparison method (frequency = 7.25 GHz, standard antenna gain = 30 dB nominal, effective radiated power = 10 dBW nominal)----------	119
4-21	Linear error accumulation for the power gain of a large microwave antenna using the gain comparison method (frequency = 7.25 GHz, standard antenna gain = 40 dB nominal, effective radiated power = 10 dBW nominal)----------	121
4-22	Linear error accumulation for the power gain of the large microwave antenna using the gain comparison method (frequency = 7.25 GHz, standard antenna gain = 50 dB nominal, effective radiated power = 10 dBW nominal)----------	122
4-23	Linear error accumulation for the power gain of the large microwave antenna using the gain comparison method (frequency = 7.25 GHz, unknown antenna gain = 60 dB nominal, effective radiated power = 10 dBW nominal)----------	123

Figure		Page
4-24	Linear error accumulation for the power gain of the large microwave antenna using the gain comparison method (frequency = 7.25 GHz, unknown antenna gain = 40 dB nominal, effective radiated power = 10 dBW nominal)	124
4-25	Quadrature error accumulation for the power gain of the large microwave antenna using the gain comparison method (frequency = 7.25 GHz, effective radiated power = 10 dBW nominal)	125
4-26	Linear error accumulation for the power gain of the large microwave antenna using the gain comparison method (frequency = 7.25 GHz, standard antenna gain = 30 dB nominal, effective radiated power = 30 dBW nominal)	127
4-27	Linear error accumulation for the power gain of the large microwave antenna using the gain comparison method (frequency = 7.25 GHz, standard antenna gain = 40 dB nominal, effective radiated power = 30 dBW nominal)	128
4-28	Linear error accumulation for the power gain of the large microwave antenna using the gain comparison method (frequency = 7.25 GHz, standard antenna gain = 50 dB nominal, effective radiated power = 30 dBW nominal)	129
4-29	Linear error accumulation for the power gain of the large microwave antenna using the gain comparison method (frequency = 7.25 GHz, unknown antenna gain = 60 dB nominal, effective radiated power = 30 dBW nominal)	130
4-30	Linear error accumulation for the power gain of the large microwave antenna using the gain comparison method (frequency = 7.25 GHz, unknown antenna gain = 70 dB nominal, effective radiated power = 30 dBW nominal)	131
4-31	Quadrature error accumulation for the power gain of the large microwave antenna using the gain comparison method (frequency = 7.25 GHz, effective radiated power = 30 dBW nominal)	132

LIST OF ILLUSTRATIONS (Continued)

Figure		Page
5-1	Practicable and low bound errors in the measurement of the flux density of Cas A	135
6-1	Practicable error in the measurement of G/T using Cas A	139
6-2	Practicable and lower bound errors in the measurement of G/T using Cas A	141
7-1	G/T measurement repeatability versus frequency	148
C-1	Block diagram of the noise adding technique	184

A STUDY OF THE MEASUREMENT OF G/T USING CASSIOPEIA A

This report describes a study intended to estimate the best possible accuracy of measuring the ratio G/T (system gain to system noise temperature) of a satellite communication ground station using the radio star Cassiopeia A (Cas A). The concept of G/T and its measurement using a radio star is briefly discussed. Results of an extensive literature search are presented, summarizing the properties of Cas A and its vicinity described by radio astronomers in order to utilize this information to assess the accuracy of a G/T measurement. Consideration is given to atmospheric effects upon a G/T measurement using Cas A based on information available in the literature. A detailed analysis of errors for gain measurements of large ground antennas, which includes the calibration of a standard gain antenna and the transfer of this calibration to the large antenna, is provided to validate radio star flux data since this analysis is not available in the literature. The results of these efforts are utilized to show that the best possible accuracy of a G/T measurement for a ground station (with practical and reasonable specifications) having a 60 ft. diameter antenna is in the neighborhood of ± 0.25 dB.

Key words: Accuracy; antenna; calibration, Cassiopeia A; G/T; star flux.

1. INTRODUCTION

This report describes a study that was undertaken to estimate the best possible accuracy of measuring the ratio G/T (gain/temperature) of a satellite communication ground station using the radio star Cassiopeia A (Cas A). The study included: an extensive literature search concerning those

properties of Cas A and atmospheric attenuation relevant to the G/T measurement; an estimate of the best possible accuracy of calibrating the gain of large ground station receiving antennas; an estimate of the best possible accuracy in the flux density measurement of Cas A; and an estimate of the best possible accuracy of measuring G/T.

The purpose for the determination of the best possibl G/T accuracy was to obtain a basis for deciding whether the measurement of G/T using Cas A could be sufficiently accurate to justify its use in the following areas: to check on the possible antenna-receiver degradation of portable ground stations after transfer from one site to another; to provide an overall performance test for the acceptance approval of new satellite communication ground stations; and to provide a means for building a history of ground station performance to ascertain the degree of reduction possible in present performance safety margins to gain a corresponding reduction in overall system costs.

The reason that G/T is an important parameter is that G/T, along with satellite ERP, determines the input signal-to-noise ratio of the satellite-ground station communication system. It is therefore intimately related to the system output performance measurands such as the output signal-to-noise ratio of an analog system or the bit error rate of a digital system, and the channel capacity or upper bound to reliable information transfer rate through the system.

This study shows that under certain conditions the direct measurement of the G/T ratio using Cas A can be performed nearly as accurately as measuring G and T separately and calculating their ratio. Furthermore, where the flux density of Cas A is available, the accuracy of the direct

measurement of G/T using Cas A is much easier to realize than the separate measurements of G and T. The study also indicates that accuracies for antenna gain measurements, flux density measurements, and G/T measurements reported in the literature are often significantly overestimated.

This study was performed for the Advanced Concepts Office, ACOM Headquarters, Fort Huachuca, Arizona, by the Noise and Interference Section of the Electromagnetics Division of the National Bureau of Standards; it is a follow-up effort by the Noise and Interference Section of a G/T measurement project begun at Camp Roberts, California, during June 1972.

The report consists of eight sections and three appendices. Section 1 is of an introductory nature, describing the reasons for the study, the concept of G/T and its measurement using a specific radio star, and the properties of some other intense radio stars.

Section 2 presents the results of an extensive literature search into the properties of Cas A relevant to the measurement of G/T and raises some questions apparently overlooked in a large part of the literature.

Section 3 presents results of a literature search related to the atmospheric effect upon radio measurements of Cas A. Although the available time did not allow an exhaustive study of this literature, some important effects are emphasized that have been considered by only a few authors.

Section 4 presents a detailed analysis of errors for the gain measurement of large ground antennas, and covers the calibration of the standard gain horn used in the measurement, and the transfer of this calibration to the larger antenna. This section is fairly extensive because much of the material is new and has not been documented in the open literature.

Sections 5, 6, 7, and 8 present the results of an analysis of the accuracy of the flux density measurement of Cas A, the potential accuracy and precision of measuring G/T, and the conclusions.

1.1 The Concept of, and a Working Definition for G/T

The ratio G/T is a figure of merit used to indicate the sensitivity of the ground station antenna and receiver in a satellite communication system. The higher the ratio, the more easily the ground station can detect a weak satellite signal. From what follows, it can be seen that this measure of sensitivity includes not only the effects of noise generated in the ground station itself, but also the effects of noise generated in the entire environment, terrestrial and cosmic, in which the ground station antenna-receiver is immersed.

For the purpose of defining this figure of merit the communication system is assumed to consist of those components appearing in figure 1-1, in which the system is considered to be functioning in its receive mode. It is clear from this figure that the system noise includes not only the circuit noise generated in the antenna and receiver, but noise from cosmic and terrestrial (including atmospheric and man-made) sources also. This system noise is characterized by a system noise temperature [1] with a magnitude equal to the average noise power divided by the product of Boltzmann's constant and the limiting bandwidth of the system. The system noise temperature can be referred to any point in the system, T_1, T_2, and T_3 being the system noise temperature as referred to ports 1, 2, and 3 respectively. T_1 is the sum of the antenna noise temperature [2] and the effective input noise temperature [1] of the receiver. G_A is the on-axis power gain of

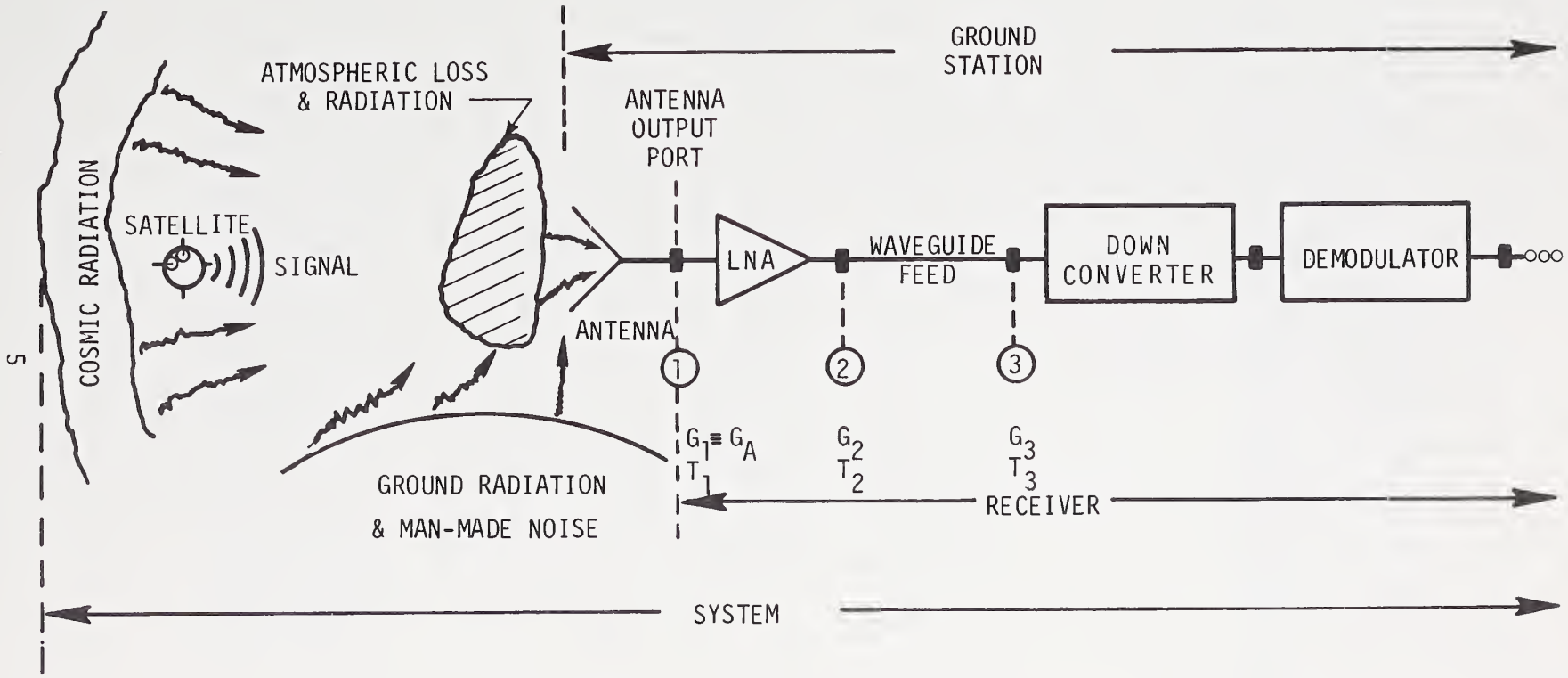

Figure 1-1. Pictorial diagram of the system as defined for the purpose of this report.

the antenna [2] and characterizes the system gain from the far field of the antenna to the antenna output port. G_2 is the system gain from the far field of the antenna to port 2, and is defined as G_A times the available power gain of the low noise amplifier (LNA). G_3 is similarly defined as G_2 times the available power gain (loss) of the waveguide feed.

The ratio G/T has the same numerical value at any of the ports 1, 2, or 3. That is

$$\frac{G_1}{T_1} = \frac{G_2}{T_2} = \frac{G_3}{T_3} \tag{1.1}$$

In other words, theory predicts that G/T could be determined at any one of these three ports with the same results. Therefore, G/T could be referenced to any of these ports and the same measure of system performance would result, indicating that the port at which G/T is defined is somewhat arbitrary.

From a search of the literature for an acceptable definition of the ground-station figure of merit G/T, it appears that the authors are fairly evenly divided in their choices of port (1, 2, or 3) to which to refer their working definitions. The only formal definition [3] that was found specifies port 1 (the antenna output port). A careful review of this formal definition is a time-consuming job more appropriately left to a later phase of the G/T project. Therefore, a working definition will have to suffice for this report.

The working definition of G/T used in this report is: the ground station figure of merit, G/T, is the ratio of the on-axis power gain of the antenna to the system noise temperature referred to the antenna output port. With reference to

figure 1 this definition corresponds to

$$\frac{G}{T} \equiv \frac{G_A}{T_1}. \tag{1.2}$$

Henceforth, whenever G and T are used separately in this report, they refer to G_A and T_1 respectively.

The magnitude of G/T is usually expressed in decibels, where the magnitude of G/T for the system under consideration is compared to a G/T of unity. That is

$$(G/T)_{dB} = 10 \log_{10} (G/T). \tag{1.3}$$

A few additional comments pertaining to the preceding ideas have been left to appendix A.

1.2 The Relationship of G/T to C/n and ERP

The desired performance of a satellite communications system is generally expressed as an output signal-to-noise ratio for an analog system, or as a bit error rate for a digital system. These parameters are related to the carrier-to-noise density ratio [4], C/n, at the antenna output, the relationship depending on the type of modulation employed. Once the desired output performance of the system is specified, C/n can be determined from equations relating it to this desired performance. The trade-off between the available satellite power and the ground station G/T is determined by finding the least expensive combination of satellite power and G/T that gives the desired C/n.

A less detailed representation than the one given in section 1.1 of a satellite communication system in its receive mode is shown in figure 1-2. Modulated RF carriers are radiated by the satellite and received by the ground

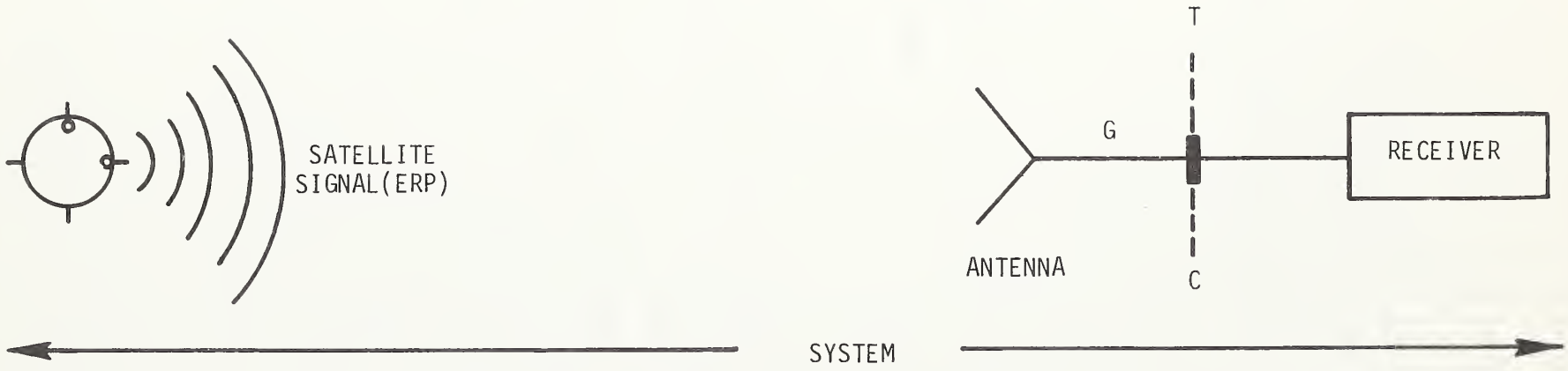

Figure 1-2. Pictorial diagram for defining the carrier-to-noise density ratio.

station antenna. The effective radiated power (ERP) [1] is the corresponding average power radiated in the direction of the antenna. C is the time average power of the received carriers that is available at the antenna output port. C is given in terms of the ERP by

$$C = ERP \times L \times G \tag{1.4}$$

where L reflects the loss in carrier power caused by the separation and the polarization mismatch between the satellite and ground station antennas, and by the atmosphere.

Under the usual assumption that the noise density kT is much larger than the noise density from the satellite received by the ground station, the noise density n at the antenna output port is given by

$$n = kT. \tag{1.5}$$

Combining eqs. (1.4) and (1.5), the ratio C/n becomes:

$$\frac{C}{n} = \left(\frac{G}{T}\right) \frac{ERP \times L}{k} \tag{1.6}$$

This equation shows that C/n can be increased by either upgrading the ground station (G/T) or by increasing the satellite ERP. It also implies an intimate relation between G/T and ultimate system performance. For example an increase in G/T could imply a more static-free voice communication, or a more error-free data communication.

See appendix A for further comments.

1.3 The Measurement of G/T -- Advantages and Disadvantages of Using Radio Stars

There are basically two approaches used to measure the ratio G/T. In one approach G and T are measured separately and their ratio is calculated. In the other approach

(sec. 1.4) G/T is measured directly in the sense that neither G nor T is explicitly measured. It is assumed here that a radio star is employed in this direct approach.

The main advantage of the direct approach is that G/T can be accurately measured using a relatively easy measurement procedure, provided the flux from the radio star is accurately known. The relative ease of this measurement procedure allows G/T to be measured more often and in much less time than with the indirect approach. This point is very important if the ground station is moved often or if a minimal allotment of time is available with which to assess performance. Although the calibration of the radio star itself is an undertaking at least as difficult as the indirect approach to the measurement of G/T, once the star is calibrated the G/T of any number of ground stations can be accurately and easily measured.

In contrast to the direct approach, an accurate determination of G/T by the separate measurement of G and T is a major measurement undertaking which includes: (1) the calibration of a standard gain horn; (2) the transfer of this calibration to the system antenna; and (3) the measurement of the system noise temperature. Even if the system antenna is small enough for direct calibration, such a calibration is in itself a major job.

The main disadvantage to the direct approach is that it can only be accurately employed on a ground station whose G/T is greater than some minimum value. As one example, Kruetel and Pacholder [5] estimate that the G/T of a ground station must exceed 35 dB if Cas A is to be used as the radio star and if the probable error in G/T is not to exceed $\pm$ 0.2 dB. If another radio star is used in place of Cas A, then the minimum G/T must be even larger.

In the event that an absolute measurement of G/T is less important than an intercomparison of the G/T radio for two similar ground stations, the accuracy of the flux from the radio star becomes unimportant, and the direct approach is even more appealing. Subsequently, as a greater accuracy in the star flux becomes available, the accuracy of the G/T for either ground station can be easily updated by simply replacing the old value of the star flux used to calculate G/T by the updated value.

1.4 A Brief Outline of the Radio Star Method of Measuring G/T

In the radio star method of measuring G/T, the ground station antenna is first directed at the radio star. The ground station receiver now registers an average noise power, P_1, that is proportional to the sum of the system noise temperature T referred to the antenna output port and the brightness temperature [6] of the radio star referred also to this port, $GT_s\Omega_s/4\pi$. That is

$$P_1 \propto T + GT_s\Omega_s/4\pi \tag{1.7}$$

where G is the antenna gain, T_s is the brightness temperature of the star, and Ω_s is the solid angle subtended by the star. For the purpose here it is assumed that the system noise temperature is independent of where the antenna is pointed.

The antenna is now directed to the cold sky just far enough to the side of the radio star that the radiated power from the star does not contribute significantly to the power emerging from the antenna output port. The receiver now registers an average noise power P_2 proportional to the system noise temperature only. That is

$$P_2 \propto T. \tag{1.8}$$

Taking the ratio Y of the two noise powers in eqs. (1.7) and (1.8) results in

$$Y = \frac{P_1}{P_2} = \frac{T + GT_s\Omega_s/4\pi}{T}. \qquad (1.9)$$

Solving eq. (1.9) for G/T yields

$$\frac{G}{T} = \frac{4\pi(Y-1)}{T_s\Omega_s}. \qquad (1.10)$$

This equation shows the basic result of a radio star measurement of G/T. Once T_s and Ω_s have been established, the measurement reduces to the relatively simple noise power ratio (or Y-factor) measurement.

Further comments on the radio star method are to be found in appendix A.

1.5 A Brief Description of Some Important Radio Stars

There are some sources of radio frequency noise beyond our own atmosphere. These cosmic sources include the moon, the sun and planets, hydrogen clouds and exploding stars within our own galaxy, and distant radio galaxies. These sources vary in angular extent from a fraction of a second of arc to many degrees, and in power from values well below the minimum perceptible level of the largest and most sophisticated antenna-receiver systems to powers easily detected by the crudest systems.

For the purpose of this report a radio star is considered to be a cosmic radio source whose angular extent is no larger than a few minutes of arc. The importance of such radio stars to the measurements of G/T stems from the fact that their angular extent is less than the angular extent of the main beam of the antenna currently under consideration, allowing G/T to be measured without measuring the entire antenna power pattern.

Radio star flux density is often expressed in flux units (f.u.), one flux unit being equivalent to 10^{-26} watt per meter squared per hertz. The curve of the flux density as a function of frequency is known as the source spectrum. Several spectra are shown in figure 1-3. The general shape of the spectral curves indicates what physical mechanism is responsible for the radio emission. For example, from figure 1-3 it can be concluded that the synchrotron mechanism (the spiraling of rapidly moving electrons around magnetic field lines) is responsible for the radiation emanating from Cas A, Cyg A, Tau A, and Virgo A, while radiation from the electrons in compact ionized hydrogen clouds is responsible for the emission from Orion A and DR 21.

Table 1-1 gives more detail concerning the radio stars whose spectra are shown in figure 1-3. The table includes the common star name in column one; the type of large-scale phenomenon believed responsible for the radio star in column two; the position of the star in equatorial coordinates in column three; the angular size of the star in column four; and the star's visibility from the north to south latitudes in column five. For the purpose of this report the visibility is defined to be that interval of terrestrial latitudes from which a source's apparent daily path through the sky rises to at least 20° above the horizon. This 20° miminum assures that the source can be seen by an antenna for at least one hour sufficiently far above the horizon to be discernible above the atmospheric and ground noise. One can tell from the visibility whether a particular source is usable in a G/T measurement at a given site. The radio stars are arranged in a table from top to bottom according to descending flux densities at 7.5 GHz.

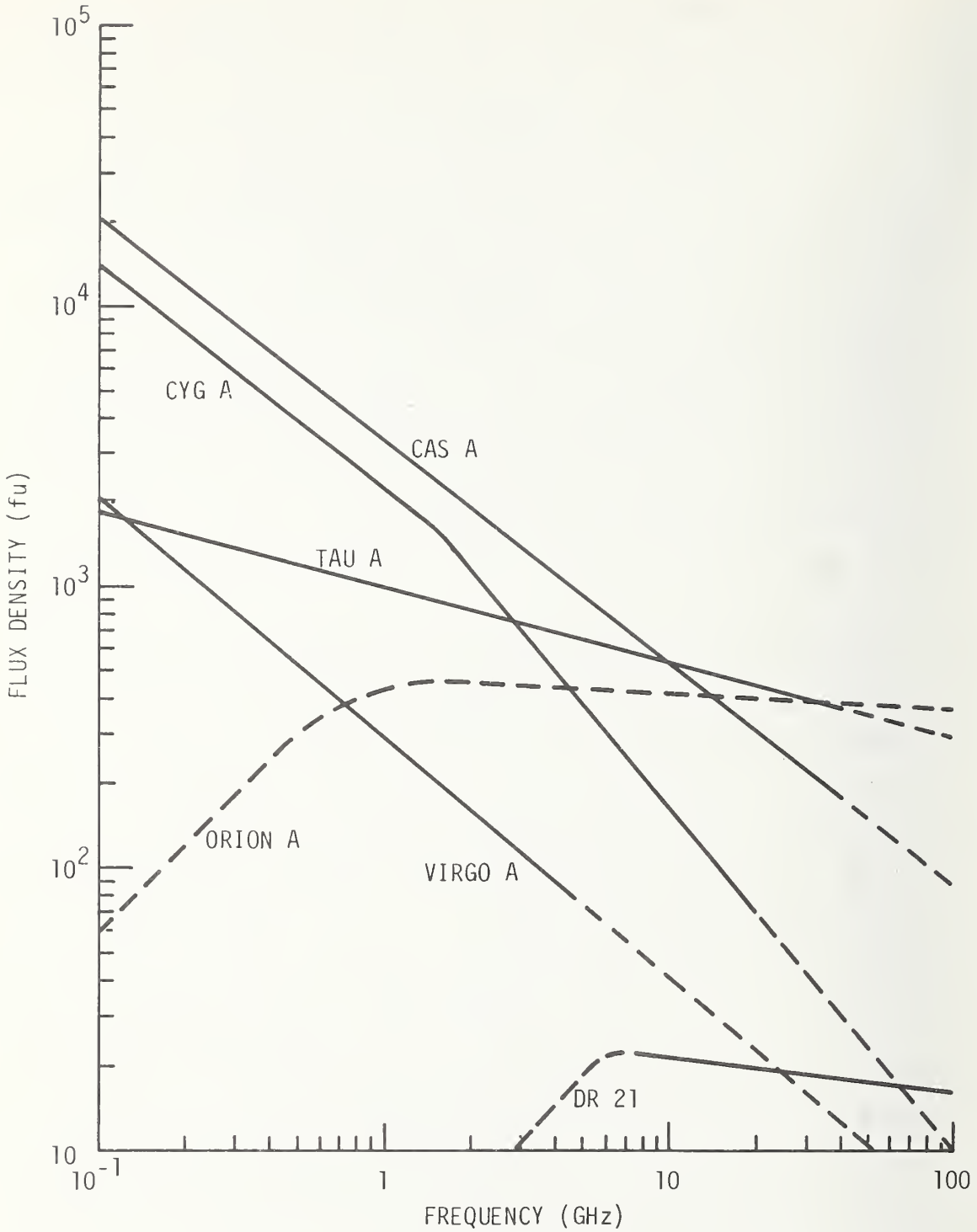

Figure 1-3. The flux density spectrum of several radio stars.

Table 1-1. Information about several radio sources.

Radio Star	Type*	Position RA^h	Dec^o	Size RA' x Dec'	Visibility NL^o to SL^o	
Cas A	SR	23.4	58.6	4 x 4	90	11
Tau A	SR	5.5	22.0	3.3 x 4	90	48
Orion A	EN	5.5	-5.4	3.5 x 3.5	65	75
Cyg A	RG	20.0	40.6	1.6 x 1	90	29
Virgo A	RG	12.5	12.7	1 x 1.8	73	57
DR 21	EN	20.6	42.2	< 0.3	90	28

*SR ≡ Supernova Remnant

EN ≡ Emission Nebula

RG ≡ Radio Galaxy

2. REVIEW OF THE PROPERTIES OF CAS A FROM THE LITERATURE

2.1 Early Measurements

The radio emission known as Cas A was discovered in 1948 by Ryle and Smith [7] while measuring rf emissions from the Constellation of Cygnus discovered two years earlier. In 1954 Baade and Minkowski [8] identified the newly discovered radio source with faint optical nebulosities located near the Constellation of Cassiopeia. From optical measurements of the nebulosities Minkowski [9,10,11] concluded: that they are traveling radially outward at a speed of 7440 km/sec; that they are approximately 11,000 light years from the earth; and that they are remnants of a supernova explosion, the visual evidence of which probably reached the earth about 1700 A.D. Subsequent rf measurements [12,13] made in 1952 to determine the center and angular size of Cas A helped Baade and Minkowski to positively identify the emission with the nebulosities.

Since these first observations, many measurements of Cas A have been made to determine its flux density and spectral distribution, angular shape, polarization, and stability. The following subsections contain discussions of the results of these measurements as they pertain to the use of Cas A as a standard source of rf noise power for the measurement of the parameters of large antennas.

2.2 The Location of Cas A

2.2.1 The Equatorial and Galactic Coordinate System

The equatorial coordinate system is the most commonly used system for locating the position of celestial bodies. It is the one used in most star catalogues and will be discussed

in detail in this subsection. The galactic coordinate system is often used in conjunction with the equatorial system in locating broad regions of cosmic background radiation and will therefore also be treated to some extent here.

Equatorial Coordinate System [6]

In the equatorial system the plane of the earth's equator is the plane of reference; the center of the earth is the coordinate origin; and the earth's geographic north pole is the northern direction. The reference direction in the reference plane is defined in conjunction with the celestial sphere, figure 2-1. This sphere is an imaginary spherical surface of arbitrarily large radius with the earth as its center, and onto which the stars appear to be projected. In the period of a year, these stars exhibit very little angular motion on the sphere and so provide a quasi-permanent reference pattern for their own locations. Objects like the sun and planets appear to move through this pattern. The intersection of the earth's equatorial plane with this sphere defines the celestial equator, and the earth's projected north and south poles define the celestial north and south poles respectively. The apparent yearly path of the sun on this sphere is called the ecliptic, which intersects the celestial equator twice a year, once at the vernal equinox and once at the autumnal equinox. Then, the line drawn from the earth's center to the vernal equinox defines the reference direction, or the direction from which the longitude of a star of the sphere is measured.

The angle α in the equatorial plane measured eastward from the vernal equinox to a projection of a particular star onto the plane is the star's longitude and is called the right ascension. It is usually expressed in hours, minutes, and seconds, 24 hours corresponding to 360°. The

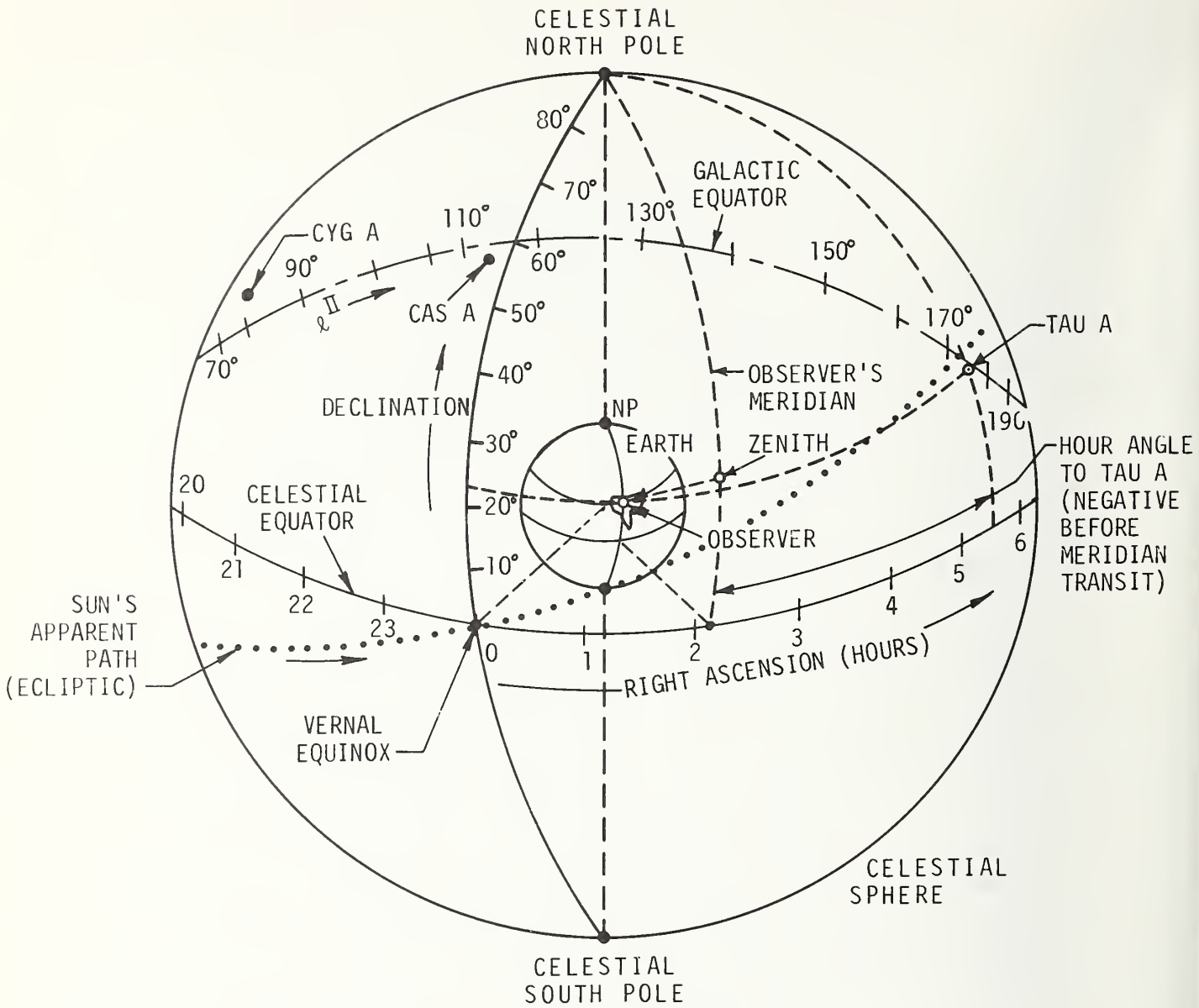

Figure 2-1. The equatorial and galactic coordinate systems superimposed onto the celestial sphere.

angle δ measured from the reference plane to the star's position is called the star's latitude on the sphere and is called the declination. It is expressed in degrees, arc minutes, and arc seconds, and is positive towards the celestial north pole and negative towards the south. For example, Tau A is located at $\alpha = 5^h\ 31^m\ 30^s$ and $\delta = 21°58'$ in figure 2-1.

The angle in right ascension between the observer's meridian (in earth coordinates) and the star is called the star's hour angle. The hour angle is defined to be negative before it transits the observer's meridian. For example, the Tau A hour angle to the observer's meridian (at $\alpha = 2^h\ 11^m$) in the figure is approximately a negative $3^h\ 20^m$.

Galactic Coordinate System [6]

Since 1958, the galactic coordinate system is defined as follows. The origin is defined by the intersection of the plane of our galaxy and the line through the center of the earth perpendicular to this plane. Angles of galactic longitude (ℓ^{II}) are measured in this plane, and angles of galactic latitude (b^{II}) are measured from this plane. The reference direction in the galactic plane is from the origin to the center of the galaxy in the plane.

The apparent intersection of the galactic plane with the celestial sphere is called the galactic equator (fig. 2-1) and provides a convenient reference circle (not a great circle) on that sphere. The north galactic pole is the intersection ($\alpha = 12^h.7$ and $\delta = 28°$) of the perpendicular from the origin with the northern hemisphere of the celestial sphere.

2.2.2 The Precession of the Earth's Axis [6]

Since the earth is not a perfect sphere, the gravitational pull exerted upon it by the sun causes a gradual precession of the earth's axis around the pole of the ecliptic, one cycle being completed in approximately 26000 years. This gradual motion shifts both the celestial equator and the celestial poles with respect to the star pattern, causing an apparent shift in the positions of the stars. Therefore, when specifying the right ascension and declination of a star, it is important to specify a date (epoch) to which they refer. The change in right ascension and declination from AD 1950.0 are given by

$$\Delta\alpha = m + n \sin \alpha \tan \delta \text{ seconds per year}$$
$$\Delta\delta = n \cos \alpha \text{ seconds of arc per year}$$

where α and δ are the right ascension and declination for 1950.0.

$m = 3.07327$ seconds

and $n = 20.0426$ seconds of arc.

2.2.3 Cas A

Through a detailed study of the shape of Cas A [14] the center of its rf emission is placed at

$$\alpha = 23^h\ 21^m\ 11^s$$

and

$$\delta = 58°32'40''$$

at the epoch of 1950.0. For comparison, the optical center of the expanding nebulosities mentioned in subsection 2.2.1 is located at [15] $23^h\ 21^m\ 11.4^s$ right ascension, and 58°32'18.9" declination.

Cas A, though not visible, is located (fig. 2-2) just west (11°) of the visible star β Cas. The effect of the earth's

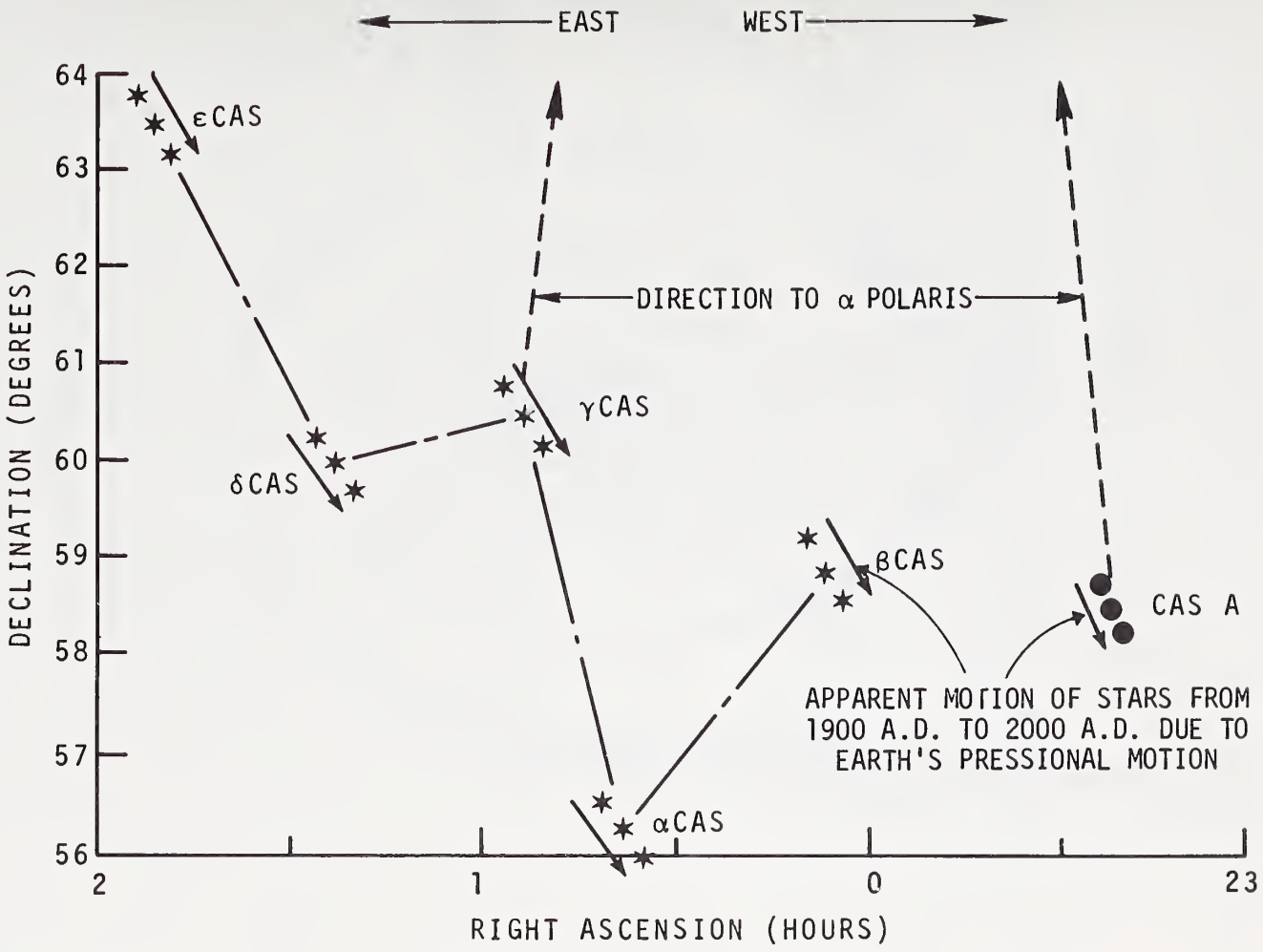

Figure 2-2. The position of the radio source Cas A relative to the visible stars in the constellation of Cassiopeia.

precessional motion upon the apparent position of the stars from 1900 AD to 2000 AD is also indicated in figure 2-2. The location of Cas A in our galaxy is shown in figure 2-3.

2.3 Flux Density and Spectral Index

2.3.1 Brightness, Brightness Temperature, and Flux Density [6]

The intensity measure of radiation from the celestial sphere is called the brightness. The brightness of a small surface on the celestial sphere can be related to the flux density, S, at an antenna on the earth. This relationship will now be developed. From figure 2-4

$$dw' = B\ dA\ d\Omega' \tag{2.1}$$

where dw' = spectral power (power per unit bandwidth) emitted by the incremental surface dA into the solid angle $d\Omega'$, watts/Hz

B = surface brightness, watts/(rad^2·m^2·Hz)

dA = elemental surface area on the celestial sphere, m^2

$d\Omega'$ = elemental solid angle, rad^2.

Thus B is a brightness whose magnitude depends upon its location on the celestial sphere, and which varies in a roughly continuous manner over the sphere except for occasional "bright spots" which correspond to highly localized or discrete sources of radio emissions. The broad continuous brightness is referred to as "background radiation," and the bright spots as radio "stars." Cas A is one of these radio stars. Figure 2-5 is a representation of the celestial sphere with the earth at its center, and with the size of the earth represented by a point relative to the radius of the celestial sphere. As seen from the earth the elemental surface area dA

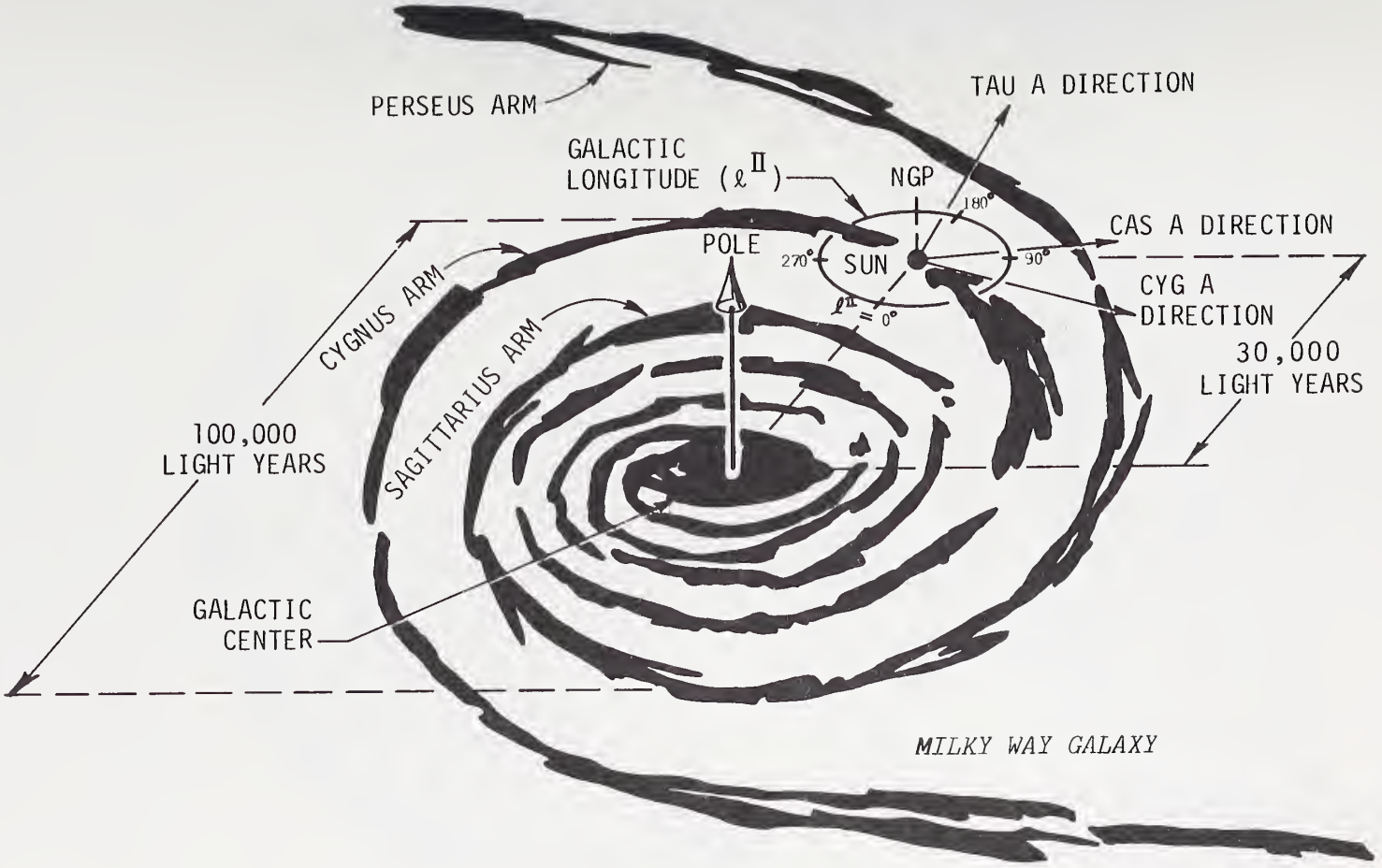

Figure 2-3. An artist's sketch of the position of the sun, and the directions to Cas A, Tau A, and Cyg A relative to the Milky Way Galaxy.

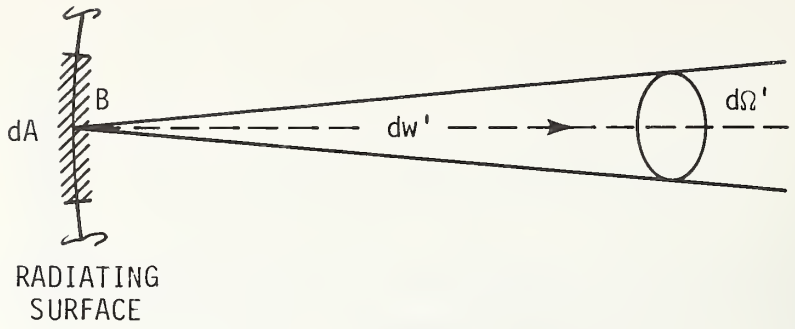

Figure 2-4 Brightness B of an elemental radiating surface dA

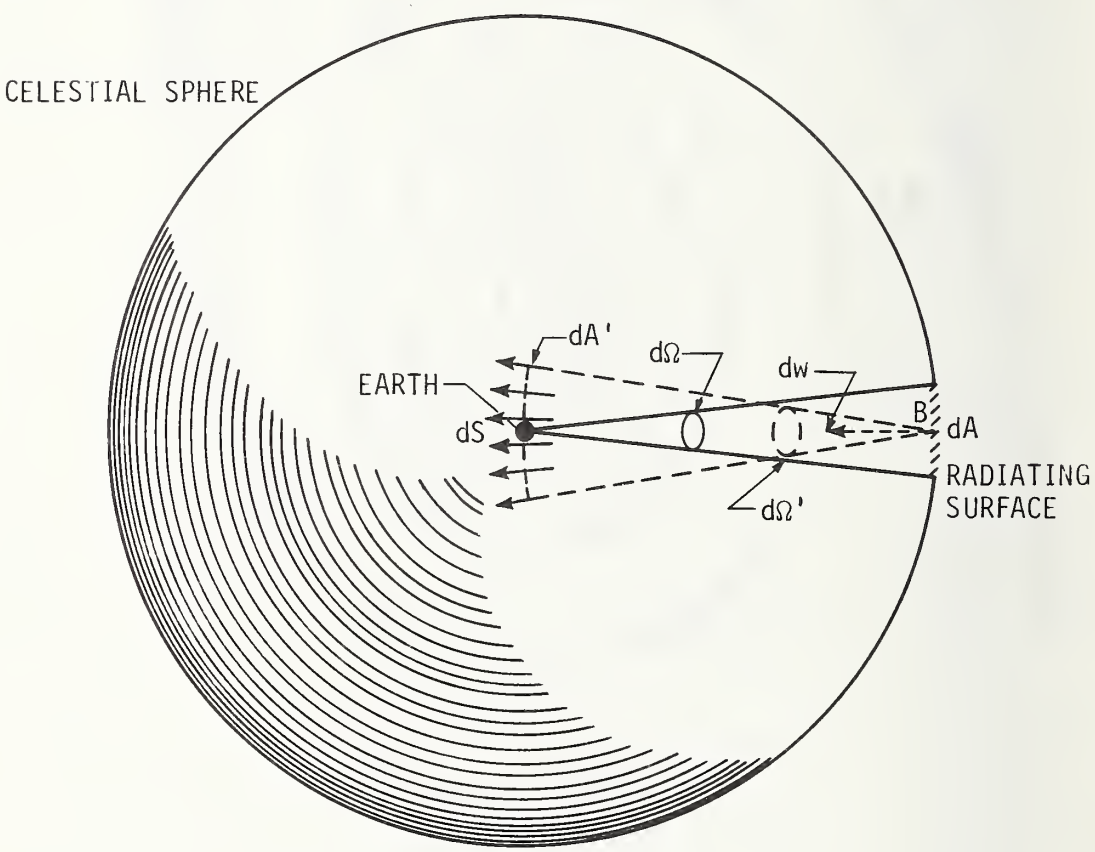

Figure 2-5 Elemental radiating surface dA on the celestial surface

on the sphere (of radius r) subtends a solid angle $d\Omega$, where the area and the solid angle are related via the equation

$$dA = r^2 d\Omega. \tag{2.2}$$

The spectral power (dw' of eq. (2.1)) leaving the surface dA proceeds within the solid angle $d\Omega'$ to the earth, becoming spread uniformly over the area dA'. Therefore the elemental flux density (dS) that reaches the earth after radiating from dA equals this spectral power divided by the elemental area dA'. That is

$$dS = \frac{dw'}{dA'}. \tag{2.3}$$

where dS = spectral power per unit area in watts/(m^2·Hz). The area dA' and solid angle $d\Omega'$ are related via the equation

$$dA' = r^2 d\Omega'. \tag{2.4}$$

Then using eqs (2.1), (2.2), and (2.4), eq. (2.3) reduces to

$$dS = B d\Omega. \tag{2.5}$$

This is the fundamental equation relating the elemental flux density (dS) arriving at the earth to the brightness B of the area of the sphere subtended by the solid angle $d\Omega$.

The flux (S) from any finite source is given by the integral of all the elemental fluxes making up the source, that is

$$S = \int_{\text{source}} B d\Omega. \tag{2.6}$$

The magnitude of the flux density is often expressed in flux units (f.u.), where one unit is 10^{-26} watts/(m^2·Hz).

The brightness temperature is a fictitious temperature associated with the brightness. It is that temperature to which a black-body radiator must be raised in order to have the same brightness B. In the low-frequency approximation it is related to the brightness through the equation [6]

$$T_B = \frac{\lambda^2 B}{2k}, \tag{2.7}$$

where T_B is the brightness temperature in kelvins; λ is the wavelength of interest in meters; and K is Boltzmann's constant.

2.3.2 Flux Density and Spectral Index of Cas A

Among other things the flux density of Cas A is both a function of frequency and time. Therefore the time and the frequency of its measurement must be specified. For example, the flux density of Cas A at 7.5 GHz for the time (epoch) AD 1965.0 is approximately 618 f.u. and is decaying at approximately 1% per year. One f.u. or flux unit is 10^{-26} w/(m^2·Hz).

It has been found that the frequency dependence of the flux density follows the equation

$$S(f) = S_1 f^{\alpha} \tag{2.8}$$

where S_1 is the flux density at 1 GHz; α is a constant called the "spectral index" and is defined by eq. (2.8); and f is the frequency in GHz (the symbol α is also used to denote right ascension). The flux density of Cas A around 7.5 GHz is given in table 2-1 and figure 2-6. The flux densities were transferred (see section 2.4) from the epochs in which they were measured (column three) to the epoch AD 1965.0 (column four) by using a decay rate of 1.1% per year.

Table 2-1

Frequency (GHz)	Epoch (AD)	Flux Density (f.u.)	AD 1965.0 Flux Density (f.u.)
5	1964.4	910 [16]	905
5.68	1968.5	740 [17]	766
6.66	1965	684 [18]	684
8	1964	590 [19]	584
9.36	1961.5	520 [20]	502
9.375	1962.7	514 [21]	502
9.38	1968.5	510 [17]	528

Figure 2-6 is a log-log plot of the AD 1965.0 flux densities in table 2-1. The line drawn through the points is a least squares fit to these points and conforms in the interval from 5 to 10 GHz to the spectral equation

$$S(f) = 3604\ f^{-0.875} \qquad (2.9)$$

where the flux density is given in flux units and the frequency is in GHz. From this equation the flux density at 7.5 GHz is found to be 618 f.u., with a corresponding brightness temperature of 336 kelvins. A method such as this is often used over a much wider frequency range to determine S at a frequency where it has not been measured, and/or to obtain a higher accuracy in S based upon the assumption that eq. (2.8) is a correct description of how S varies with frequency. In this context it should be pointed out that the values of α (-0.875) and S_1 (3604 f.u.) found from this table using only data over the restricted frequency range do not agree with α's and S_1's generally found in the literature. This

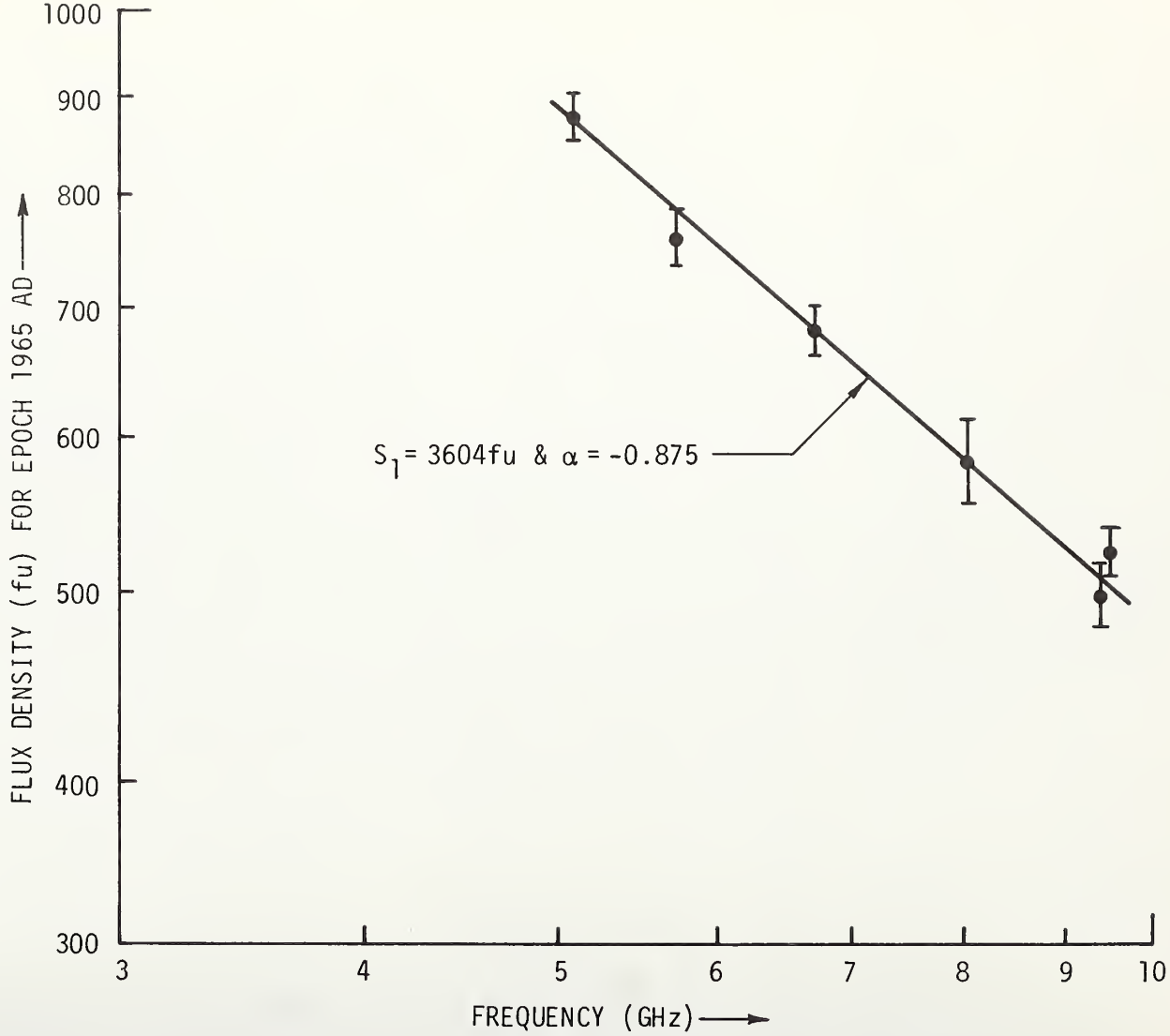

Figure 2-6. The flux density of Cas A around 7 GHz.

disagreement reopens the question of whether the flux density (at 7.5 GHz for example) can actually be more accurately determined by a curve-fitting process on a number of measured points close to 7.5 GHz as done in figure 2-5, by a curve-fitting process over a wider frequency range or by direct measurement of G/T at 7.5 GHz. The curve-fitting process for finding α and S over the wider frequency range correspondingly requires α to be constant over this larger range, a requirement that may not be met [22].

The characteristics (spectral index, polarization, decay rate, intensity distribution, and shape) for Cas A are explained to first order [23] by an expanding shell model wherein the rf emission is assumed to come from synchrontron radiation within the shell. One of the predictions of this model will be used in the next subsection where the Cas A decay rate is discussed.

2.4 Secular Decay

2.4.1 Decay Rate

The shell model [23] of Cas A predicts its flux density S at its age t. According to this model S can be calculated from the measured flux density S_o measured at age t_o from the equation

$$S = S_o(t_o/t)^{\beta}. \qquad (2.10)$$

Where β is a decay constant that is related to the spectral index α through the equation ($\alpha < o$)

$$\beta = 2(1-2\alpha). \qquad (2.11)$$

Based on eq. (2.10) the flux density S from Cas A should decay with time as roughly indicated in figure 2-7. The (normalized)

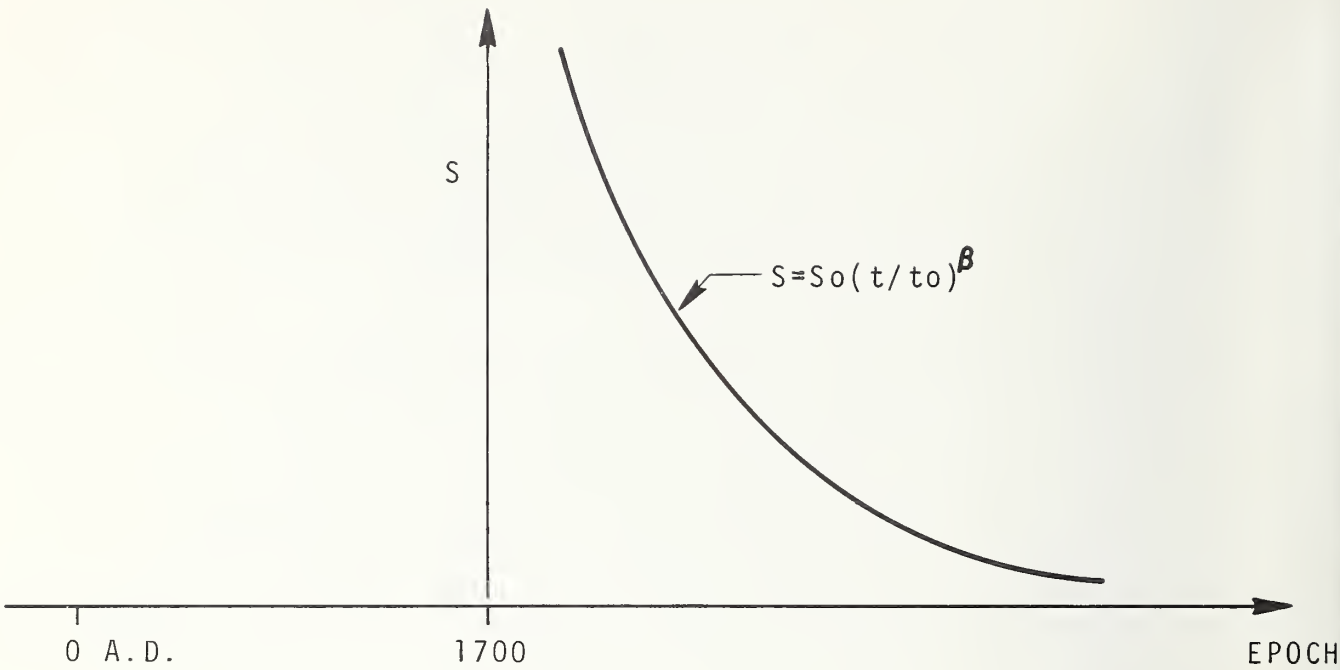

Figure 2-7. Decay curve of the Cas A flux density as calculated from the shell model.

differential decay rate, r, can be found by differentiating eq. (2.10) and is

$$r = -\frac{1}{S}\frac{dS}{dt} = \frac{\beta}{t}. \qquad (2.12)$$

The decay rate calculated for Cas A using epoch AD 1950.0 from eqs. (2.11) and (2.12) is 2%, while the measured value is closer to 1%. Minkowski's [10] birth date (AD 1700) for Cas A has been used in this calculation along with a spectral index equal to -0.8. It is interesting to note in this regard that Brosche [24] has drawn attention to some Korean records that indicate a "guest star" in the region of Cassiopeia around AD 1592, which "star," if it were the birth of Cas A, would yield a decay rate (AD 1950.0) of 1.3% per year, much closer to the measured values than the rate given by Minkowski's data.

While the shell model is not a perfect description of the Cas A decay, it indicates in a rough way (fig. 2-7) how the flux density should decay with time. As will be seen, the time dependence of r as indicated in eq. (2.12) shows that more care should be exercised in the application of average decay rates measured over long periods.

The decay rate predicted by eq. (2.12) decreases with time. At the present time insufficient receiver sensitivity, coupled with the small yearly decrease in the flux of Cas A, prevents a short-term measurement of the Cas A decay rate. One is forced therefore to compare the flux from Cas A over long periods of time, a process which yields an average decay rate instead of the differential rate. It can be seen from figure 2-8 that this average decay rate, R, where ($\Delta t = t - t_o$)

$$R = \frac{S_o - S}{S\Delta t} \qquad (2.13)$$

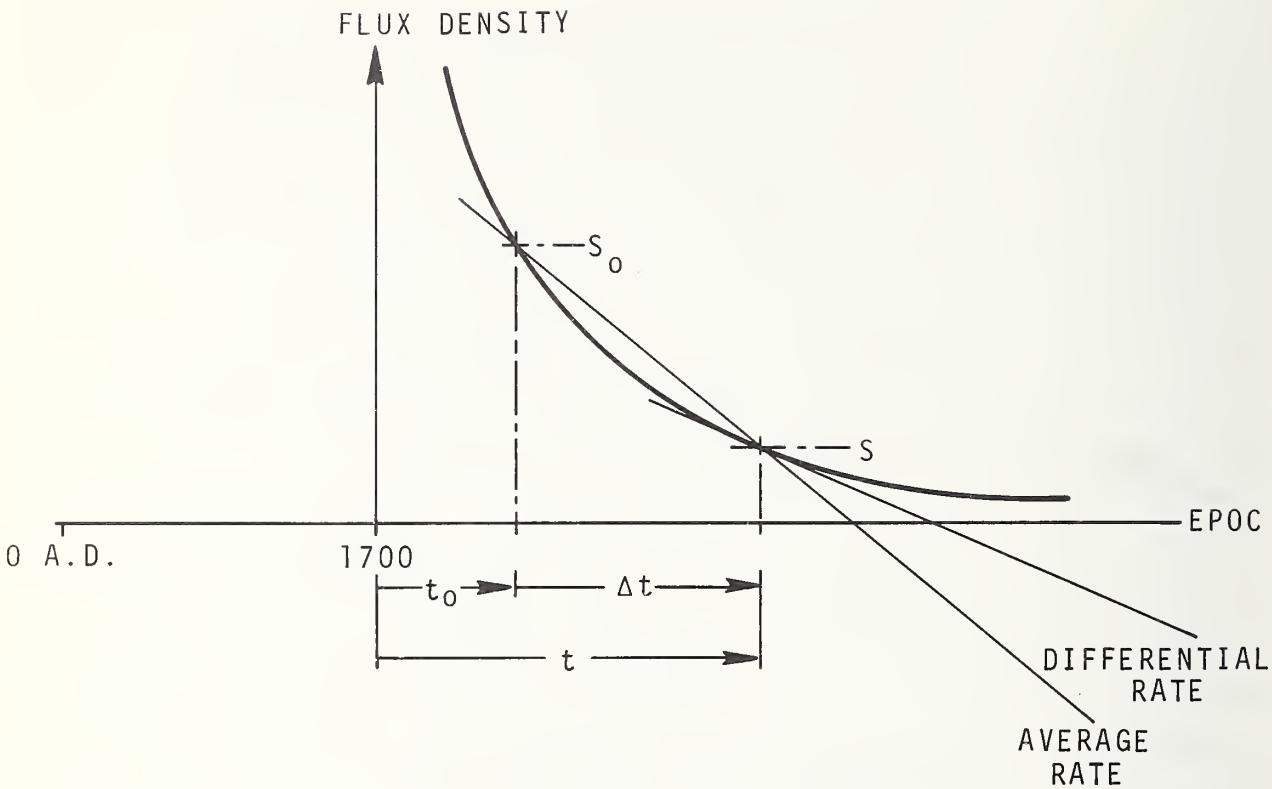

Figure 2-8. Decay curve of the Cas A flux density showing the relation between the differential and average decay ratio.

is related to the differential decay rate, r, at age t to first order in $\Delta t/t_o$ by

$$r \simeq R(1-\Delta t/t_o) \tag{2.14}$$

and that the differential rate is always less than the average rate. An estimate of the magnitude of $\Delta t/t_o$, or the relative correction needed to reduce R to r, can be obtained by taking the birth of the radio star to be AD 1700, t_o to be AD 1948, and Δt to be 25 years. The resulting $\Delta t/t_o$ is 0.1. In other words the differential decay rate is 10% less than the average decay rate measured over the 25 year period, a difference that should not be ignored when using the decay rate to predict the flux density of Cas A. Therefore, the model, while not perfect, does indicate that the average decay rate (R) used in the literature to transfer flux densities from one epoch to another should probably be reduced, in some cases possibly by as much as 10%. Moreover, if it is assumed that the shell velocity has not increased since the explosion that gave rise to Cas A, then it can be easily shown that the star birth cannot be earlier than AD 1700 under certain simplifying assumptions in which case it can be conjectured that the difference between the average and differential decay rates is probably greater than 10% for a 25-year measurement period. In any case, these results derived from the shell model do strongly suggest that the practice of using the average decay rate to transfer flux densities from one epoch to another should be examined more closely if a high accuracy in the resulting flux densities is desired.

Flux densities are deduced in the literature from known values by use of the following equation

$$S = S_1(1-R)^{\Delta t} \tag{2.15}$$

where S_1 is the flux measured at age t_1; R is the average decay rate discussed above; and Δt is the time difference between t_1 and the time of interest t. From the preceding discussion it is seen that a better approximation to S is obtained when one uses r instead of R, that is,

$$S = S_1(1-r)^{\Delta t}, \tag{2.16}$$

where r is calculated from R by using eq. (2.14). Even eq. (2.16) is not exact in the sense that it is equivalent to eq. (2.10). However, it is a sufficiently good approximation for even the most accurate of today's measurements and has the great advantage that β need not be known, and only a rough estimate of the star's birth date need be used in calculating r from eq. (2.14).

2.4.2 Some Measured Values of R

Some measured values of the average decay rate R are shown in table 2-2.

Table 2-2

Freq. GHz	Decay Rate (percent)	Error in Decay Rate (percent)	Epochs Used	Year Span	Reference
0.082	1.06	13	1948-1960	12	Högbom [25]
0.082	1.29	6	1948-1969	21	Scott [26]
3.2	1.14	23	1953.9-1962.7	8.8	Mayer [27]
1.4	1.38	11	1965-1971	11	Findlay [28]
1-3	0.90	11	1960-1971	15	Baars [29]

These results indicate that the average decay rate is not known to a high degree of accuracy. Add to this the fact

that the rates used are possibly 5% to 10% high and that the rate possibly changes with frequency [30], and it is easily seen that the state of knowledge concerning decay rate is not at a very high level and that much more work along this line needs to be done.

2.5 Polarization

2.5.1 Polarization and Faraday Rotation

Polarization [6]

The emission from a celestial radio source extends over a wide frequency range, and therefore within any finite bandwidth, consists of the super-position of many statistically independent waves of various polarizations. Generally these emissions are partially polarized, some sources tending toward complete nonpolarization and others toward a significant degree of polarization. Partially polarized emission can be decomposed into a completely random wave plus completely polarized waves. The degree of polarization d is then defined as the ratio of the power contained in the polarized wave to the total power in all the wave. It is this total power, or the power contained in both the random and polarized waves, that is proportional to the source flux density.

The "position angle" on the celestial sphere of the polarization of a source is measured the northerly direction, increasing in the eastwardly direction. The manner in which the antenna polarization and the linear source polarization affect the available power from the antenna output port is shown in table 2-3, on the assumption that the antenna is pointed directly at the source, and that the source is a point source.

Table 2-3

Type of Antenna Polarization	Spectral Power at Antenna Waveguide Port
Linear	$1/2\ SA_e(1 + d \cos 2\theta)$
Right or Left Circular	$1/2\ SA_e$

The first column of the table shows the type of antenna polarization assumed for the antenna receiving flux from the sources. The second column shows the power per unit bandwidth available at the antenna waveguide port as a result of the source flux impinging on the antenna aperture. A_e is the effective antenna aperture [2]; d is the degree of linear polarization of the source; and θ is the angular difference between the source's polarization position angle and the antenna's linear polarization angle measured relative to the source's north.

Faraday Rotation [6,31]

Much of the galactic medium between the earth and Cas A is ionized and contains a small magnetic field roughly parallel to the direction between them. Because of the presence of the magnetic field, this medium is anisotropic and causes the direction of polarization of a polarized wave traveling through it to rotate as the wave proceeds. This rotation is proportional to the square of the wavelength of the polarized wave. Therefore, as the observed wavelength is increased, the observed position angle of the source polarization will increase or decrease according to whether the proportionality constant is positive or negative respectively. This proportionality constant is called the "rotation measure," and in the direction of Cas A is thought to be [14] approximately -130 rad./m^2.

2.5.2 Measured Polarization of Cas A

The literature [14,32,33,34] suggests that above 1 GHz the linear polarization of Cas A is approximately 1%, and that below 1 GHz the polarization falls to zero. Table 2-4 is representative of the values reported, and shows that the degree of polarization and the position angle are not accurately known.

Table 2-4

Frequency (GHz)	Polarization (%)	Position Angle (Degree)	Reference
1	< 1	--	32
3	< 1	--	32
5	1.4 ± 0.5	37 ± 15*	14
8.25	0.5 ± 0.2	114 ± 15	33
10	1.5	40*	32
14.5	1.2 ± 0.5	41 ± 9*	35
15.25	1.9 ± 0.2	71 ± 3*	33
15.75	2.2 ± 0.3	79 ± 3	33
19.4	1	31*	34

*Indicates values used in figure 2-9.

The scheme depicted in figure 2-9 might be used to obtain usable values of position angle versus frequency. The position angle values in the table identified by an asterisk have been plotted against wavelength in the figure. The wavelength is indicated on a squared scale so that theoretically the data should fall along a straight line assuming the position angle is proportional to wavelength squared. Then the least squares fit linear curve, curve (a) in the figure, gives at least an idea of the position angle as a function of wavelength that

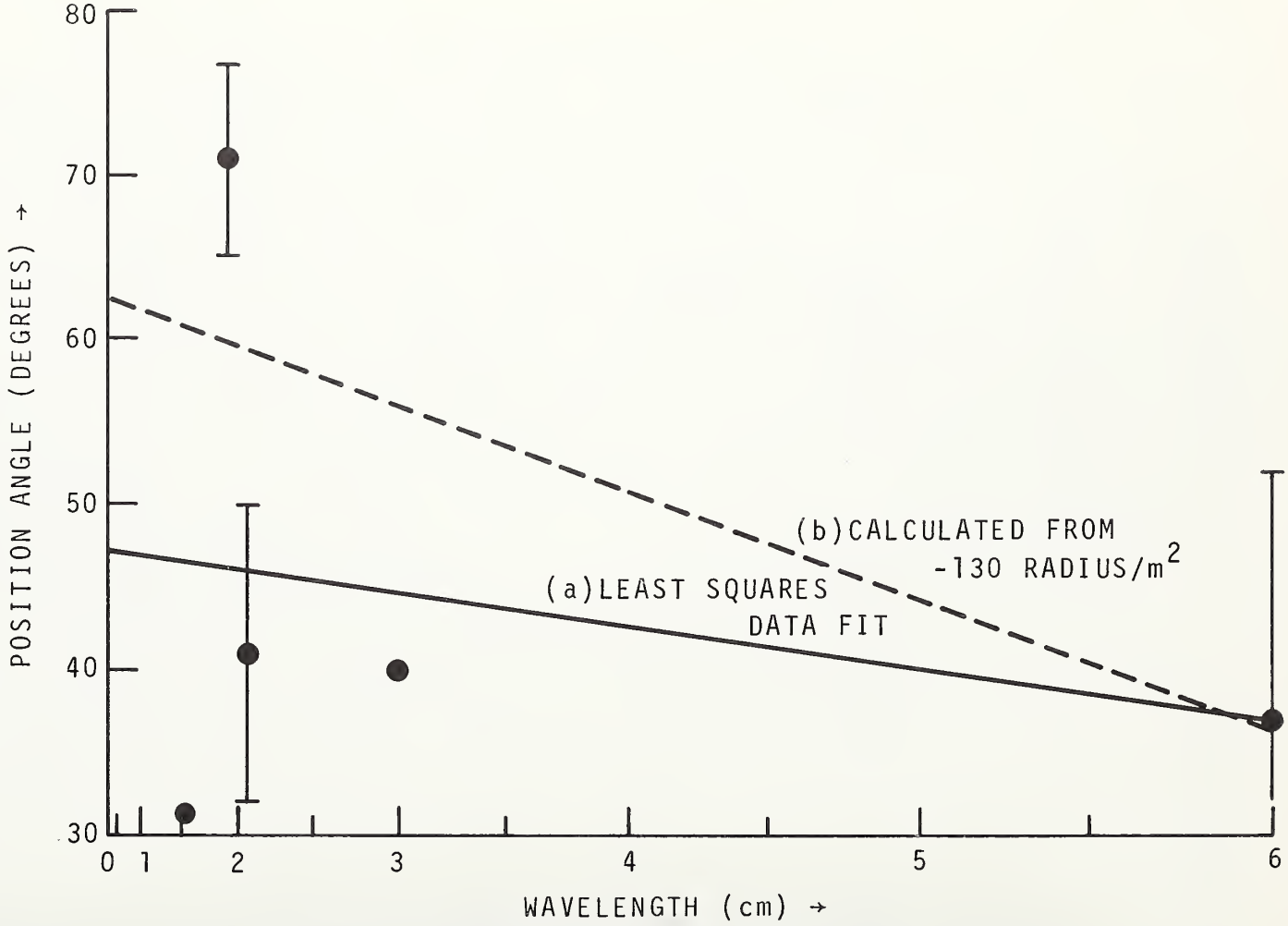

Figure 2-9. Hypothetical position angle curve for the linearly polarized flux from Cas A.

might be used in calculations involving linearly polarized antennas. Curve (b) is included in the figure to indicate the slope that corresponds to the measured [14] rotation measure (-130 rad./m^2).

2.6 High Resolution Maps

For the purpose of this report Cas A is considered to be a discrete source with a single value assigned to its flux density, spectral index, degree of polarization and position angle, and secular decay rate for a given epoch and frequency of observation. However, there have been a number [14,34,36] of investigations made into the detailed structure of this source which, from our point of view, are worth examining for several reasons: 1) they aid in understanding the nature of the background radiation in the neighborhood of Cas A, and therefore in the interpretation of broadbeam measurement results; 2) they help determine at what antenna resolution Cas A can no longer be treated as a discrete source with no structure; and 3) they can be used to obtain more accurate source-antenna convolution corrections. The high-resolution maps of Cas A will show that all of the parameters of Cas A which are considered to be constants in the broad beamwidth picture do in fact vary across the face of the source in a highly irregular manner.

Figure 2-10 shows a brightness temperature contour map [14] of Cas A measured around epoch AD 1969.8, where the thick dashed curve represents the zero contour (relative to a cold area of the sky well separated from the source), and where the contour interval is 200 kelvins. The brightness temperature is plotted in right ascension versus declination, and the highly structured nature of Cas A is clearly evident. It is also clear that the source is well localized with a slight bulge towards the east.

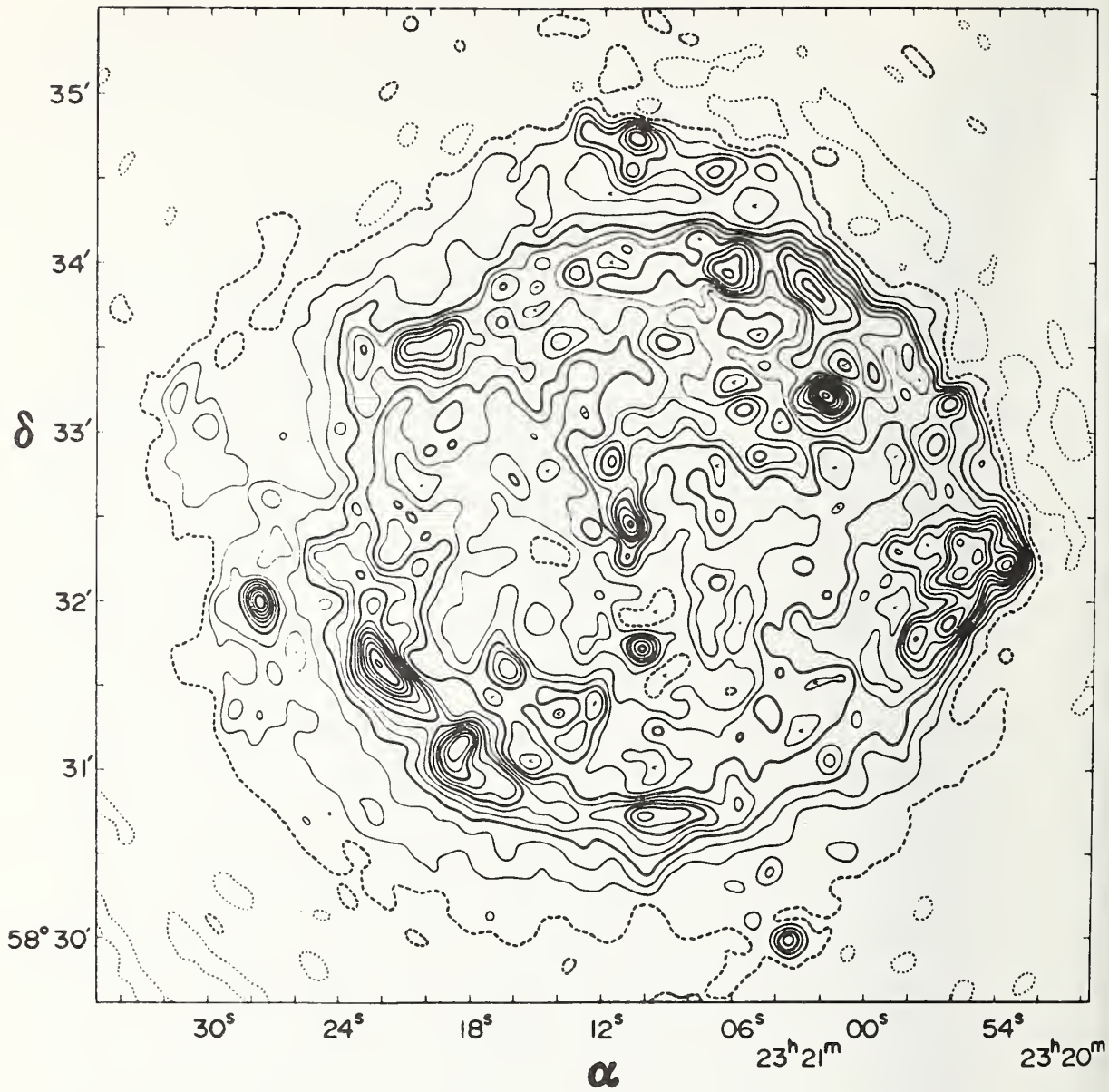

Figure 2-10. Brightness temperature contour map of Cas A (coordinates for Epoch AD 1950.0, 5.0 GHz). (Courtesy of Monthly Notices of the Royal Astronomical Society, Vol. 151, No. 1, p. 112, 1970.)

Figure 2-11 is another brightness temperature map [14] (epoch AD 1968.4, frequency 1.407 GHz) with a dashed zero contour and 6700 kelvins contour intervals. On this map the numbers representing the spectral index and their locations are noteworthy. It can be seen that the index varies from a negative -0.5 to a negative -1.2 in a highly irregular manner. The resulting spectral index averaged over this map is a negative -0.75, in fair agreement with Baars' [29] negative -0.787.

Figure 2-12 (epoch AD 1966.8, frequency 19.4 GHz) shows two profile views [34] of Cas A, curve (a) being proportional to the brightness temperature relative to the uniform background around Cas A, and curve (b) being proportional to the linearly polarized component (amplified 20 times) of this brightness temperature. A characteristic "valley" of reduced polarization can be seen running from southwest to northeast across the source. This "valley" is also evident in figure 2-13, which shows the distribution [14] (epoch AD 1950, frequency 5 GHz) of this polarized component. The bars in figure 2-13 are oriented along the electric vector position angles, the longest bar corresponding to a brightness temperature of about 100 kelvins. The degree of polarization averages about 5% around the rim of the shell, with peaks of about 10% in the southeast region and of about 6% in the northwest region. Toward the central part of the shell the polarization falls to 1% or less. The average polarization over this map is 1.4% at a position angle of 37°.

To get an idea of the average shape of the Cas A, annular rings about the center of the source 5 arc seconds wide were extracted from the intensity map in figure 2-10, and the intensity around each ring averaged. Figure 2-14 (epoch AD 1950, frequency 5 GHz) shows the resulting

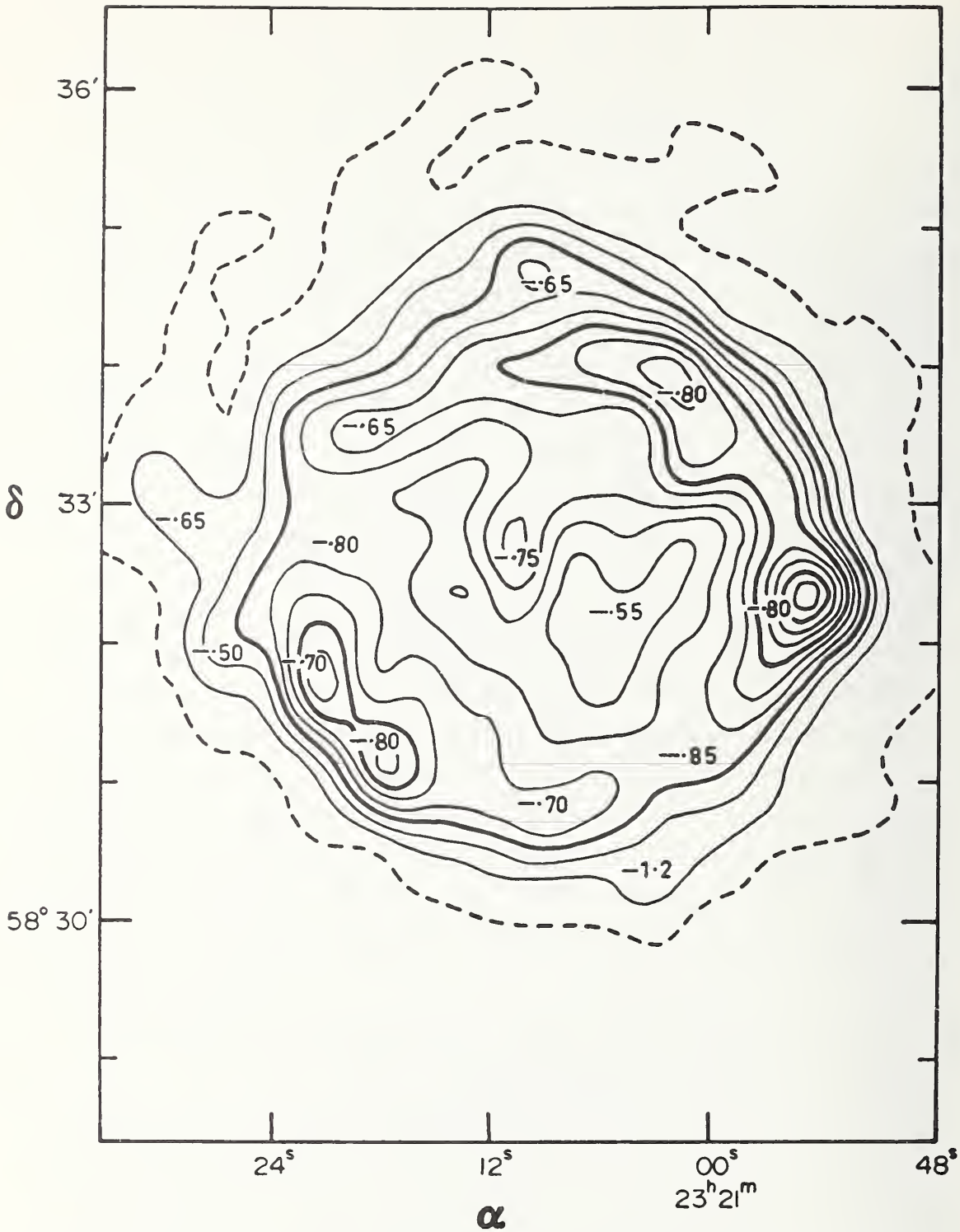

Figure 2-11. Brightness temperature contour map of Cas A (Epoch 1968.4, 1.4 GHz) showing the variation of the spectral index across the source. (After Monthly Notices of the Royal Astronomical Society, Vol. 151, No. 1. p. 114, 1970.

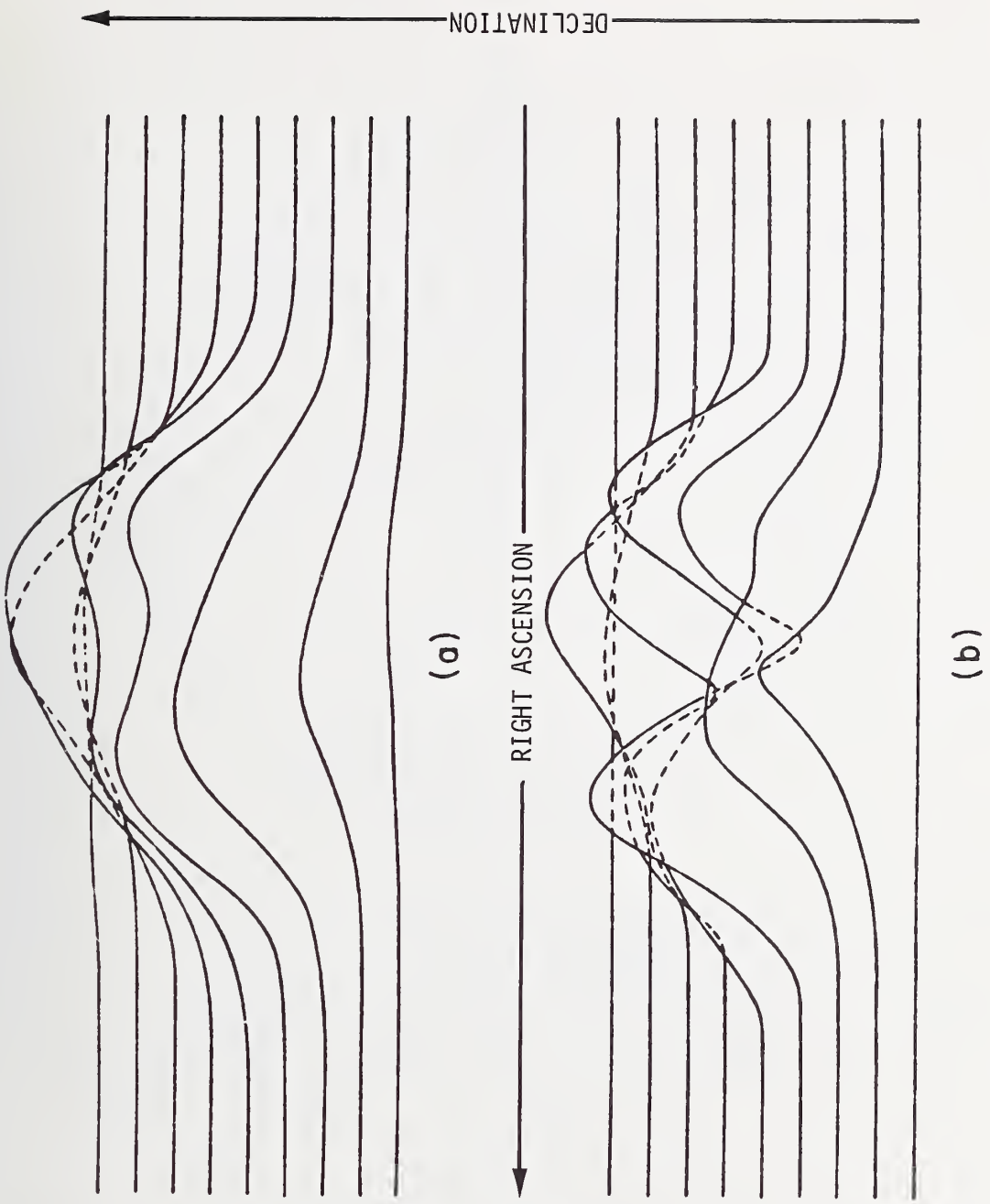

Figure 2-12. Brightness temperature contour map of Cas A (Epoch AD 1966.8, 19.4 GHz) showing (a) the brightness temperature, (b) the linearly polarized component of (a) amplified 20 times. (Courtesy of Astrophysical Journal, Vol. 151, p. 56, 1968; C.H. Mayer and I.P. Hollinger; University of Chicago Press.)

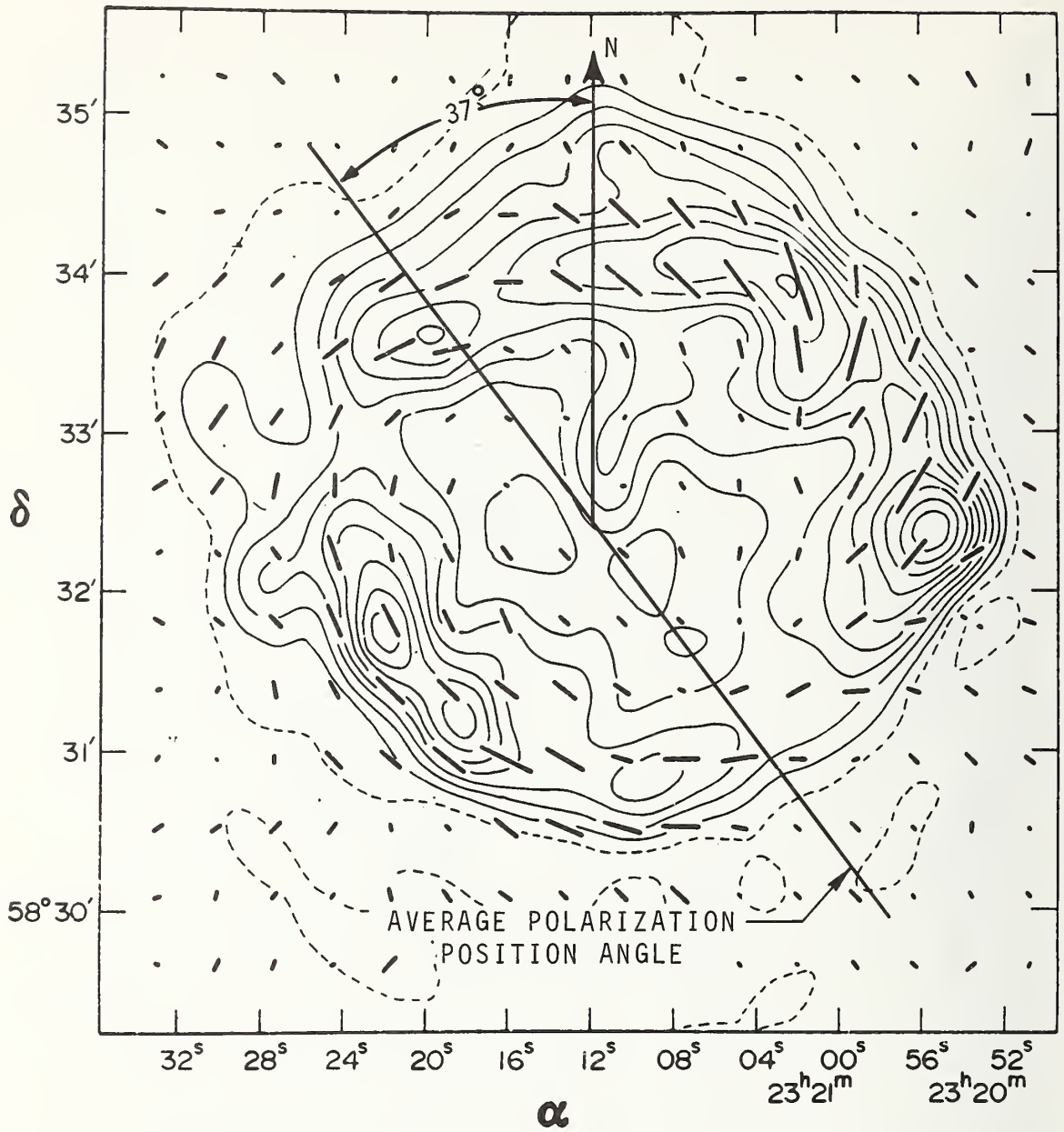

Figure 2-13. Brightness temperature contour map of Cas A (Epoch 1950.0, 5.0 GHz) showing the distribution of polarized emission across the source with the average position angle of the electric vectors superimposed. (After Monthly Notices of the Royal Astronomical Society, Vol. 151, No. 1, p. 116, 1970).

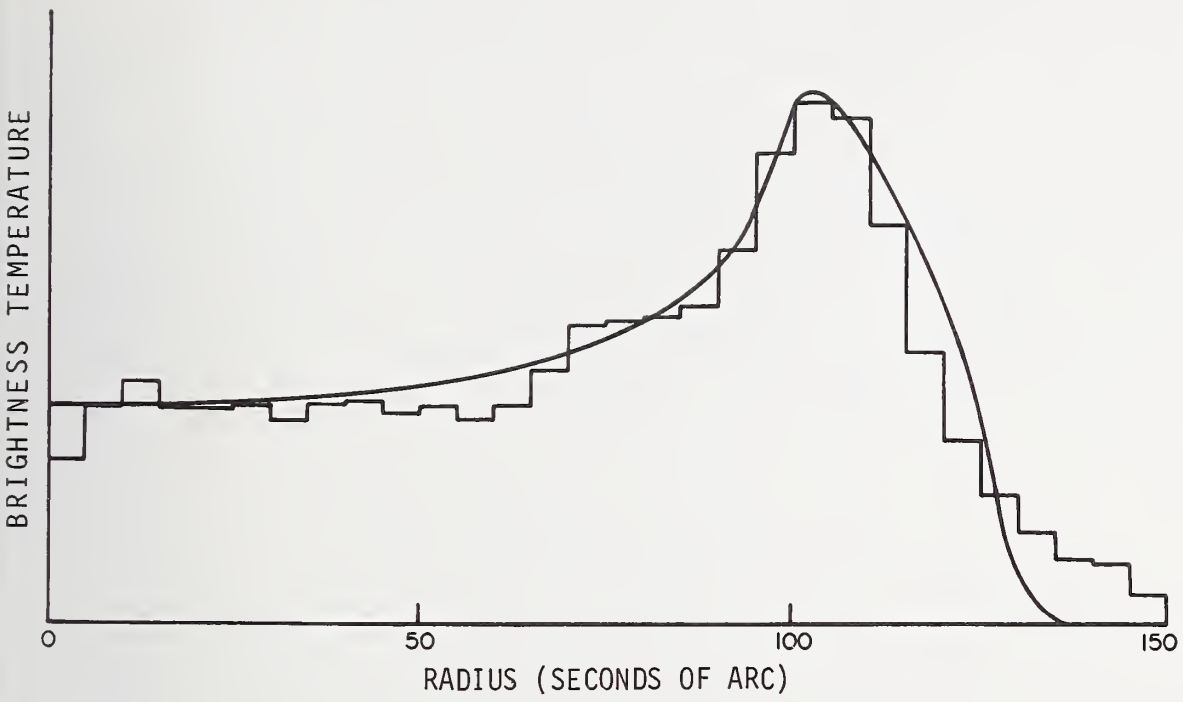

Figure 2-14. Mean brightness temperature profile from the center of Cas A outward (Epoch AD 1950.0, 5.0 GHz). (After Monthly Notices of the Royal Astronomical Society, Vol. 151, No. 1, p. 118, 1970).

histogram [14]. The abscissa represents the arc radius from the center of the source ($\alpha = 23^h\ 21^m\ 11^s$, $\delta = 58°,32',40''$, Epoch AD 1950), and the ordinate is proportional to the brightness temperature relative to the uniform background around Cas A. This histogram agrees well with other measurements which indicate that the source has an average shape resembling a disk with an enhanced outer ring. The smooth curve drawn through the histogram is the best-fit curve predicted from the spherical shell model with a small radial magnetic field. This curve or its histogram could be convolved with the main beam of broad beamwidth antennas to obtain the usual star size correction.

2.7 Cosmic Background Radiation

Besides the discrete sources of radio emission like Cas A, the cosmic or extraterrestrial radio sky contains a more or less continuous background of radiation which consists of a thermal and a nonthermal component. In the context of this report one needs to know this background radiation because 1) this background radiation contributes to total system temperature of any satellite ground station -- the contribution depending upon where the satellite is; 2) the background around Cas A may be different from the background around the satellite; and 3) the background around the calibrating source (Cas A) determines where the antenna should be pointed in the course of performing G/T ratio measurements.

2.7.1 Nature of the Cosmic Radio Background

The origin of the continuous cosmic radio background radiation is still open to question, and it appears that a number of measurements in the microwave region and above remain to be done.

Kraus [6] distinguishes three sources of continuous background radiation, extragalactic and galactic nonthermal (synchrotron) radiation, and galactic thermal radiation originating in the galactic HII (ionized hydrogen) regions. The nonthermal synchrotron radiation predominates below about 1 GHz with a spectral index of from about -0.2 to -0.5, and the thermal radiation predominates above 1 GHz. From a review of the literature one receives the impression that above 1 GHz it is not clear what the source of the continuous thermal radiation is. Some of the references suggest that the radiation comes from the galactic HII regions, while others suggest a cosmic black-body origin (to be discussed). In what follows it will be seen that the radio background maps support the latter conclusion.

A radio map [6] of the cosmic radiation at 250 MHz is shown in figure 2-15. The contours are at 6-kelvin intervals above the coldest parts of the sky, which are at a temperature of about 80 kelvins. Since the dotted line represents the galactic equator it is seen that the background peaks up in the galactic plane and falls off from this plane. Since the measurements were done at 250 MHz, the contours are predominantly nonthermal in nature (see fig. 2-16). Furthermore, since the contour lines run parallel to the galactic equator, it can be implied, consistent with remarks in the preceding paragraph, that the nonthermal radiation has a strong component associated with the galactic plane. In the following it will be seen that the same conclusion does not appear to be applicable to the thermal radiation above 1 GHz.

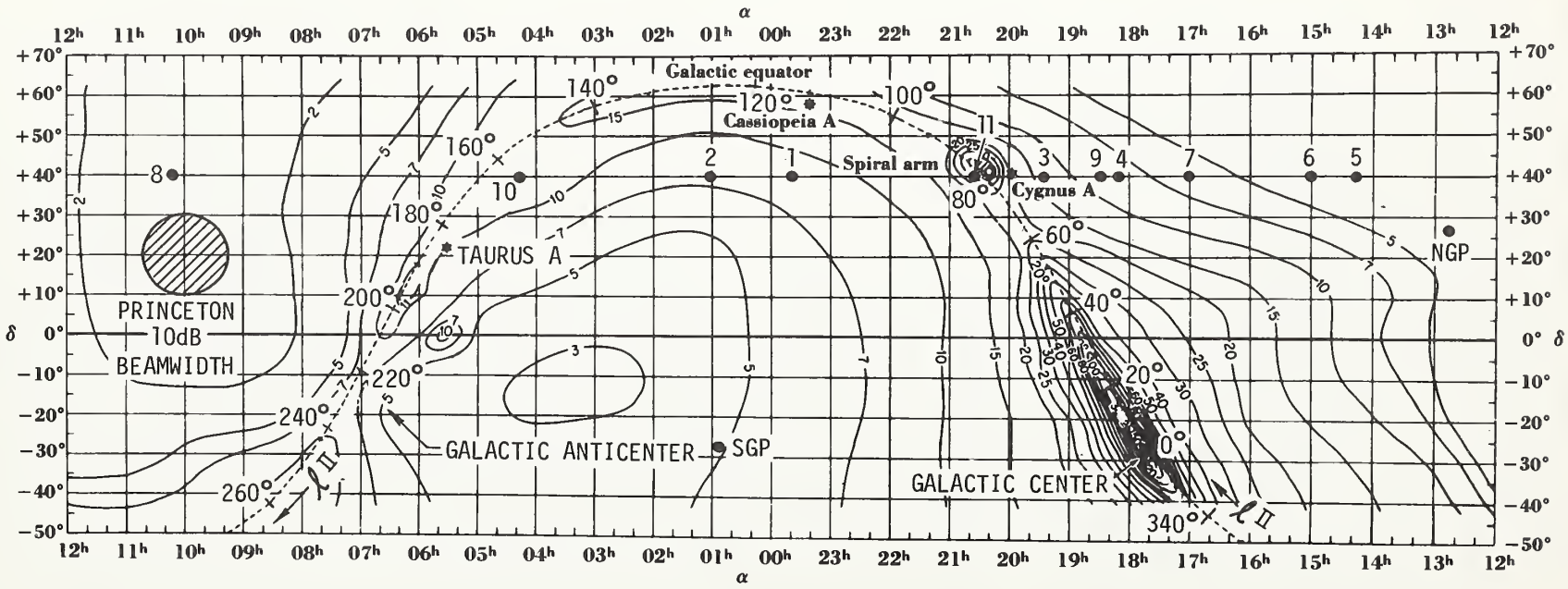

Figure 2-15. The cosmic radio sky at 250 MHz. (After Sky and Telescope, Vol. 16, p. 160, 1957).

In addition to the three sources of continuous radio emission mentioned earlier there is mention in the literature of a possible fourth [37] source, cosmic black-body radiation. According to hypothesis it originated when the universe was in a highly condensed and heated state, and as the universe expanded, the cosmological red shift cooled the radiation while preserving its thermal character. A number of measurements [38,39,40] of the absolute cosmic background tend to support this idea, the most convincing of which is the set taken at Princeton [39]. Referring again to figure 2-15, the eleven numbered points along the 40th declination represent positions where the Princeton measurements (9.375 GHz) were made. Table 2-5 gives the values of these measurements which, although they should be considered to be the same within the ± 0.5 kelvin experimental error, are listed in order of descending magnitude.

Table 2-5

Measurement Number	Location (Right Ascension)	Brightness Temperature (kelvins) at 9.375 GHz
1	$23^h\ 40^m$	3.32
2	1^h	3.16
3	$19^h\ 30^m$	3.14
4	$18^h\ 10^m$	3.12
5	$14^h\ 20^m$	3.07
6	15^h	3.02
7	17^h	2.98
8	$10^h\ 10^m$	2.89
9	$18^h\ 30^m$	2.80
10	$4^h\ 20^m$	2.78
11	$20^h\ 30^m$	2.76
	Average	3.0 ± 0.5 kelvins

It is important to note from the distribution of these points along the 40th declination that there seems to be no correlation between the position of the measured values and the position of the galactic equator, leading to the conclusion that the continuous radiation above 1 GHz received at the earth is isotropic and not primarily associated with the galactic plane. If there were a continuous increase of thermal radiation towards the galactic equator, then measurement number 11 should be considerably greater in magnitude than measurement number 1, yet these two points represent respectively the lowest and highest values in the table. This leads to the conclusion that, except for HII regions (which emit thermal radiation) localized along the galactic equator, the continuous thermal radiation above 1 GHz is isotropic and does not peak-up along the galactic equator like the nonthermal case below 1 GHz (fig. 2-15). In other words, it appears that the continuous thermal radiation is not associated with the galactic HII regions, but that it stems from a universal blackbody radiation and is spread uniformly over the celestial sphere. This conclusion is further supported by the contour maps to follow. In addition to the Princeton measurement, Penzias and Wilson [38] and Roll, et al. [39] have made measurements (averaging the absolute cosmic background along declinations close to the 40th declination) which agree with the Princeton measurements, and are summarized in table 2-6.

Only the direction of the contour lines in the following maps is germane to the discussion in this section. Therefore no attempt has been made to reconcile contour-line magnitudes from one map to another, their values being those appearing on the maps in the literature.

Table 2-6

Frequency GHz	Brightness Temperature (kelvins)
4.08	3.1 ± 1 [38]*
9.375	3.0 ± 0.5 [39] (average of Princeton measurements)
32.5	3.16 ± 0.2 [40]

*The value quoted by Penzias and Wilson [38] is 3.5 ± 1 kelvin. A later measurement by the same authors with a modified horn feed mentioned by Roll, et al. [39] gave the lower (and presumably better) value reported in table 2-6.

The preceding remarks lead to the following picture (fig. 2-16) of the continuous cosmic radio background. Below approximately 1 GHz the brightness (c.f. section 2.3.1) consists mainly of synchrotron radiation [6] lying in magnitude between that emanating from the galactic center and that from the galactic pole, and peaking up along the galactic equator. Above 1 GHz the brightness consists of isotropic black-body radiation at 3 kelvins. Superimposed on this continuous radiation are numerous localized HII regions of thermal radiation associated with the galaxy. For reference the brightness of Cas A is included in figure 2-16. While this picture of the continuous background seems to be consistent with the available data and radio maps, many more measurements, primarily in the microwave region and above, need to be performed to adequately justify it. It is nevertheless the most consistent picture that can be pieced together from the available literature. With figure 2-16, the positions of the contours with respect to the galactic equator in the maps to follow can be easily understood and lend further support to the conclusions drawn.

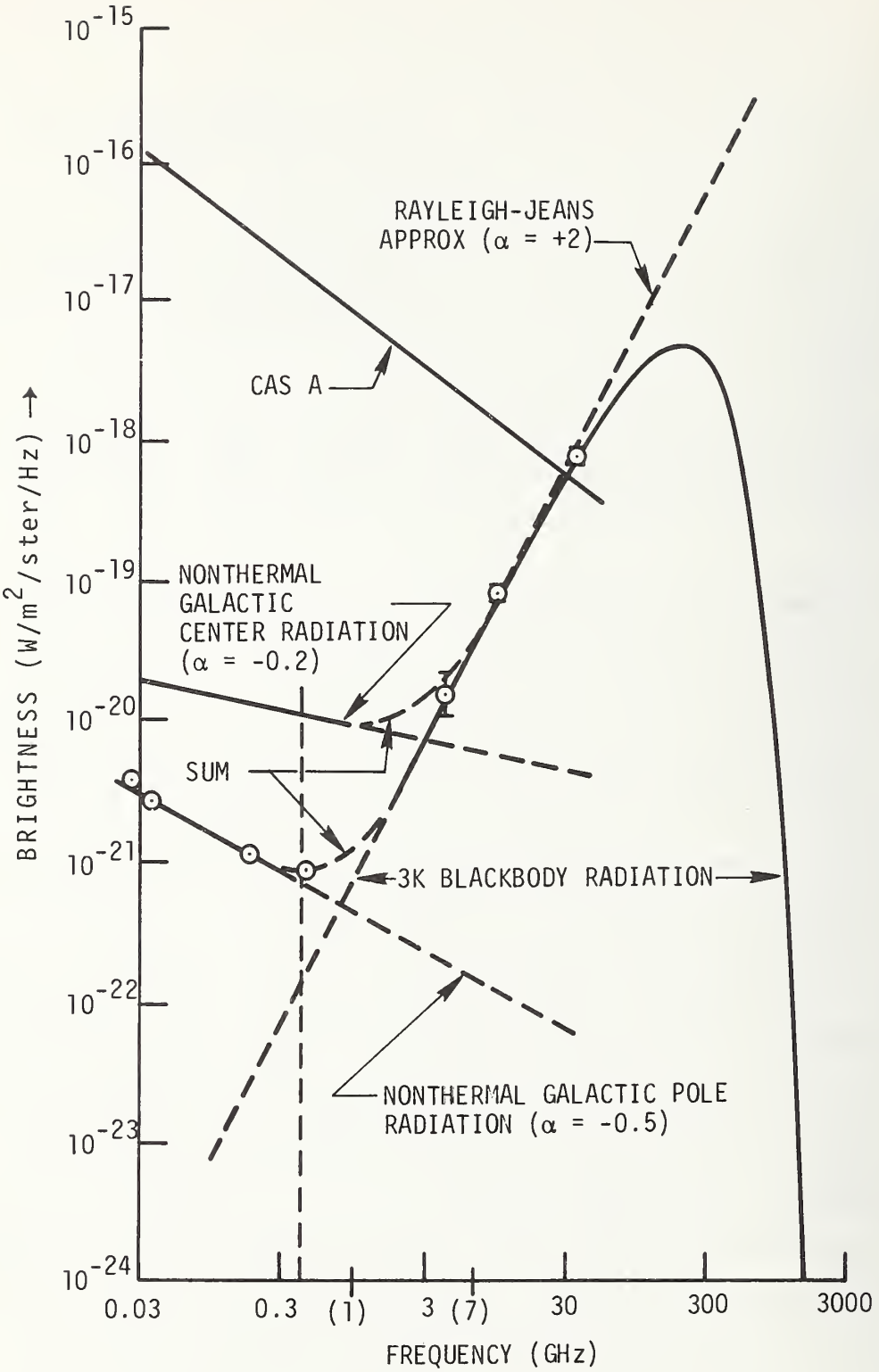

Figure 2-16. Brightness spectrum of the continuous cosmic radiation as deduced from the literature.

In addition to the map shown in figure 2-15 (250 MHz), figures 2-17 [30], 2-18 [41], 2-19 [42], and 2-20 [43] show radio maps around Cas A at 404 MHz, 960 MHz, 1.4 GHz, and 3.2 GHz, respectively, with the galactic equator drawn in, and lend support to the previously drawn conclusions concerning the nature of the thermal radiation above 1 GHz. It is apparent that in the 250 MHz, 404 MHz, and 960 MHz maps the contours run predominantly parallel to the galactic equator, while in the 1.4 GHz and 3.2 GHz maps this is not the case. In fact the contours in the 1.4 GHz and 3.2 GHz maps arise from localized HII regions around Cas A, and in the frequency region above 1 GHz where the synchrotron radiation is expected to die out (fig. 2-16), the distinct absence of contour lines parallel to the galactic equator indicates a lack of continuous thermal radiation emanating from the galactic plane. In other words, at about 1 GHz, consistent with figure 2-16, the continuous synchrotron radiation dies out leaving only the isotropic black-body component, with the HII radiation manifesting in localized regions only.

2.7.2 Cosmic Background Contribution to the System Noise Temperature

Assuming the validity of the above conclusions, the contribution to the cosmic background on the system noise temperature can now be predicted. When an antenna is pointed at a stationary satellite, the satellite appears to describe a path on the celestial sphere along one of the celestial declinations. In the process, the antenna beam and sidelobes pick up cosmic radiation along this path which, in the microwave region, is a uniform 3 kelvin black-body radiation on which the occasional localized HII regions are superimposed.

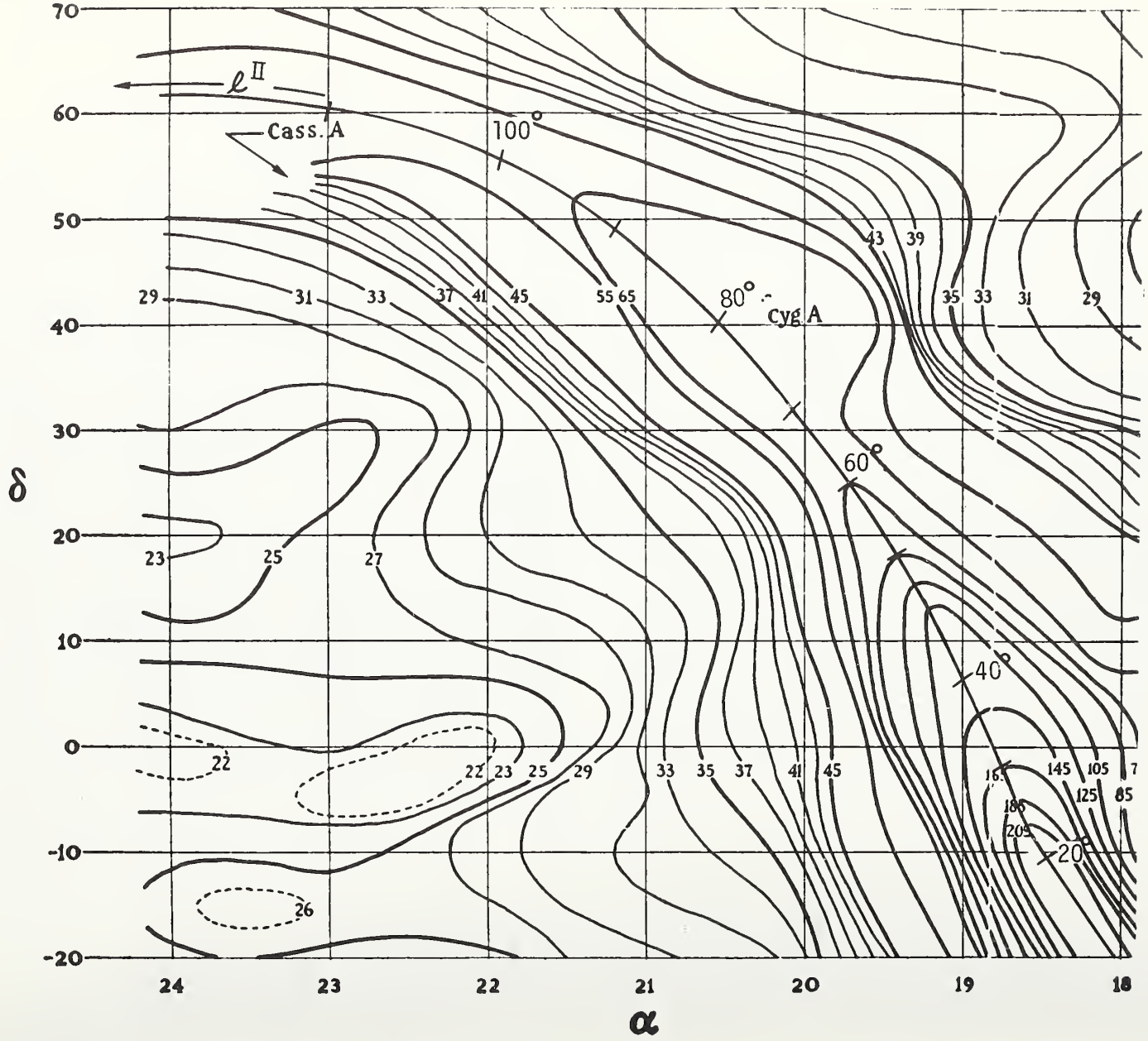

Figure 2-17. Cosmic radio background at 400 MHz. (After Monthly Notices of the Royal Astronomical Society, Vol. 124, No. 1, p. 74A, 1962).

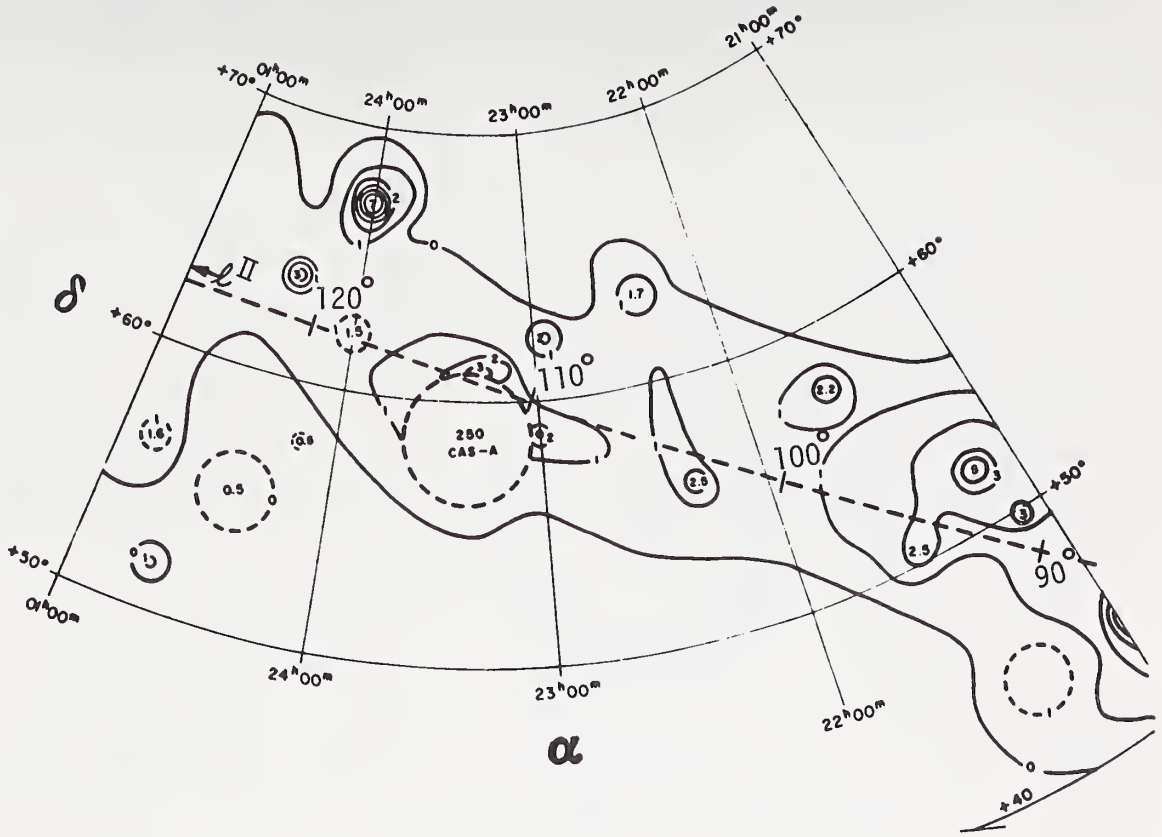

Figure 2-18. Cosmic radio background at 960 MHz. (After Publications of the Astronomical Society of the Pacific, Vol. 72, No. 428, p. 336, 1960).

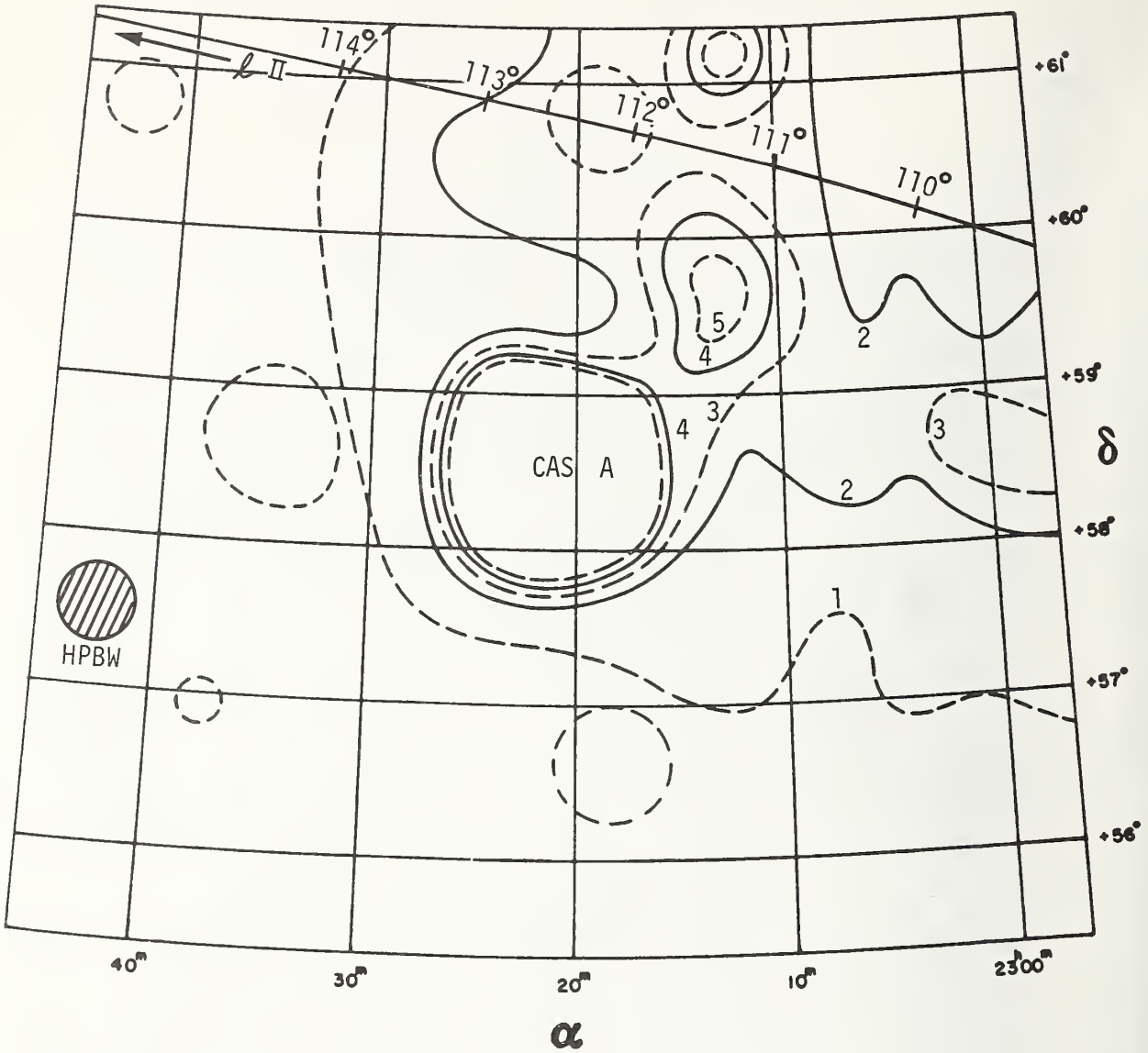

Figure 2-19. Cosmic radio background at 1.4 GHz. (After Publications of the National Radio Astronomy Observatory, Vol. 1, No. 3, p. 55, 1961).

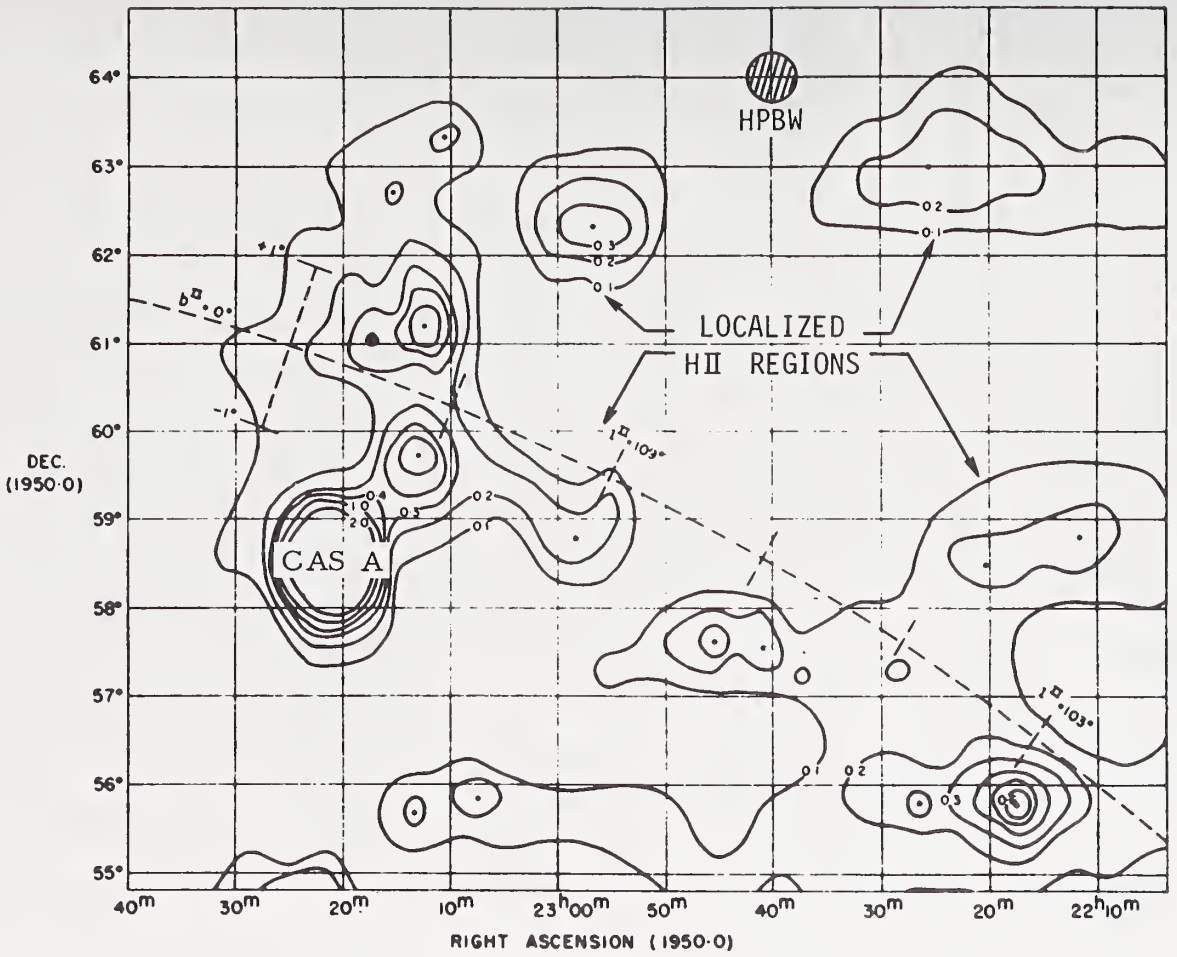

Figure 2-20. Cosmic radio background at 3.2 GHz. (After Monthly Notices of the Royal Astronomical Society, Vol. 129, No. 2, p. 166, 1965).

The contribution to the system noise temperature from this background radiation varies along this path in a corresponding manner. For example, consider what happens when the antenna beam encounters the various HII regions along the 60th declination in figure 2-19. The contour intervals are designated by integers which are multiples of 0.8 kelvins above a uniform background, presumably the 3 kelvin black-body radiation. As the beam (assumed small compared to the distances between the contours) traverses the contours along the 60th declination from right to left the antenna temperature is increased from 3 kelvins by 1.6, 2.4, 3.2, 3.2, 2.4, 1.6, and 0.8 kelvins in succession. This gives an idea of the possible variation of the antenna temperature for a narrow-beam antenna as it traverses a localized HII region. To know this variation in detail a radio map along the declination traversed by the satellite for the frequency in use is clearly necessary.

For the greatest accuracy, the preceding implies that when measuring the ground station G/T using the direct radio star method described in section 1.4, the offsets from Cas A used to establish P_2 or the system noise temperature should be made to an area of the celestial sphere free from localized HII radiation. These regions are apparent from figures 2-19 and 2-20. Furthermore, since figures 2-19 and 2-20 indicate that there is some HII radiation surrounding Cas A, the contribution of this radiation to the system noise temperature should be subtracted when Cas A is used as a calibrating source. In order to do this, a good map of the HII radiation around Cas A is needed. Figures 2-19 and 2-20 give an idea of the problems involved in obtaining such maps at a given frequency. The symmetry of contour lines around Cas A in these figures strongly suggests that the high synchrotron radiation from Cas A in the sidelobes of the antenna used to

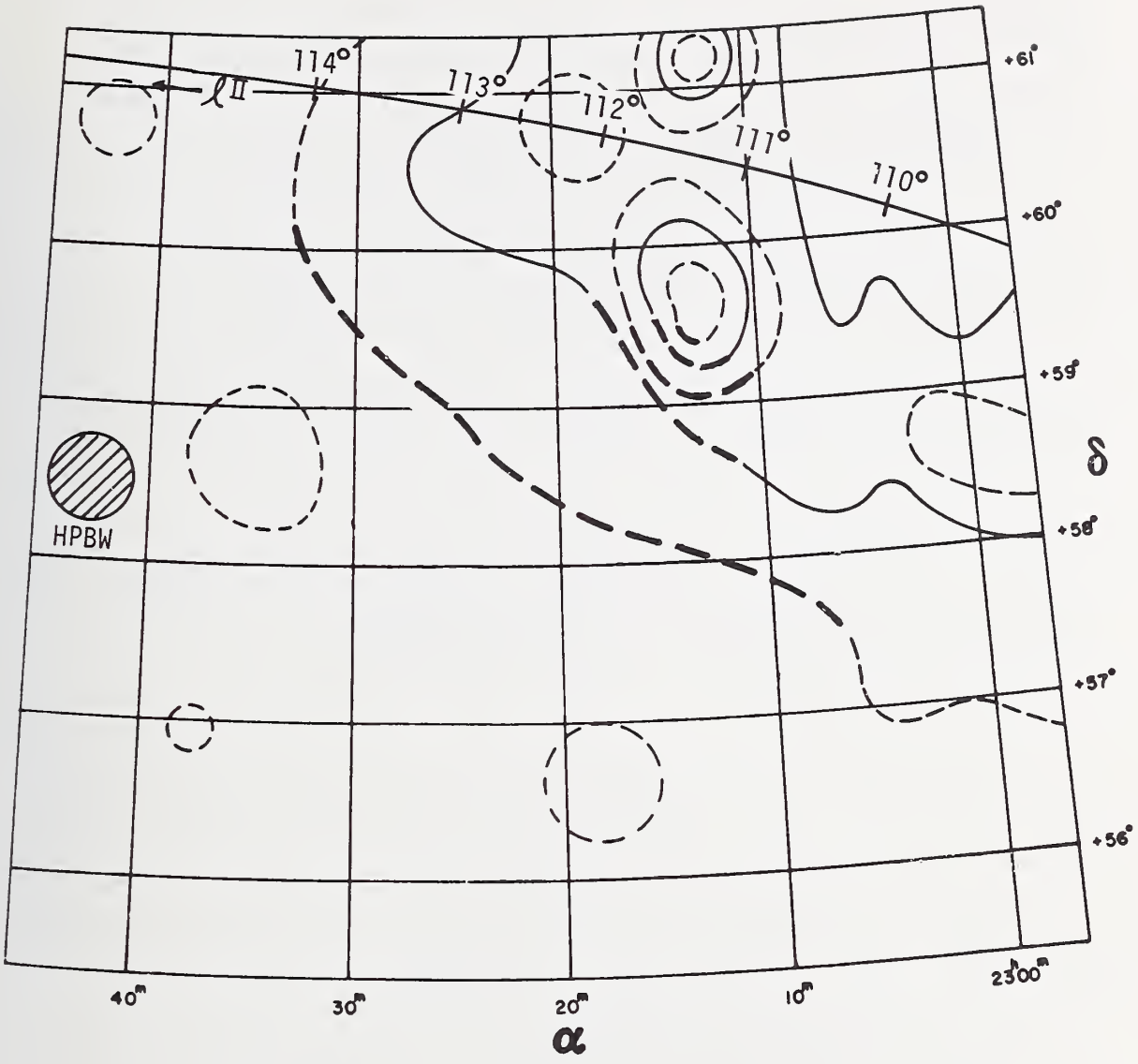

Figure 2-21. Hypothetical cosmic radio background at 1.4 GHz with effect of Cas A removed.

determine these contours has distorted the resulting picture of the HII radiation, and one is tempted to replace the maps with a (hopefully) "corrected" map that might look like figure 2-21. When this is done at 1.4 GHz, Cas A appears to be bathed in HII radiation approximately equal to 1.2 kelvins (1.5 x 0.8) above the 3 kelvin black-body level. Since the brightness for the HII regions is expected [6] to be flat above 1.4 GHz, this leads to a 0.04 kelvin (using eq. (2.8)) increase at 7.25 GHz. Thus, given the validity of the assumptions made in arriving at 0.04 kelvins, the HII background around Cas A at this frequency should cause negligible error (less than 0.01 dB) in the use of Cas A as a calibrating source.

In summary, it appears that there are many gaps in the literature concerning the cosmic background in general, and the background around Cas A in particular.

3. THE ATMOSPHERIC EFFECTS IN VIEWING CAS A

The problems associated with the effects of the atmosphere upon the flux from Cas A passing through it are varied and complex. Therefore, within the time allotted a penetrating review of the problems involved was not possible, and correspondingly the exposition given in this section will be brief and somewhat incomplete. However, with this first reading of the literature it was possible to delineate most, if not all of these problems. As will be seen, the usual problems concerning absorption by atmospheric constituents (O_2, H_2O, rain, fog, snow, etc.) emerge. In addition, problems associated with the distortion of the component of the flux falling on the receiving antenna aperture by the inhomogeneous refractive index of the earth's atmosphere also emerge. These latter problems are overlooked by most authors, and it is not clear which of the remaining few authors handle them correctly. The versions of refractive distortion presented here come from references [44] and [45].

Table 3-1 is a list of those mechanisms by which the atmosphere affects a flux passing through. They fall into two distinct categories: Attenuation of the flux by the atmospheric constituents and refractive distortion and addition of noise from the atmospheric constituents. The references included in table 3-1 are only a sampling of the papers read during this survey and don't necessarily represent the best possible sources of information concerning the effects they describe.

Table 3-1

Mechanisms	References
Attenuation:	
Apparent Source Solid Angle	44,45
Atmospheric Turbulence	
Diffusion	45
Aperture Perturbations	45
O_2 and H_2O	46,47,48
Clouds, fog, rain, snow, etc.	*
Enhancement:	
Refractive Index	
O_2 and H_2O Emission	
Emissions from clouds, fog, etc.	*

*It is practically impossible to make accurate measurements during periods of bad weather. Therefore, the corresponding literature, although accumulated, was not seriously reviewed.

According to the literature [44,45] the apparent solid angle subtended at the antenna by the radio source decreases with increasing zenith angle. The magnitude of this decrease depends upon what percentage of the antenna main beam is subtended by the radio star, being greatest for a point source and practically zero for an extended source of greater angular extent than the beam. For example, according to the literature the flux density S from an unpolarized "point" source appears to have a magnitude S_z when viewed by an antenna set at a zenith angle z, where

$$S_z = S\Omega_z/\Omega_s \qquad (3.1)$$

and where Ω_z is the apparent solid angle of the source viewed at zenith angle z, and Ω_s is the true source solid angle. The flux density S is thus seen to suffer a refractive attenuation of Ω_z/Ω_s.

Atmospheric turbulence causes an irregular variation in the atmospheric refractive index, which in turn causes rays from the radio star to diffuse and to reach the antenna aperture with phase and magnitude perturbations. The resulting diffusive attenuation is greatest for point sources.

The largest source of flux density attenuation at microwave frequencies is absorptive attenuation by molecular oxygen and water vapor. The magnitude of attenuation depends upon the temperature, pressure, and water vapor content of the atmosphere along the path traveled by the signal and is difficult to estimate accurately. An approximate expression for this attenuation is given by [47,48]

$$A(z) = (a_o \ell_o + \rho a_w \ell_w) \text{ Sec } z \text{ (dB)} \qquad (3.2)$$

where ℓ_o (4 km) and ℓ_w (2 km) are characteristic heights for the atmospheric oxygen and water vapor respectively, and where a_o and ρa_w are the frequency-dependent attenuation coefficients (dB/km) for molecular oxygen and water vapor respectively. For a standard atmosphere [49] with a water vapor content of ρ = 10 g/cm^3, the CCIR report [47] gives values of 0.011 dB/km and 0.00081 dB/km for a_o and ρa_w respectively at 6.4 GHz. It may be more accurate to measure this effect than to calculate it from eq. (3.2) [50].

The relative importance of these attenuation effects for large zenith angles can be seen in table 3-2, the values for which were derived from measurements at 6.4 GHz of Cas A and the moon [45] using a 22-meter antenna with a 10' half-power-beamwidth.

Table 3-2

Zenith Angle (Deg.)	Absorptive Atten (dB)	Diffusive Atten (dB)	Refractive Atten (dB)
60	0.1	0.1	0.0
75	0.19	0.17	0.02
86	0.47	0.31	0.19

The surprisingly large values of diffusive attenuation were obtained by comparing the attenuation of the flux from Cas A with that of the moon; they follow well the predicted frequency squared dependence of this type of attenuation when compared with measurements at 4 GHz.

Excluding bad weather, table 3-1 lists two mechanisms which enhance or add to the flux density: the refractive index change from unity at the upper "edge" of the atmosphere to n at the earth's surface [44]; and emissivity from atmospheric O_2 and H_2O. When expressed in terms of the change in the source's brightness temperature, this refractive index change yields

$$\Delta T_B = (n^2-1)T_B \tag{3.3}$$

where ΔT_B represents an apparent increase in the brightness temperature, and n represents the refractive index of the atmosphere at the earth's surface. A value of 1.0004 for n gives a relative increase ΔT_B of 0.003 dB.

The increase in the apparent brightness temperature of the flux density due to atmospheric emissivity can be approximated by

$$\Delta T_B = 0.23\ A\ T_{ma} \tag{3.4}$$

where ΔT_B represents the apparent increase, A is the attenuation (dB) given by eq. (3.2), and T_{ma} is the mean temperature of the troposphere [49]. Equation (3.4) gives a relative increase of 0.09 dB in the Cas A zenith brightness temperature at 6.4 GHz. Some of the literature indicates that this ΔT_B may be more accurately measured [50] than calculated from eq. (3.4). Accurate versions [46] of eqs. (3.2) and (3.4) involve a ray-path integration of the attenuation coefficient, taking into account the atmospheric variables along this path. A more penetrating review of this important aspect of the problem was not possible in the time allotted.

4. THE MEASUREMENT OF POWER GAIN OF A LARGE GROUND ANTENNA FOR CALIBRATING COSMIC RADIO STARS

4.1 Introduction

The strongest radio stars, Cas A, Cyg A, and Tau A have received much attention because of their intensity in the calibration of large antennas. One of radio astronomy's most important and difficult problems is to determine by use of well calibrated antennas the precise, absolute values of the flux densities from these stars. Therefore, the purpose of this chapter is to discuss the measurement of the power gain of large ground-based antennas to be used in calibrating radio stars.

The power gain of a standard horn antenna was calculated theoretically by Schelhunoff [51] and Slayton [52]. The theory has usually been applied satisfactorily to a relatively small standard horn antenna of fairly low-power gain. If a low-gain, standard horn antenna is used in the calibration, then the signal-to-noise ratio associated with the measurement is poor, and the horn's angular resolution is low; this results in confusion between adjacent radio sources. Moreover, the accounting for the effects of the horn's mechanical imperfections is very difficult, and the computation of its power gain is usually unsatisfactory.

The most common experimental method of determining antenna gain and polarization is a substitution technique, which includes the response of an antenna under test to an incident "plane-wave" field compared with that of one or more standard antennas. With conventional "far-field" antenna ranges, the plane-wave condition is attempted by using large separation distances between the transmitting and receiving sites.

But at large distances the errors due to ground reflections and scattering from other objects can be significant. Availability (in the substitution techniques when used in medium ranges) of reliable correction procedures for proximity and multiple reflections between a large antenna and the horn used to calibrate it would permit the use of medium antenna ranges and reduce ground reflections. Braun [53], Chu and Semplak [54], Tseytlin and Kinber [55], and others have computed proximity corrections for horns separated by medium distances. However, these computations involve approximations and idealizations which limit the accuracy of the corrections.

In the extrapolation method of gain calibration of the antenna [56-59] measurements are made at shorter distances and lower tower heights than the more traditional methods. In this method the measured variation in the received signal with distance is then used to correct for errors caused by both proximity and multiple reflections between antennas. The extrapolation method gives the best accuracy currently available for the power gain of an antenna. The extrapolation method has been implemented only for relatively small standard gain antennas primarily because of the physical limitations of the special extrapolation antenna ranges at NBS. Thus it is generally necessary to determine the power gain of a large ground antenna used to make an absolute flux density measurement from a gain comparison with a smaller standard gain horn antenna whose gain has been measured by the extrapolation method. This comparison can be made directly by observing with both antennas the radiation from a satellite.

In section 4.2, the calibration of a small standard gain antenna by the generalized three-antenna extrapolation method is discussed. An analysis of the errors in the generalized three-antenna extrapolation method for calibrating the small standard gain antenna is also given.

In section 4.3, the gain transfer from a standard gain antenna to a larger ground antenna is discussed. An analysis of the errors in this gain comparison method is also given.

4.2 Calibration of Standard Gain Antennas by Use of the Generalized Three-Antenna Extrapolation Technique

4.2.1 Introduction

The generalized three-antenna extrapolation method is applied to the calibration of standard gain antennas with power gains of 30 or 40 dB. This technique has the following advantages: (1) the measurements are made at shorter distances in order to eliminate ground reflections; and (2) it is possible to make accurate corrections for errors arising from both proximity and multiple reflections between antennas.

Section 4.2.2 describes the characterization of antennas in terms of the scattering matrix parameter. Then, this formulation is used in section 4.2.3 to develop a generalized three-antenna technique for obtaining the power gain and the polarization ratio. In this technique, no a priori quantitative information concerning the power gain and the polarization ratio of any of the three antennas is required. Although the generalized three-antenna method can be used at the conventional far-field distances, for large antennas more accurate values can be obtained by the extrapolation method.

Section 4.2.4 briefly describes the extrapolation method, which is based on the antenna scattering theory and detailed mathematical constraints upon the functional relations involved in the antenna-antenna interaction. The accuracy consideration for the power gain of the standard gain antenna is given last in section 4.2.5.

4.2.2 Antenna Scattering Matrix Analysis

The extrapolation method is based upon the plane-wave scattering matrix analysis developed by Kerns [60-62], and is covered in detail in his publications [56-59]. Therefore, this analysis is only briefly discussed to clarify the basic approach to the reader who may not be familiar with it.

Consider the antenna shown schematically on figure 4-1, oriented in the coordinate system Oxyz, and let $\underline{k}$ be the propagation vectors for plane-waves in the space surrounding the antenna. The X, Y, and Z directions are fixed in space and with respect to the antenna. We choose a terminal surface S_o in the waveguide feed and define a supplementary surface S_a, such that $S_a + S_o$ forms a closed surface enclosing the source or detector associated with the antenna (fig. 4-1).

For simplicity we assume that only one mode need be considered in the vicinity of S_o. This is also the most common use in practice. The formulation for multimode feeds is discussed elsewhere [63]. It is convenient to denote the combined x and y components of the propagation vectors $\underline{k}$ by $\underline{K}$, so that $\underline{K} = K_x\underline{e}_x + K_y\underline{e}_y$ where $\underline{e}_x$, $\underline{e}_y$, and $\underline{e}_z$ are unit vectors. In order to set up representations for the antenna scattering matrix, it is assumed that a set of outgoing wave amplitudes b_o and $b_m(\underline{K})$ in figure 4-1 is determined by a set of incident wave amplitudes, a_o and $a_m(\underline{K})$ as shown in figure 4-1, where a_o and b_o are the incident and emergent wave

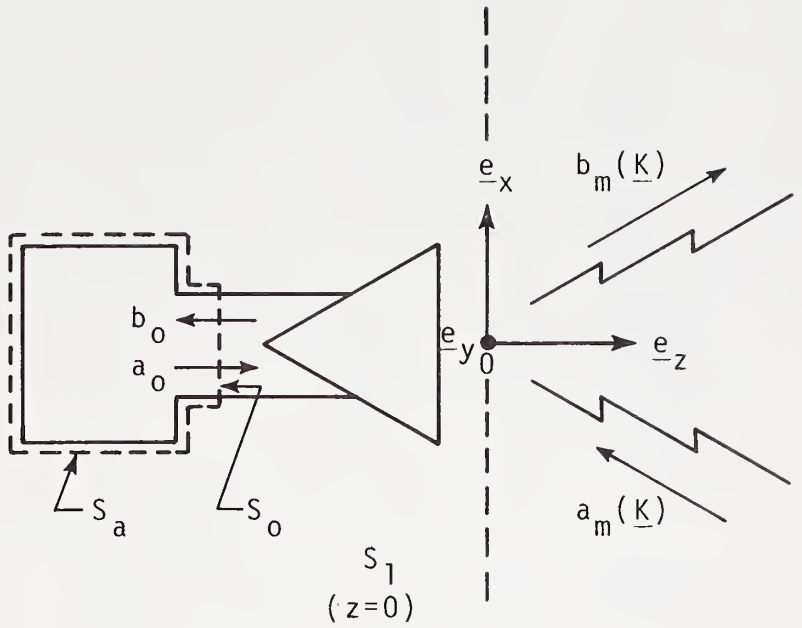

Figure 4-1 Antenna in the measurement coordinate system

amplitudes at the surface S_o, and $a_m(\underline{K})$ and $b_m(\underline{K})$ are spectral density functions for incoming and outgoing plane waves in the $\underline{K}$ space. The index m in $a_m(\underline{K})$ and $b_m(\underline{K})$ assumes the value 1 and 2 corresponding to the two orthogonal polarizations, $\underline{\kappa}_1$ and $\underline{\kappa}_2$ of the wave component in the XY plane, where $\underline{\kappa}_1 = \frac{\underline{K}}{K}$ and $\underline{\kappa}_2 = \underline{e}_z \times \underline{\kappa}_1$. The plane wave antenna scattering matix is now defined by

$$b_o = S_{00}a_o + \int \sum_{m=1,2} S_{01}(m,\underline{K})a_m(\underline{K})\,d\underline{K} \qquad (4.1)$$

$$b_m(\underline{K}) = S_{10}(m,\underline{K})a_o + \int \sum_{n=1,2} S_{11}(m,\underline{K};n,\underline{L})a_n(\underline{L})\,d\underline{L}, \qquad (4.2)$$

where the antenna characteristics are embodied in the four scattering parameters S_{00}, $S_{01}(m,\underline{K})$, $S_{10}(m,\underline{K})$ and $S_{11}(m,\underline{K};n,\underline{L})$, which are respectively the input reflection coefficient, and the receiving, transmitting and scattering characteristics. n and $\underline{L}$ play the same role as m and $\underline{K}$. This equation is derived on the assumption that the antenna system is a passive linear system, where the relation between the set of outgoing wave amplitudes and the set of incident amplitudes is linear.

If the antenna is reciprocal, then the receiving characteristic $S_{01}(m,\underline{K})$ is related to the transmitting characteristic $S_{10}(m,\underline{K})$ by the reciprocity relation [60]

$$-\eta_o S_{01}(m,\underline{K}) = \eta_m(\underline{K})S_{10}(m,-\underline{K}), \qquad (4.3)$$

where $\eta_1 = \omega\varepsilon/\gamma$ and $\eta_2 = \gamma/\omega\mu$ are the wave admittances associated with the polarizations $\underline{\kappa}_1$ and $\underline{\kappa}_2$ respectively, η_o is the wave admittance for the waveguide mode involved, ε and μ represent the permittivity and permeability of the medium, $\gamma = (k^2-K^2)^{\frac{1}{2}}$, and $k^2 = \omega^2\mu\varepsilon$.

Antenna power gain and antenna effective area are very useful basic quantities that are here expressed in terms of $S_{10}(m,\underline{K})$ and $S_{01}(m,\underline{K})$ respectively of the antenna scattering matrix. In accord with IEEE Definitions of Terms for Antennas (1973) [2], the power (for a transmitting) gain is defined by

$$G(\underline{K}) = \frac{\text{Power radiated per steradian as a function of direction}}{\text{net power into antenna}/(4\pi)}. \quad (4.4)$$

It will follow that in terms of antenna scattering matrix parameters, the power gain is given by

$$G(\underline{K}) = \frac{4\pi Y_o k^2 [|S_{10}(1,\underline{K})|^2 + |S_{10}(2,\underline{K})\gamma/k|^2]}{\eta_o(1-|S_{00}|^2)}, \quad (4.5)$$

where Y_o is the value of $\sqrt{\varepsilon/\mu}$ for the ambient medium. It should be noted that the power gain is a characteristic of the antenna under consideration and is independent of the source used to excite the antenna; also that the value of the power gain is independent of the insertion or adjustment of a lossless tuner in the feed waveguide, whether or not this tuner is counted as a part of the antenna.

For an antenna functioning in a receiving mode, the counterpart of the power gain is the effective area, A_e. In accordance with IEEE Standard Definitions of Terms for Antenna (1973) [2], the effective area is defined by

$$A_e(\underline{K}) = \frac{\text{The power available at the terminals of a receiving antenna}}{\text{The power per unit area of a plane wave incident on the antenna from a given direction which is polarized coincident with the polarization that the antenna would radiate, and which gives rise to the power available at the terminals.}} \quad (4.6)$$

Then in terms of plane-wave scattering matrix parameters, the effective area is given by

$$A_e(\underline{K}) = \frac{4\pi^2\eta_o[|S_{01}(1,\underline{K})\gamma/k|^2 + |S_{01}(2,\underline{K})|^2]}{Y_o(1-|S_{00}|^2)}. \quad (4.7)$$

For a reciprocal antenna, the power gain and effective area functions satisfy the well-known relation

$$A_e(\underline{K}) = \frac{\lambda^2}{4\pi} G(-\underline{K}). \quad (4.8)$$

The far-field characteristics, i.e., the power gain, the effective area, the polarization ratio, etc., of an antenna can be determined from $S_{10}(\underline{K}) = S_{10}(1,\underline{K})\underline{\kappa}_1 + S_{10}(2,\underline{K})\underline{\kappa}_2$. The purpose of the extrapolation technique is, therefore, to determine $S_{10}(\underline{K})$.

4.2.3 Generalized Three Antenna Measurement Technique

There are a variety of measurement techniques that take full account of polarization characteristics and that do not necessarily require reciprocal antennas; namely 1) one-unknown (and one standard) antenna; 2) generalized two identical unknown antennas [56]; and 3) generalized three (unknown) antenna measurement techniques [58,59]. Of all antenna measurement methods, the generalized three-antenna measurement technique requires a minimum of *a priori* information about the antennas involved in the measurements. In addition it is the method chosen for treatment in this report because it yields the best accuracy.

In this discussion of the generalized three-antenna technique, for convenience reciprocity is postulated for all three antennas. There is a further generalization of the theory to a four-antenna measurement technique [63] in which

no antenna need satisfy a reciprocity or similar known constraint. The antenna coordinate system is defined with its Z axis in the electromagnetic boresight direction, and with the X and Y axes referred to arbitrary marks on the antenna structure as shown in figure 4-1.

With the above choice of references axes, let antenna number 1 be placed at the origin and used as the transmitting antenna. Let one of the other antennas, number two, be placed in a receiving orientation, i.e., located at Z = d and pointing in the $-\underline{e}_z$ direction. The two antennas are shown schematically in figure 4-2 with appropriate terminal surfaces and wave amplitudes shown. The coupling equation which relates the received wave amplitude b_o' to the wave amplitude a_o in terms of the transmitting characteristic is given by [58],

$$b_o'(d) = \frac{a_o}{1 - \Gamma_\ell \Gamma_2} \int_{\underline{K}} \sum_m {}^2S_{01}'(m,\underline{K}) \cdot {}^1S_{10}(m,\underline{K}) \exp(i\gamma d)\, d\underline{K}, \quad (4.9)$$

where ${}^2S_{01}'(m,\underline{K})$ is the receiving characteristic for antenna 2 in the receiving orientation; ${}^1S_{10}(m,\underline{K})$ is the transmission characteristic of antenna 1 in the transmitting orientation; and Γ_2 and Γ_ℓ are the reflection coefficients as shown in figure 4-2. Equation (4.9) neglects the multiple reflections between antennas.

We consider only the on-axis values ($\underline{K}=\underline{0}$ and $k=\gamma$) of the antenna characteristics and refer to these quantities as the antenna characteristics. The linear and circular components of $S_{10}(\underline{0})$ are referred to as X, Y, R and L. For example

$$S_{10}(\underline{0}) = X\underline{v}_y + Y\underline{v}_y = R\underline{v}^+ + L\underline{v}^-, \quad (4.10)$$

where $\underline{v}_x$ and $\underline{v}_y$ are unit basis vectors for linear polarizations, $\underline{v}^+$ and $\underline{v}^-$ are the unit basis vectors for right and

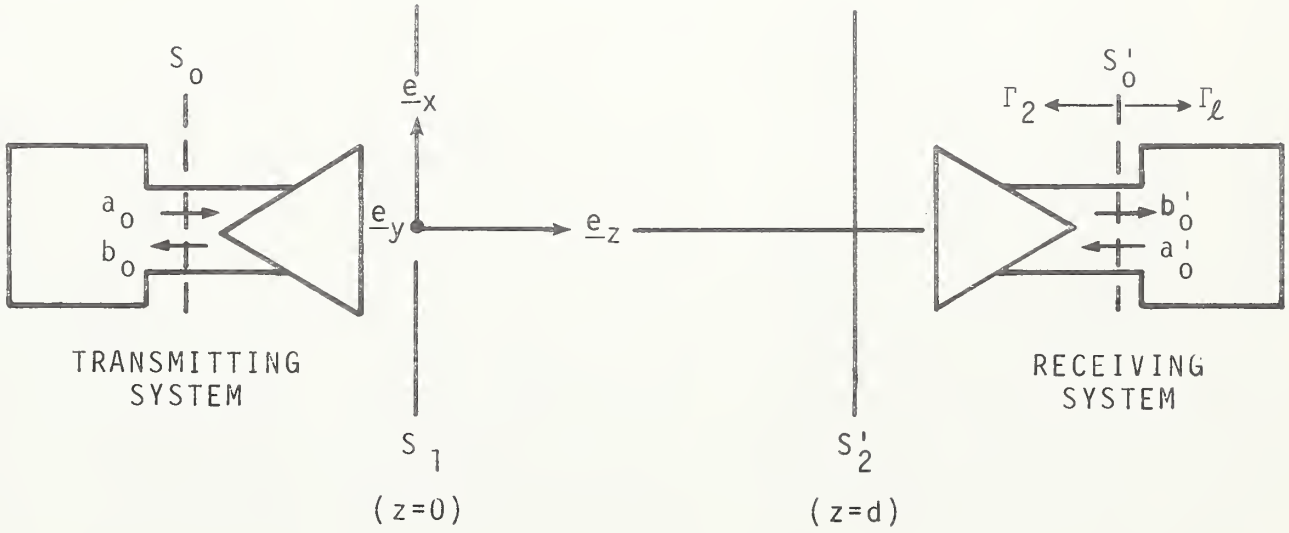

Figure 4-2 Schematic of two antennas oriented for measurement

left circular polarization. $\underline{v}^+$ and $\underline{v}^-$ are defined as

$$\underline{v}^+ = \frac{\underline{v}_x + i\,\underline{v}_y}{\sqrt{2}}, \quad \underline{v}^- = \frac{\underline{v}_x - i\,\underline{v}_y}{\sqrt{2}}, \tag{4.11}$$
$$\tag{4.12}$$

where the time dependence is assumed to be $\exp(-i\omega t)$. Then the transformation equations between X, Y, R and L are given by

$$R = \frac{X - iY}{\sqrt{2}}, \qquad \frac{X + iY}{\sqrt{2}} . \tag{4.13}$$
$$\tag{4.14}$$

Using this simplified notation for $S_{10}(\underline{0})$ and the reciprocity relations given in eq. (4.3) by which the change in ${}^2S_{01}(\underline{0})$ due to reorienting antenna 2 is expressed in terms of ${}^2S_{10}(\underline{0})$, the asymptotic value of eq. (4.9) for large d is

$$b_o'(d) \sim \frac{2\pi i k a_o \exp(ikd)}{(1-\Gamma_\ell\Gamma_2)d}\,[X_1X_2 - Y_1Y_2], \tag{4.15}$$

where subscripts 1 and 2 on X and Y referred to the X and Y components of $S_{10}(\underline{0})$ for antenna 1 and antenna 2 respectively. Equation (4.15) can be rewritten as

$$X_1X_2 - Y_1Y_2 = \lim_{d\to\infty}\left\{\frac{b_o'(d)\,d(1-\Gamma_\ell\Gamma_2)\exp(-ikd)}{a_o 2\pi i k}\right\} \equiv D_{12}' , \tag{4.16}$$

where $b_o'(d)$ is the output wave amplitude and D_{12}' is determinable from measurements as explained later. Now let the receiving antenna be further reoriented by rotating about the Z axis by 90° in the direction from X and Y; then eq. (4.16) becomes

$$X_1Y_2 + X_2Y_1 = \lim_{d\to\infty}\left\{\frac{b_o''(d)\,d(1-\Gamma_\ell\Gamma_2)\exp(-ikd)}{a_o 2\pi i k}\right\} \equiv D_{12}'', \tag{4.17}$$

where $b_o''(d)$ denotes the output wave amplitude for the second orientation, and D_{12}'' is determinable from measurements.

Equations similar to eq. (4.16) and eq. (4.17) can be written for the other two antenna pair combinations (i.e., antennas 1 and 3, and antennas 2 and 3) for a total of six complex equations in six complex unknown quantities. This is perfectly general even for asymmetrical antennas. These six equations may be expressed by the two general equations for transmission from antenna m to antenna n as

$$X_i X_j - Y_i Y_j = D'_{ij}, \qquad (4.18)$$

$$i,j = 1,2,3$$

and

$$X_i Y_j + X_j Y_i = D''_{ij}. \qquad (4.19)$$

To solve the resulting set of six complex equations we define

$$\Delta_{ij} = \frac{D'_{ij} - iD''_{ij}}{2}, \qquad (4.20)$$

and

$$\sum_{ij} = \frac{D'_{ij} + iD''_{ij}}{2}. \qquad (4.21)$$

Then eqs. (4.18) and (4.19) can be replaced by

$$R_i R_j = \Delta_{ij}, \qquad (4.22)$$

and

$$L_i L_j = \sum_{ij}. \qquad (4.23)$$

For example the solution for circular components gives

$$R_1 = \pm \left\{ \frac{\Delta_{21}\Delta_{13}}{\Delta_{32}} \right\}^{1/2}, \qquad (4.24)$$

and

$$L_1 = \pm \left(\frac{\Sigma_{21}\Sigma_{13}}{\Sigma_{32}} \right)^{1/2}, \tag{4.25}$$

where the double signs are mathematically uncorrelated. The X and Y linear polarization components corresponding to eqs. (4.24) and (4.25) are

$$X_1 = \pm \frac{1}{\sqrt{2}} \left(\sqrt{\frac{\Delta_{21}\Delta_{13}}{\Delta_{32}}} \pm \sqrt{\frac{\Sigma_{21}\Sigma_{13}}{\Sigma_{32}}} \right), \tag{4.26}$$

and

$$Y_1 = \pm \frac{i}{\sqrt{2}} \left(\sqrt{\frac{\Delta_{21}\Delta_{13}}{\Delta_{32}}} \mp \sqrt{\frac{\Sigma_{21}\Sigma_{13}}{\Sigma_{32}}} \right), \tag{4.27}$$

where the signs are correlated vertically but not horizontally. Which solution-pair pertains to a given measurement cannot be determined from the equations above. With regard to the more significant double signs within the brackets, it is easily seen that, if one choice yields $|Y|^2 < |X|^2$, then the other will yield $|Y|^2 > |X|^2$. Thus, if it is known that one or the other of the inequalities holds, one simply takes the solution yielding the known inequality.

It should be noted that a variety of singular cases arise if one or more of the three unknown antennas is nearly circularly polarized. For example if antenna 3 has a nearly left-circular polarization, then both Δ_{13} and Δ_{23} are nearly zero. R_1 and R_2 are, therefore, indeterminate, but R_3 and all the left components may be obtained if the other two antennas are not circularly polarized. The most common combinations occurring in practice are, therefore, either three linearly polarized antennas or two linear and one

circularly polarized antenna. In the first case the gains and polarizations are determined for all three, while in the latter, the characteristics of only the circular antenna will be completely determined.

Finally, using eqs. (4.5) and (4.10) the power gain and polarization in the boresight direction ($\underline{K}=\underline{0}$) are unambiguously determined in terms of the linear or circular components of $S_{10}(\underline{0})$.

The power gain:

$$G(\underline{0}) = \frac{4\pi Y_o k^2(|X|^2+|Y|^2)}{\eta_o(1-|S_{00}|^2)},$$

or

$$G(\underline{0}) = \frac{4\pi Y_o k^2(|L|^2+|R|^2)}{\eta_o(1-|S_{00}|^2)}. \tag{4.28}$$

The complex linear polarization factor is

$$P_\ell = \frac{Y}{X}. \tag{4.29}$$

The complex circular polarization factor is

$$P_c = \frac{R}{L}. \tag{4.30}$$

The axial ratio is

$$A = \frac{|R| + |L|}{|R| - |L|}. \tag{4.31}$$

The tilt angle is

$$\tau = \frac{1}{2}\arg(P_\ell). \tag{4.32}$$

4.2.4 Extrapolation Technique

The data required to determine D_{ij} in eqs. (4.16) and (4.19) are the asymptotic values of $b_o'(d)\cdot d/a_o$ for large

d with the frequency and the necessary reflection coefficients. D_{ij} may be evaluated experimentally in at least three ways.

1) Conventional far field measurement method.
2) Near-field scanning technique [56], [57], [61].
3) Extrapolation method [58], [59], [64].

To avoid the error due to ground reflections and to make accurate corrections to reduce errors arising from both proximity and multiple reflections between antennas, the extrapolation measurement approach is employed to determine D_{ij}. The extrapolation technique requires the measurement of $b_o'(d) \cdot d/a_o$ as a function of antenna separation distance d. For any two essentially arbitrary antennas, the received signal can be accurately expressed as a formal series representation given by Wacker [64]. For the antenna pair 1, 2 considered earlier with $\underline{K} = 0$

$$\frac{b_o'(d)}{a_o} = \frac{1}{1 - \Gamma_2\Gamma_\ell} \sum_{p=0}^{\infty} \frac{\exp[i(2p+1)kd]}{(d)^{2p+1}} \sum_{q=0}^{\infty} \frac{A_{pq}}{d^q}$$

$$= \frac{1}{1 - \Gamma_2\Gamma_\ell} \left\{ \frac{\exp ikd}{d} \left(A_{00} + \frac{A_{01}}{d} + \cdots \right) \right.$$

$$+ \frac{\exp 3ikd}{d^3} \left(A_{10} + \frac{A_{11}}{d} + \cdots \right)$$

$$\left. + \frac{\exp 5ikd}{d^5} \left(A_{20} + \cdots \right) + \cdots \right\}, \quad (4.33)$$

where the A's are complex coefficients. It is clearly shown that eq. (4.33) includes both proximity effects (in the series in $\frac{A_{pq}}{d^q}$) and multiple reflection effects (in the exponential series) without approximation. For example, the first series represents the directly transmitted wave; the second

series the first order multiple reflection between two antennas, and the third, fourth, etc., series the higher order multiple reflections. In the proper application of this technique, the antennas are sufficiently close and high enough off the ground that ground reflections are negligible; eq. (4.33) includes no terms due to such reflections.

It can be seen from eqs. (4.16) and (4.33) that

$$D'_{ij} = \frac{A_{00}}{2\pi ik}. \tag{4.34}$$

Thus the determination of the leading coefficient in eq. (4.33) is the immediate measurement objective.

The basic idea of conventional far-field techniques is to have d large enough so that other terms in eq. (4.33) are negligible compared to the leading term, A_{00}, in the series. This requires very large ranges for some antennas and even at $d = 64 \frac{D^2}{2\lambda}$, where D is the major aperture dimension of the antenna, the proximity correction for a common type of standard gain horn is still approximately 0.05 dB. Moreover, as the distance is increased, the error due to ground reflection tends to increase.

In the extrapolation technique, measurements are made as a function of separation distance, and the plotted data points are curve fitted with as many terms of eq. (4.33) as may be significant. When all significant terms are included, A_{00} will be determined more accurately than when the higher terms are ignored. The power gain, the effective area, the polarization ratio, etc., will be, therefore, determined with more accuracy when this value of A_{00} is used.

4.2.5 Accuracy Consideration

The general character of the averaged extrapolation data fitted with 4-term polynominals is shown in figure 4-3, where the abscissa is expressed in terms of the

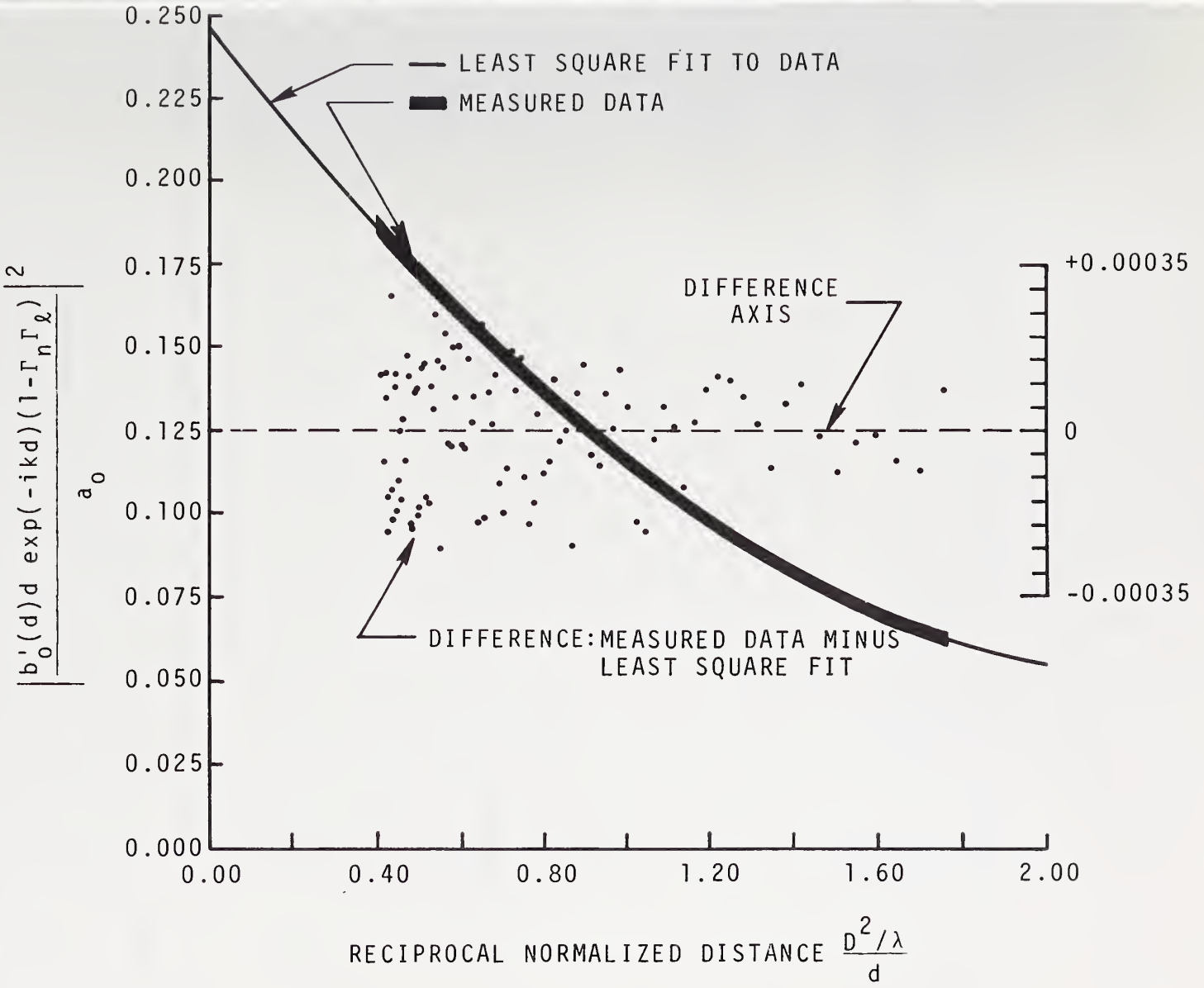

Figure 4-3 Measured data, 5-term polnominal fit, and residual for x-band standard horn (frequency = 7.25 GHz, antenna power gain 23 dB, major aperture dimension of antenna = 23.5 cm).

reciprocal normalized distance $\frac{D^2/\lambda}{d}$, and the ordinate is expressed in terms of the power ratio:

$$\left|\frac{b_o'(d)d\ \exp(-ikd)(1-\Gamma_n\Gamma_\ell)}{a_o}\right|^2 .$$

The difference between the measured and fitted waves is also shown as the point plot in figure 4-3, where one point corresponds to each data point. These differences are amplified by 500 in this figure.

The errors which have the largest effect are those which vary with distance because the extrapolation process can amplify the effect of small errors in the data to significant errors in A_{00}. Those errors are due to receiver nonlinearity, atmospheric loss uncertainty, range misalignment and distance uncertainty. The analysis of the errors in the measurement of the power gain of standard gain antennas is performed using a computer program basically developed by the Fields and Antennas Section of the Electromagnetics Division, NBS, and is discussed below in detail.

A. Error in Mismatch Factors

As stated earlier, the power gain of an antenna is a characteristic of the antenna under consideration, and is independent of the source used to excite the antenna. Therefore a lossless tuner in the feed waveguide, whether or not the tuner is counted as a part of the antenna, will not change its power gain. However, mismatch error is involved in the measurement of b_o' and a_o. At NBS this mismatch factor is carefully taken into account by carefully measuring the amplitude and phase of the reflection coefficients of the antenna, the receiver and the generator using an automated network analyzer. If the amplitudes of the reflection coefficients of an antenna, a receiver, and a generator are about

0.05, and the amplitude and phase can be measured to within an accuracy of 10%, then the resulting error corresponds to about ± 0.006 dB uncertainty in the power gain of the antenna. In calculating total errors in section 4.2.6 to follow, it is assumed that when the amplitude and phase of the reflection coefficients of the antenna, receiver, and generator can be measured to within an accuracy of 10%, then the mismatch error contribution to the power gain of the antenna is around 0.006 dB.

B. Attenuator Error

There is a large difference in wave amplitude between b_o' and a_o. Therefore, an attenuator is used to reduce a_o to a level that the receiver can handle. Moreover, to avoid the possible nonlinearity error associated with the receiver, it may be desirable to further reduce the a_o signal level to the same level as b_o' by use of a calibrated precision attenuator. A precision attenuator can be calibrated to within an accuracy of 0.01 dB including the multiple reflections and mismatch error by the series substitution, dc substitution, modulated subcarrier, or i-f substitution technique [65]. In calculating errors in section 4.2.6 to follow, it is assumed that a 0.01 dB error in the precision attenuator causes 0.01 dB error in the power gain of the antenna.

C. Receiver Nonlinearity and Gain Instability

The linear response of a receiving system is determined by measuring the change in output signal resulting from a change in an input precision attenuator used to set various receiver input power levels. Thus, the receiver nonlinearity is determined by systematically varying the precision attenuator over a 10-12 dB range and recording the

corresponding receiver output values. The resulting calibration curve is then used to correct the measured data, if necessary. The error in the power gain of an antenna due to receiver nonlinearity and receiver gain instability is of the same nature and is shown in figure 4-4 as a function of the receiver nonlinearity and/or gain instability. If the gain instability of a receiving system is characterized as a random uncorrelated fluctuation phenomenon, the errors due to this source are then considered to be random and uncorrelated, and could be taken out by statistical averaging. In calculating errors in section 4.2.6 to follow, it is assumed that after suitable corrections, the receiver nonlinearity is about 0.002 dB per 1 dB, which contributes an error of about 0.03 dB to the power gain of the antenna.

D. Atmospheric Loss Uncertainty

Uncertainty in the atmospheric loss between a transmitting and a receiving antenna cause an error in the measured power gain of an antenna. This becomes particularly severe at millimeter wavelengths where the absorption of electromagnetic power is very large and is highly dependent on frequency. Typical atmospheric losses are shown in figure 4-5 as a function of frequency. Figure 4-6 shows the error due to uncertainty in atmospheric loss in the calibration of the power gain as a function of the uncertainty in atmospheric loss. In the 5 to 10 GHz frequency range the atmospheric loss is about 0.008 dB per kilometer. In calculating errors in section 4.2.6 to follow, its uncertainty is assumed to be 12.5%, i.e., 0.001 dB per kilometer for the analysis of the error estimates.

E. Range Misalignment

Means must be provided for accurately aligning the two antennas involved in a given measurement and for maintaining

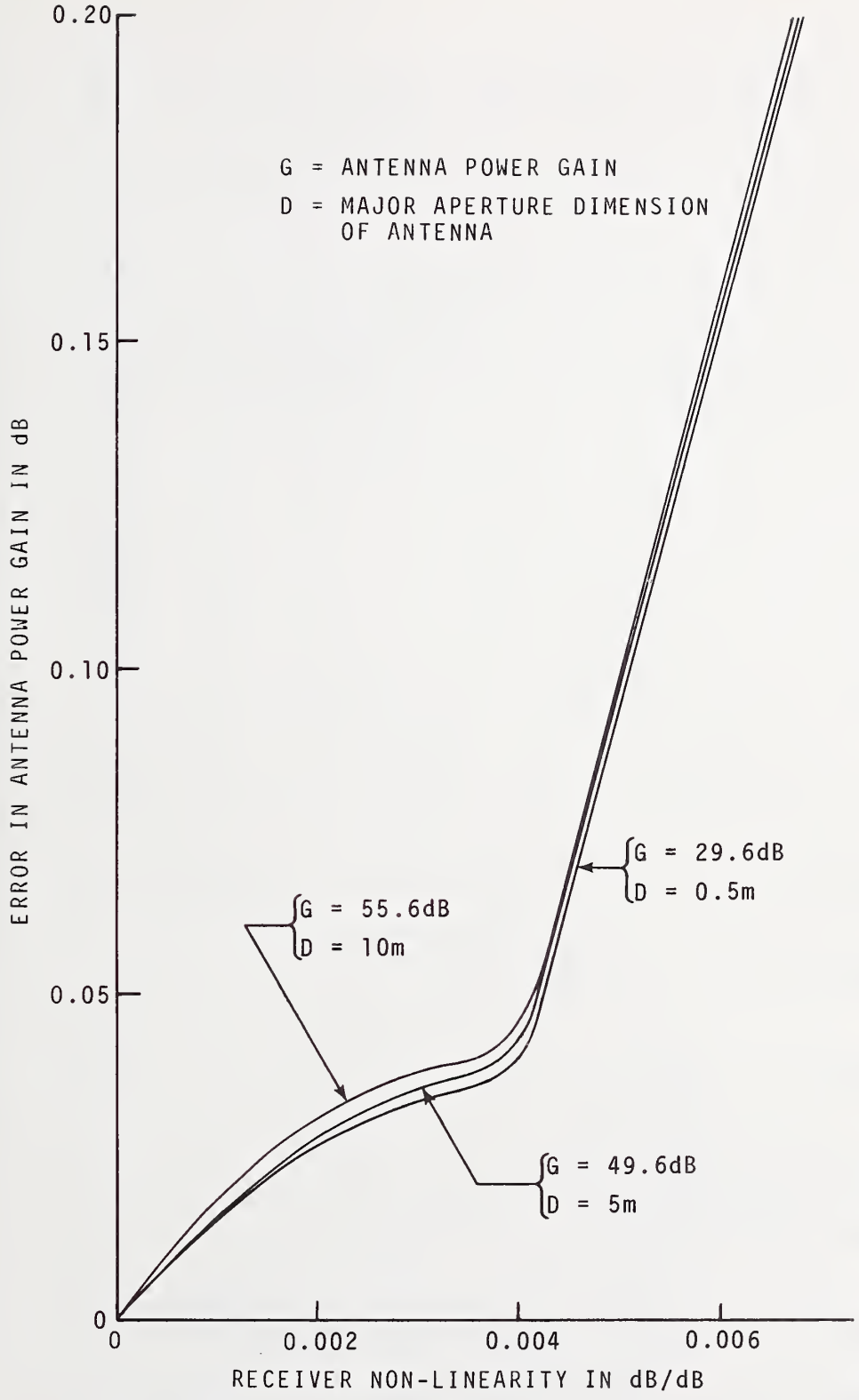

Figure 4-4 Error in the measured antenna power gain due to receiver non-linearity (Frequency = 7.25 GHz).

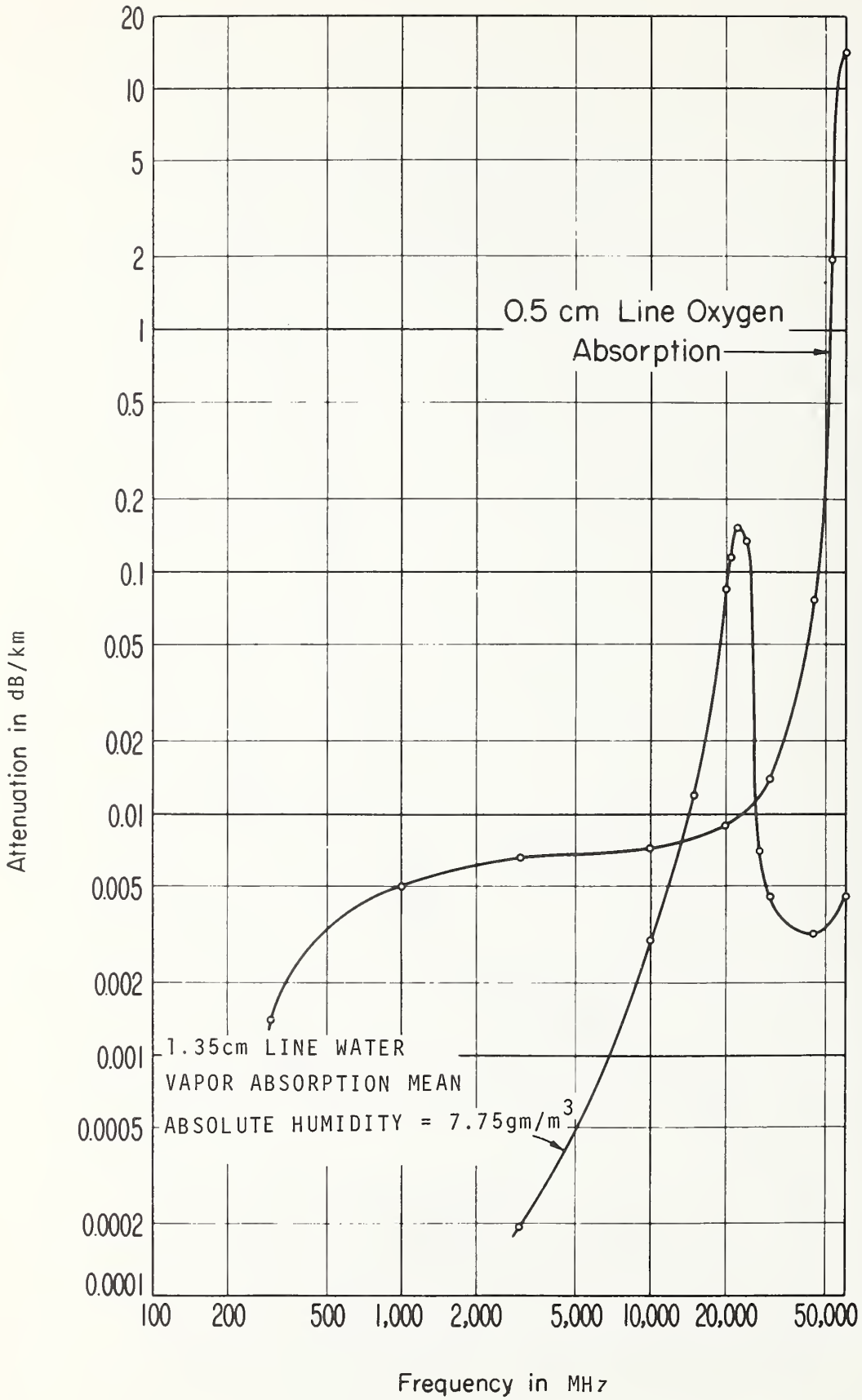

Figure 4-5 Atmospheric attenuation versus frequency (courtesy of Bean and Dutton)

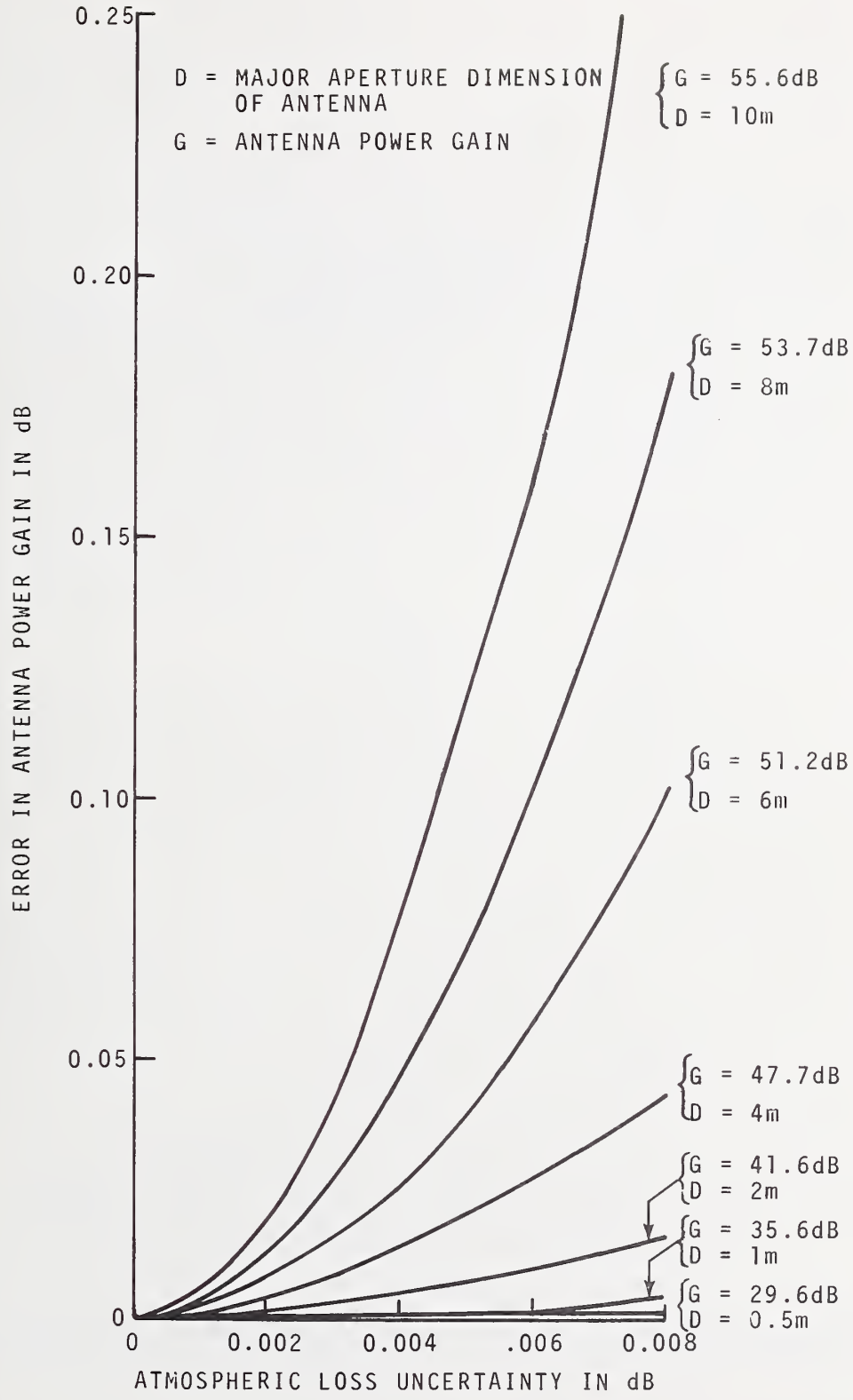

Figure 4-6 Error in the measured antenna power gain due to atmospheric loss uncertainty (Frequency = 7.25 Ghz).

this alignment as the separation distance is varied from almost zero to about one or two D^2/λ. Assuming that in the far-field the power gain can be very closely approximated by $G(\phi) = G_o \, \mathrm{sinc}^2(\frac{2.784\phi}{\theta_{hp}})$, where G_o is an on-axis power gain, θ_{hp} (half power beamwidth) = 70 λ/D, and ϕ is the misalignment angle, the error in the calibration of the power gain of the antenna due to range misalignment is shown in figure 4-7 as a function of maximum angular misalignment. Here it is postulated that the angular deviation is zero at the maximum separation distance (typically 2 $\frac{D^2}{\lambda}$) and is maximum at the minimum separation distance (typically 0.2 $\frac{D^2}{\lambda}$). In calculating errors in section 4.2.6 to follow, it is assumed that the maximum angular deviation is about 0.01 degree about any axis for the analysis of error estimates.

F. Distance Inaccuracy

The separation distance, d, between two antennas, or more specifically, between terminal surfaces S_1 and S_2' of figure 4-2 must be accurately measured. A laser interferometer is very convenient for this purpose. The separation distance can be measured to within 0.05%. The error in the measured power gain of an antenna due to the distance inaccuracy is shown in figure 4-8 as a function of that distance inaccuracy in percent. In calculating errors in section 4.2.6 to follow, it is assumed that the distance inaccuracy is about 0.05% for the final analysis of the error estimates.

4.2.6 Summary and Concluding Remarks

An estimate of the best total accuracy that one can expect for the calibration of the power gain of a standard gain antenna using the generalized three-antenna extrapolation

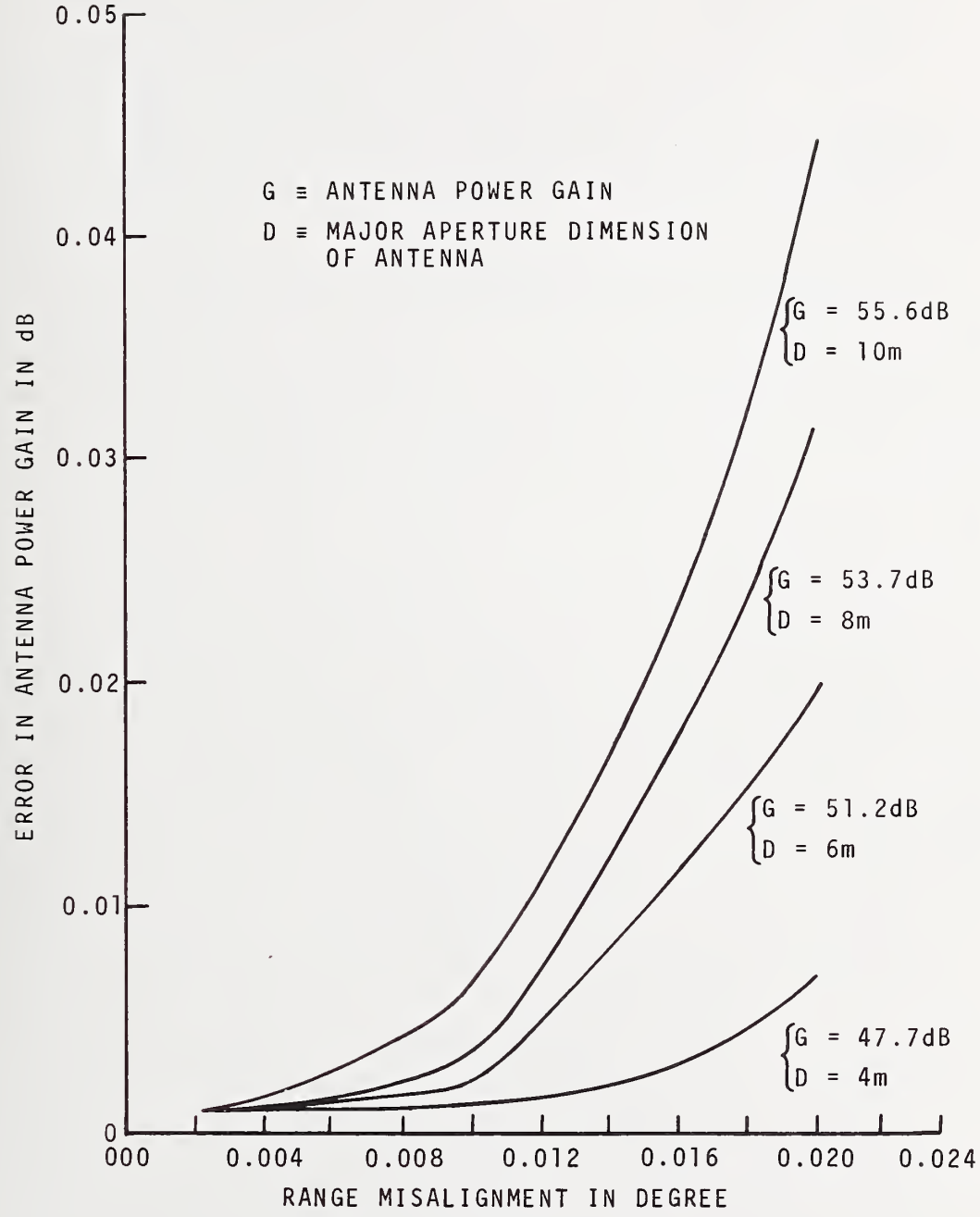

Figure 4-7 Error in the measured antenna power gain due to range misalignment (Frequency = 7.25 GHz).

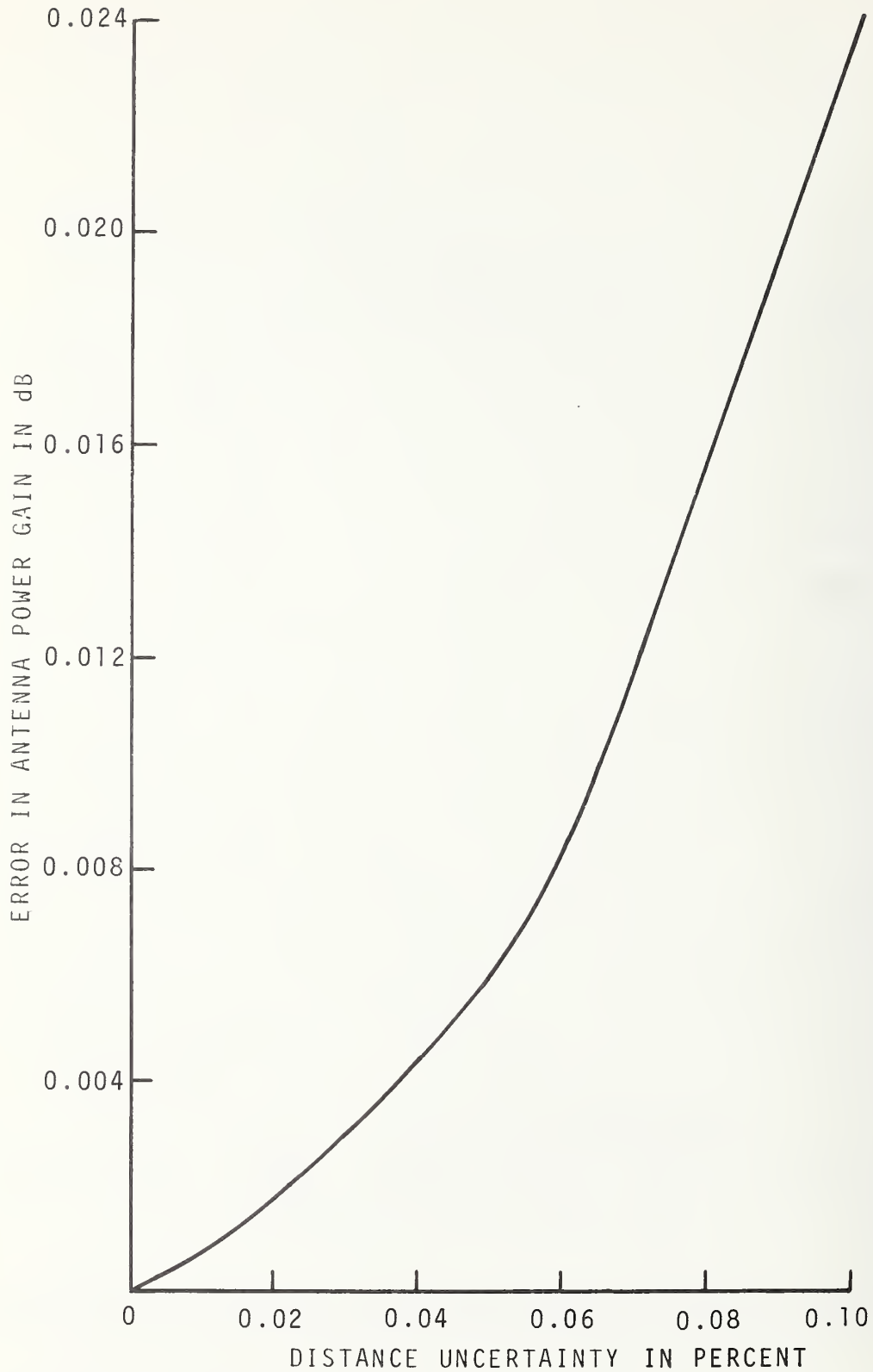

Figure 4-8 Error in the measured antenna power gain due to distance uncertainty (frequency = 5 to 10 GHz, antenna power gain = 20 to 50 dB, major aperture dimension of antenna = 0.5 to 10 m).

method is shown in figure 4-9 as a function of the major aperture dimension of the antenna. Figure 4-10 shows the accuracy of the power gain for a standard gain antenna as a function of the operating frequency. In these error estimates, the following assumptions are made:

1. Amplitude (< 0.05) and phase of the reflection coefficient are measured to within an accuracy of 10%.
2. An attenuator is calibrated with an accuracy of 0.01 dB.
3. Receiver nonlinearity is 0.002 dB per dB.
4. Uncertainty in the atmospheric loss is 0.001 dB per kilometer.
5. Maximum range misalignment is 0.01 degree about any axis.
6. Separation distance is measured to within 0.05%.
7. Random error contribution from all sources is 0.03 dB (3σ). This number is based on experience at NBS in very careful measurements, where much data was taken and then statistically processed.

The total errors shown in figures 4-9 and 4-10 were calculated using a linear addition of the various constituent errors, although some of the contributing sources of error are independent and therefore satisfy the condition for quadrature error addition. The errors due to an attenuator and the receiver linearity may not be independent and therefore may not satisfy the condition for quadrature error addition. The reason for this is that the receiver linearity is usually determined by use of an attenuator. However, other sources of errors, namely, the errors due to mismatch uncertainty, atmospheric loss uncertainty, range misalignment, and distance inaccuracy, are independent and do satisfy the condition for

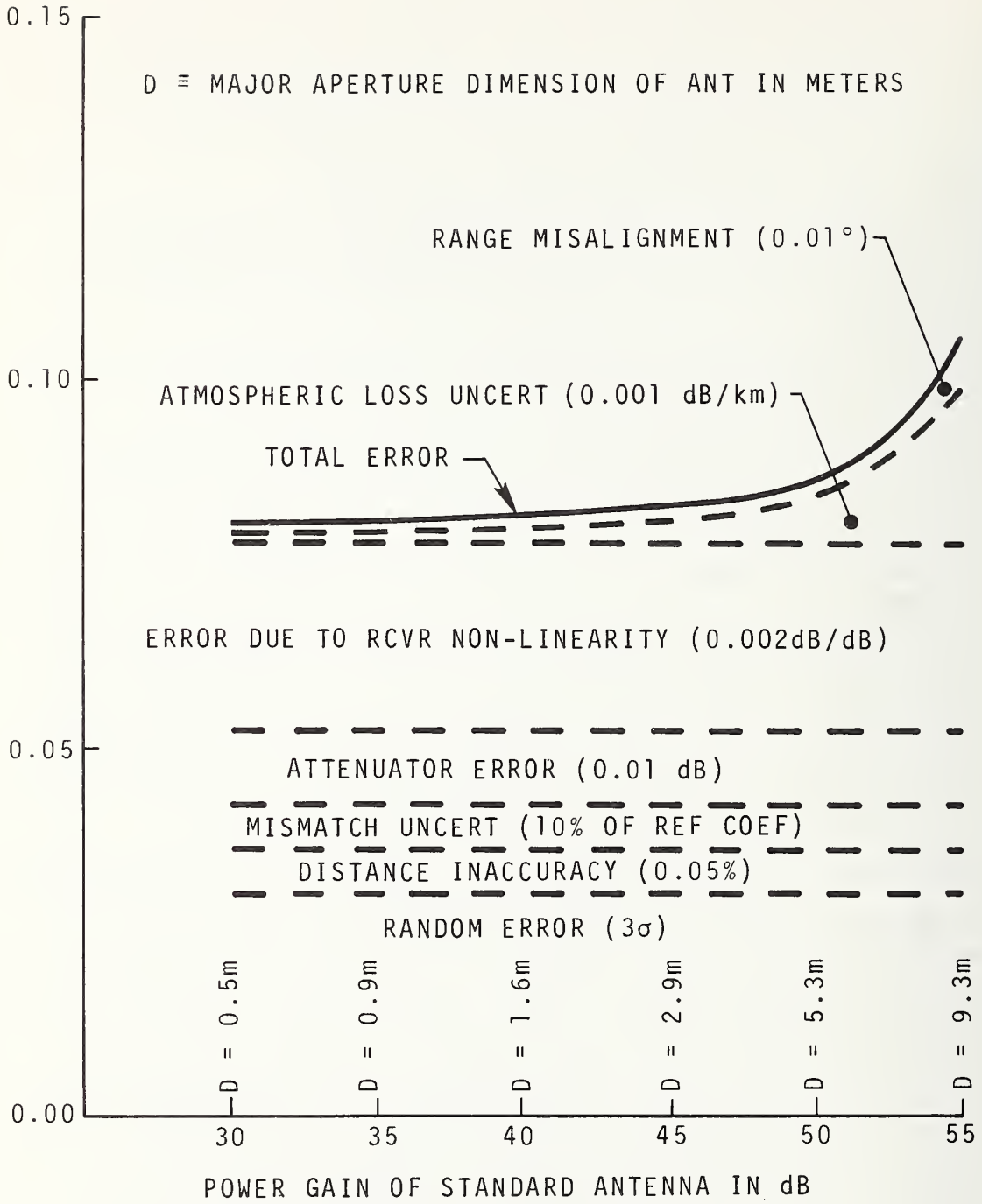

Figure 4-9 Accumulated error in the measured power gain of the generalized three-antenna extrapolation method (frequency = 7.25 GHz).

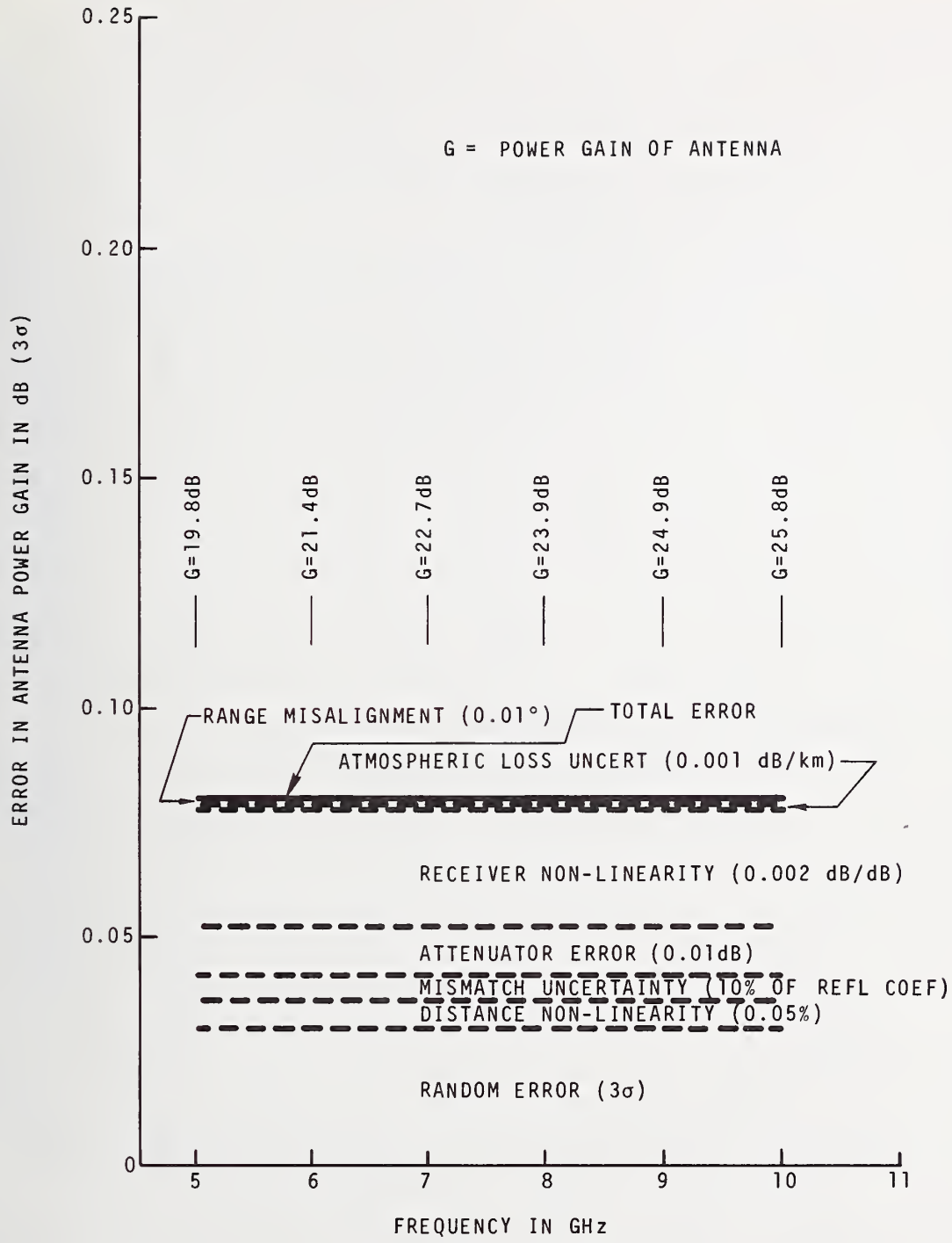

Figure 4-10. Linear error accumulation for the measured power gain of the standard antenna using the generalized three-antenna extrapolation method (major aperture dimension of antenna = 23.5 cm).

quadrature error addition. Under these assumptions, the limiting accuracy of the power gain of a standard gain horn antenna using the generalized three-antenna extrapolation method is shown in figure 4-11 as a function of the major aperture dimension of the antenna and in figure 4-12 as a function of operating frequency.

In conclusion, using the extrapolation technique, it seems possible to calibrate the power gain of a standard gain antenna, with a typical power gain of 40 dB and whose major aperture dimension is approximately 1.6 m, to within linear accumulation error of 0.08 dB for 3σ limits or a quadratic accumulation error of 0.04 dB for 3σ limits. The typical length of the extrapolation range required for the extrapolation measurements is approximately 120 m, and the separation distance (for D = 1.6 m and f = 7.25 GHz) is to be varied from typically $0.2\ \frac{D^2}{\lambda}$, that is 12 m, to $2\ \frac{D^2}{\lambda}$, that is 120 m. In principle, it is possible to calibrate the power gain of a larger standard gain antenna, say, with power gain of 50 dB whose major aperture dimension is approximately 5.3 m using this method. However in order to achieve the separation distances varying from 0.2 to $2\ \frac{D^2}{\lambda}$, the required length of an extrapolation range is approximately 1.4 km. In practice, it is very difficult to construct and maintain such a long extrapolation range with good stability and alignment. Therefore, it is generally necessary to calibrate the power gain of a relatively small standard gain antenna, typically with power gain of 40 dB and major aperture dimension of 1.6 m at 7.25 GHz by use of the extrapolation method, and then to determine the power gain of a larger ground antenna, typically with power gain of 60 dB and major aperture dimension of 16.6 m by a gain comparison technique which uses a radiation from a satellite as a common source. This gain comparison method is discussed in the next section.

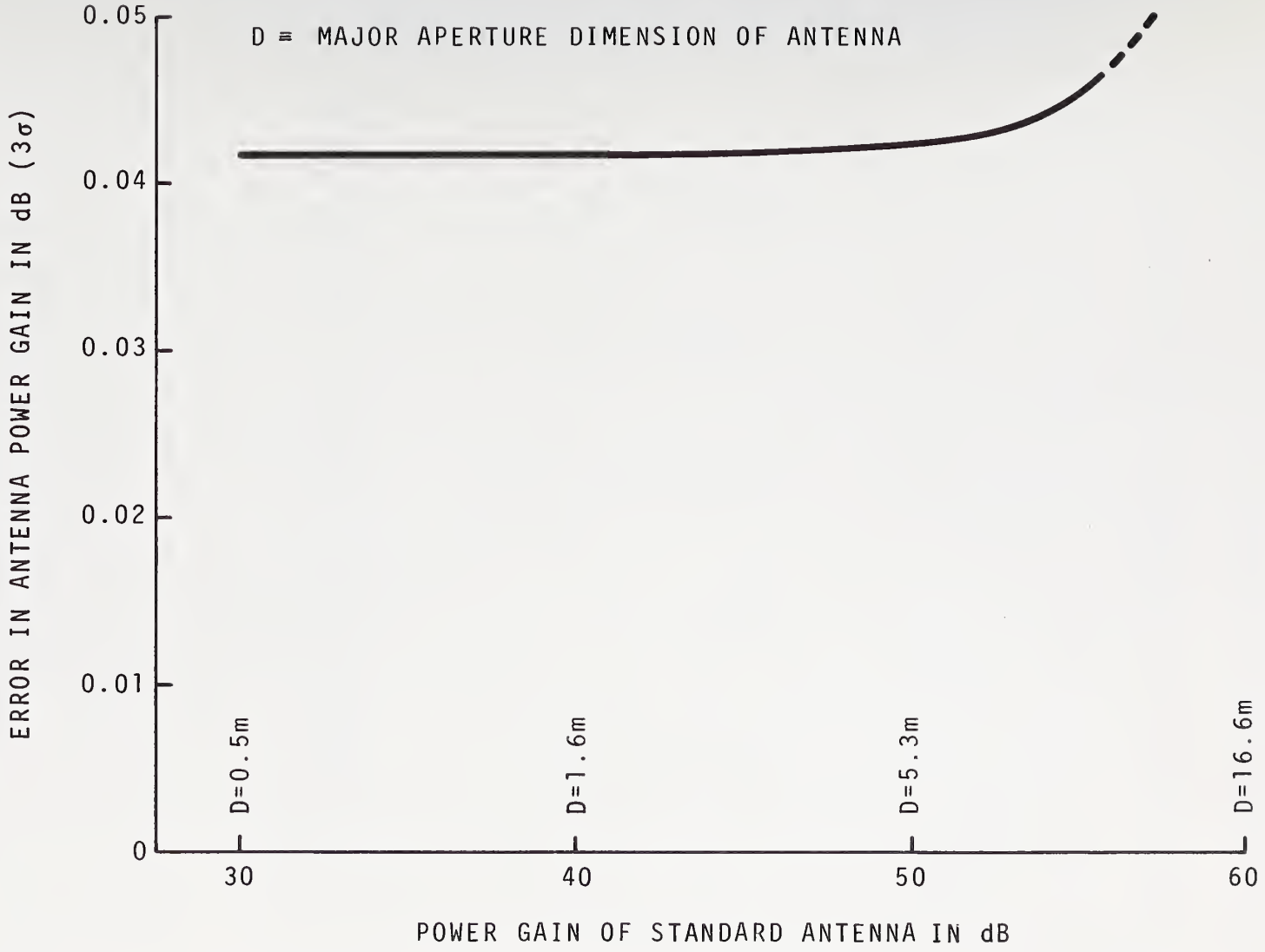

Figure 4-11 Quadrature error accumulation for the measured power gain of the standard antenna using the generalized three-antenna extrapolation method (Frequency = 7.25 GHz).

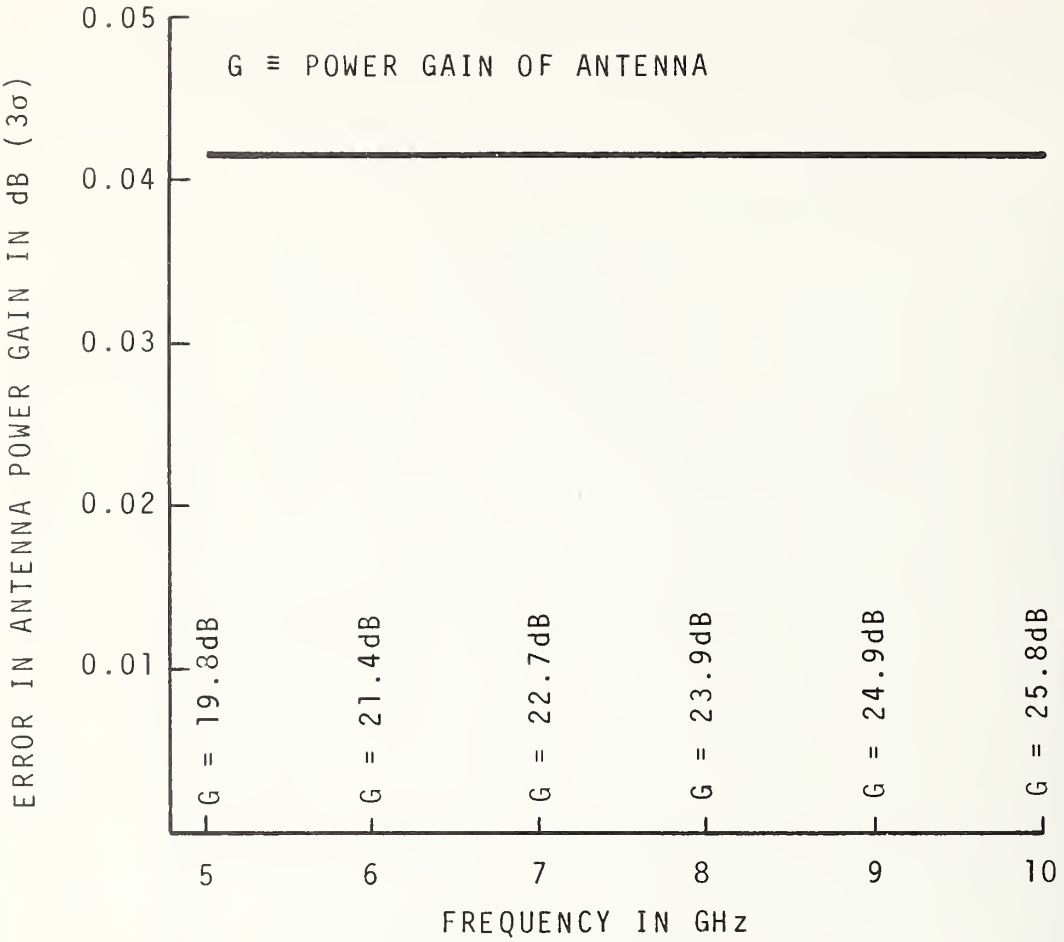

Figure 4-12 Quadrature error accumulation for the measured power gain of the standard antenna using the generalized three-antenna extrapolation method (major aperture dimension of antenna = 23.5 cm).

4.3 The Calibration of a Large Ground Antenna by the Gain Comparison Method

4.3.1 Introduction

Utilization of an accurately calibrated large ground antenna with 60 dB power gain is typically required for an accurate calibration of Cas A (see section 6). Unfortunately, accurate calibrations of large antennas are very difficult. There are various methods in common use which yield fairly accurate gain figures, but which may require elaborate technical preparation. Some of these methods are: gain comparison, pattern measurements and subsequent integration, extrapolation measurements, planar or spherical scanning techniques.

It is found in general that the extrapolation method gives best accuracies for the power gain of relatively small standard gain antennas, but is not suitable for large antennas as indicated in section 4-2. Therefore the decision is often made to calibrate the power gain of large ground antennas by the gain-comparison technique, utilizing a standard gain antenna. In this method, a received signal is successively measured with the standard gain antenna whose absolute gain is accurately known and then with the large ground antenna under test, both being connected to the same receiving systems. The ratio of the received powers is then related to the ratio of the power gain of a standard gain antenna to that of the large ground antenna under test.

In this part of the report we discuss the gain comparison method and assume that the calibration signal is stable and is transmitted by a geostationary satellite. The major advantages of the gain-comparison method are: 1) the signal source is in the far-field of even larger ground antennas

because the distance between a satellite and a ground station is typically 35,000 kilometers; and 2) the power radiated by a typical satellite is approximately 10 dBW or higher (dBW means dB above one watt) and is strong enough to acquire with even a low-gain standard antenna.

4.3.2 Theory

In the gain-comparison method the total power received from the satellite is measured in rapid succession: first with the large ground antenna under test, then with the standard gain antenna. These two measurements are then repeated without the satellite signal. The setup for the gain-comparison measurement is shown in figure 4-13. The advantages of this technique are: 1) a priori knowledge of the following is not required: satellite performance characteristics, effective radiated power from the satellite, path loss between the satellite and the ground antenna, the system temperatures when the standard gain antenna or the large ground antenna under test are connected to a receiver, the bandwidth of the receiver, etc.; and 2) it is possible to perform the measurements of power ratio with more accuracy than measurements of absolute power.

Referring to figure 4-13, the total power delivered to the receiver output port is symbolized by P. For a large ground antenna while receiving a signal from the satellite

$$P_1 = \left\{ \left(\frac{4\pi}{\lambda_u^2} \cdot ERP_u \cdot (1-L_u) \cdot M_u \cdot t_u \cdot A_u + k \cdot T_{au1} \cdot B_1 \right) \cdot \alpha_{u1} + kT_{e1}B_1 + k \cdot (1-\alpha_{u1}) \cdot T_{ou1} \cdot B_1 \right\} \cdot g_1, \qquad (4.35)$$

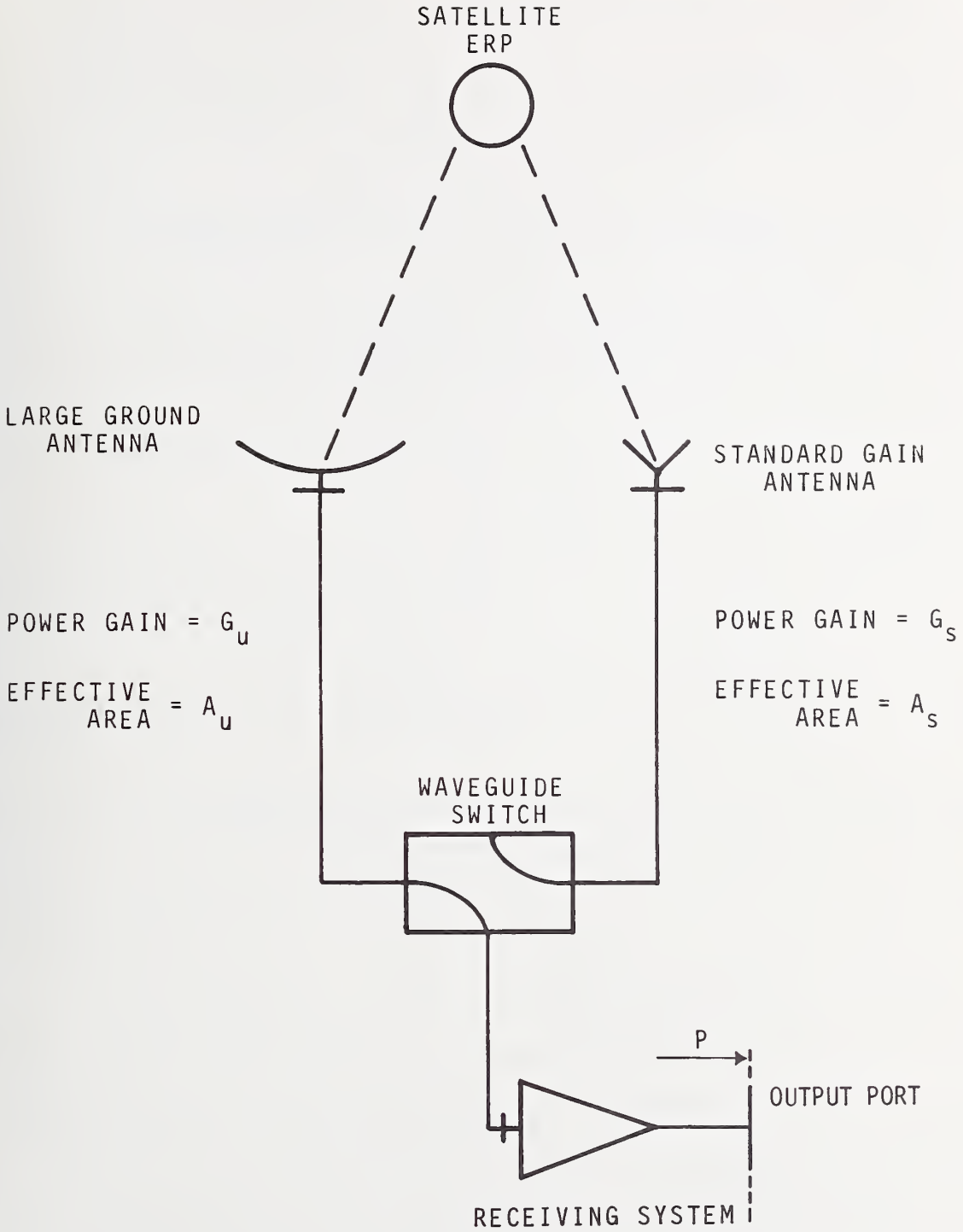

Figure 4-13 Schematic for experimental gain comparison method

and for a standard gain antenna,

$$P_2 = \left\{\left(\frac{4\pi}{\lambda_s^2}\cdot ERP_s\cdot(1-L_s)\cdot M_s\cdot t_s\cdot A_s + k\cdot T_{as2}\cdot B_2\right)\cdot\alpha_{s2} + kT_{e2}B_2 + k\cdot(1-\alpha_{s2})\cdot T_{os2}\cdot B_2\right\}\cdot g_2. \quad (4.36)$$

For the ground antenna under test when the antenna is pointing away from the satellite,

$$P_3 = k\cdot[T_{e3}+T_{au3}\cdot\alpha_{u3}+(1-\alpha_{u3})\cdot T_{ou3}]\cdot B_3\cdot g_3, \quad (4.37)$$

and similarly for the standard gain antenna

$$P_4 = k\cdot[T_{e4}+T_{as4}\cdot\alpha_{s4}+(1-\alpha_{s4})\cdot T_{os4}]\cdot B_4\cdot g_4. \quad (4.38)$$

Here, λ is the wavelength,

ERP is the effective radiated power of the satellite,

L is the path loss between the satellite and a ground antenna, expressed as a power ratio,

M is the polarization mismatch factor,

t is the tracking factor that takes tracking inaccuracy into account,

A is the effective area of the antenna,

k is the Boltzmann's constant,

T_a is the antenna noise temperature referred to the antenna output port and includes external noise and noise due to antenna loss,

B is the bandwidth of the receiving system,

g is the available power gain of the receiving system,

α is the ratio of the available power at the antenna output port to the available power at the receiver input port,

T_o is the physical temperature of the waveguide, etc. between the antenna output port and the receiver input port,

and T_e is the effective input noise temperature of the receiver.

The subscript "u" denotes factors associated with the measurement when the system is connected to the ground antenna, and the subscript "s" denotes factors associated with the measurement when the system is connected to a standard gain antenna.

The effective area of the ground antenna is then given by

$$A_u = A_s \cdot \frac{\lambda_u^2 \cdot ERP_s \cdot (1-L_s) \cdot M_s \cdot t_s \cdot \alpha_{s2}}{\lambda_s^2 \cdot ERP_u \cdot (1-L_u) \cdot M_u \cdot t_u \cdot \alpha_{u1}} \cdot \frac{g_2}{g_1} \cdot \frac{XZ}{Y} \cdot \left(\frac{Y - \frac{g_1}{g_3} \cdot (1+\delta_2)}{Z - \frac{g_2}{g_u} \cdot (1+\delta_1)} \right), \tag{4.39}$$

where

$$X \equiv \frac{P_1}{P_2}, \tag{4.40}$$

$$Y \equiv \frac{P_1}{P_3}, \tag{4.41}$$

$$Z \equiv \frac{P_2}{P_4}, \tag{4.42}$$

$$\delta_1 \equiv \frac{[T_{e2}+T_{as2} \cdot \alpha_{s2}+(1-\alpha_{s2}) \cdot T_{os2}] \cdot B_2 - [T_{e4}+T_{as4} \cdot \alpha_{s4}+(1-\alpha_{s4}) \cdot T_{os4}] \cdot B_4}{[T_{e4}+T_{as4} \cdot \alpha_{s4}+(1-\alpha_{s4}) \cdot T_{os4}] \cdot B_4}, \tag{4.43}$$

and

$$\delta_2 \equiv \frac{[T_{e1}+T_{au1} \cdot \alpha_{u1}+(1-\alpha_{u1}) \cdot T_{ou1}] \cdot B_1 - [T_{e3}+T_{au3} \cdot \alpha_{u3}+(1-\alpha_{u3}) \cdot T_{ou3}] \cdot B_3}{[T_{a3}+T_{su3} \cdot \alpha_{u3}+(1-\alpha_{u3}) \cdot T_{ou3}^2 \cdot B_3}. \tag{4.44}$$

It should be emphasized that the ratios X, Y, and Z should nominally be measured rather than the absolute powers P_1, P_2, P_3, and P_4. The expression for the effective area of a ground antenna given in eq. (4.39) applies to the very general case where the effective radiated power, antenna

temperature, path loss, front-end loss, gain of receiving system, bandwidth, etc., are assumed to change during the series of four measurements. It is useful only for the purpose of an error analysis. For actual measurement purposes, however, one assumes the following to hold during the measurements:

1. Operating frequency stays constant.
2. ERP stays constant.
3. Antenna temperature stays constant for each antenna.
4. Path loss is the same between the satellite and each antenna and stays constant.
5. The polarization mismatch between the incident wave from the satellite and both antennas is the same.
6. Tracking factor is the same for both antennas.
7. Losses between the antennas and the receiver system are equal for both antennas.
8. The gain of the receiving system stays constant.
9. The physical temperature of the antennas and between the antennas and the receiving system is the same for both antennas.
10. The effective input noise temperature of the receiver stays constant.

With these assumptions, eq. (4.39) simplifies to

$$A_u = A_s \frac{XZ}{Y} \frac{Y - 1}{Z - 1} = A_s \frac{P_1 - P_3}{P_2 - P_4} . \qquad (4.45)$$

It is easy to see that the factor Y - 1 is the signal-to-noise ratio for the large ground antenna when receiving the signal from the satellite. Similarly, Z - 1 is the signal-to-noise ratio for the standard gain antenna when receiving the signal from the satellite.

For a reciprocal antenna, the power gain is obtained from

$$G = \frac{4\pi}{\lambda^2} A, \tag{4.46}$$

and the final analysis of the error estimate is discussed in terms of the power gain of the large ground antenna.

4.3.3 Accuracy Consideration

The power ratio measurements cause the largest uncertainty in the calibration of the power gain of the large ground antenna under many circumstances, and should be carefully noted. In this section the various sources of error in the gain-comparison method are discussed.

A. The Power Gain of a Standard Antenna

The summary of the power gain accuracy of the standard gain antenna using the extrapolation technique is given in section 4.2.4. Typically the power gain of a 40-dB standard gain antenna can be determined to within a linear accumulation error of 0.08 dB for 3σ limits by use of the extrapolation technique, or to within a quadrature accumulation error of 0.04 dB. This error in the power gain of the standard gain antenna reflects directly on the error in the measured power gain of the ground antenna.

B. Frequency Instability

The receiving system is assumed to be tuned to the frequency of the signal from the satellite. The signal from the satellite used for calibration is assumed to be CW so that its bandwidth is much narrower than that of the receiving

system. It is possible to control the frequency of a satellite signal and of a receiving system to within one part in 10^9 with a good synchronizer. Therefore the error due to this source is negligible.

C. Effective Radiated Power (ERP)

According to IEEE standard definitions of terms for antennas [2], the effective radiated power is defined as

ERP = in given direction, the power gain of a transmitting antenna multiplied by the net power accepted by the antenna from the connected transmitter.

It is assumed for the purpose of the present error analysis that the effective radiated power from a satellite is either 10 dBW or 30 dBW. It should be noted that the value of ERP is needed only for the error analysis and does not need to be known for the measurement of the power gain of the ground antenna, provided ERP is stable during the measurements. In practice, an assumed 0.01 dB instability of ERP exists during the power measurements and causes an uncertainty of again 0.01 dB in the measured power gain of the ground antenna.

D. Path Loss

The path loss consists of the free-space loss and the loss due to atmospheric absorptions. The free-space loss is the loss between two isotropic antennas in free space, expressed as a power ratio [2]. The free-space loss is usually expressed in decibels and is given by $20 \log(4\pi r/\lambda)$ where r is the distance between two antennas. For a typical distance of 35,000 km between a satellite and a receiving antenna, the free-space loss at 7.25 GHz is approximately 200 dB.

The terrestrial atmosphere causes radio wave attenuation, which usually divides into three different types: absorptive, refractive, and diffusive attenuation. Absorptive attenuation is caused by a resonance in the oxygen and water vapor molecules and is about 0.1 dB at a 40° elevation angle. Smooth variations in the refractive index of the atmosphere cause refraction of the radio wave from a satellite, and irregular variations in the refractive index of the atmosphere due to turbulence cause diffusion and distortion of a radio wave. The attenuation due to refraction and diffusion (as sensed by the antenna) is dependent on the aperture dimension of the antenna [66].

The average atmospheric loss at 7.25 GHz is about 0.008 dB per kilometer as previously shown in figure 4-5. Path loss instability between satellite and ground introduces an error which is assumed to be 0.01 dB to the power gain of the ground antenna.

E. Polarization Mismatch

To determine the mismatch between the polarization patterns of the signal from the satellite and that of the receiving ground antenna (or the standard gain antenna) it is necessary to know the on-axis polarization characteristics of each antenna and the polarization characteristics of the field incident from the satellite.

The polarization mismatch factor, M, is defined here as follows (M relates to a specific receiving antenna and the on-axis component of a specific incoming wave): M is given by the ratio of the power at the antenna output port when an arbitrarily polarized and oriented wave is being received, to the same output power when a wave that is polarized and oriented for optimum reception is being received.

The expression for M that holds when either field or antenna is elliptically or circularly polarized is given by [67]

$$M = \frac{(R_1 R_2 \pm 1)^2 \cos^2 \theta + (R_1 \pm R_2)^2 \sin^2 \theta}{(R_1^2+1)(R_2^2+1)} . \qquad (4.47)$$

R_1 and R_2 are the electric field axial ratios (maximum divided by minimum) for an antenna and an incident electric field, respectively. θ is the polarization mismatch angle, i.e., the angular difference between the major axes of two polarization ellipses.

In eq. (4.47) the plus sign is used when the polarizations of the antenna and the incident electric field from the satellite are in the same sense, and the minus sign applies when both polarizations are in the opposite sense. When one of the polarizations is linear, the polarization mismatch factor, M, becomes

$$M = \frac{(R^2+1) + (R^2-1)\cos 2\theta}{2(R^2+1)}. \qquad (4.48)$$

When both polarizations are linear, M is simply given by $\cos^2 \theta$. When the electric field axial ratios of the elliptically polarized incoming wave from a satellite and of a ground (or standard horn) antenna are assumed to be 1.2 and can be measured with 0.1% accuracy, the error for the gain calibration of a ground antenna due to this source is about ± 0.005 dB. Similarly, when the polarization mismatch angle or orientation of the major axis of the polarization pattern can be ascertained to within 1 degree, the resulting error is 0.005 dB.

F. Tracking Accuracy

The tracking accuracy is the accuracy with which an antenna can track a source. The tracking error is a measure

of tracking accuracy and is defined as the instantaneous space angle difference, ϕ, between the directions of the power pattern maxima of a receiving antenna and a (satellite) transmitting antenna. The tracking error is usually specified in terms of its rms value, which is usually normalized to half-power beamwidth, in this case that of the ground antenna.

To estimate the error introduced in the measured power gain by the tracking error, it is reasonable to assume that the tracking error has a normal probability distribution [68], namely,

$$p(\phi) = \frac{1}{\sqrt{2\pi}\ \delta\theta_{hp}} \exp\left\{-\frac{\phi^2}{2\delta^2\theta_{hp}^2}\right\}, \quad -\pi \leq \phi \leq \pi , \qquad (4.49)$$

where δ is the rms value of the tracking error normalized to θ_{hp}, the half-power-beamdwidth of the ground antenna. At far-field distances, the power gain of the antenna can be very closely approximated by the sinc x function. Knowing that the function $\text{sinc}^2\ x = 0.5$ when $x = 1.392$ radian, the power gain can be given by

$$G(\phi) \doteq G_o\ \text{sinc}^2\left(\frac{2.784\phi}{\theta_{hp}}\right). \qquad (4.50)$$

The expected value of the power gain is then

$$E\{G(\phi)\} = \int_{-\pi}^{\pi} G(\phi)p(\phi)d\phi$$

$$= \frac{G}{\sqrt{2\pi}\ \delta\theta_{hp}} \int_{-\pi}^{\pi} \text{sinc}^2\left(\frac{2.784\phi}{\theta_{hp}}\right)\exp\left\{-\frac{\phi^2}{2\delta^2\theta_{hp}}\right\}d\phi. \qquad (4.51)$$

The expected reduction in measured power loss due to tracking inaccuracies is given by the ratio of the expected values of

the power gain and G_o;

$$\frac{E\{G(\theta)\}}{G_o} = \frac{1}{\sqrt{2\pi}\,\delta\theta_{hp}} \int_{-\pi}^{\pi} \operatorname{sinc}^2\left(\frac{2.784\phi}{\theta_{hp}}\right) \exp\left(-\frac{\phi^2}{2\delta^2\theta_{hp}^2}\right) d\phi. \qquad (4.52)$$

The numerical computation of the integral was performed by Zolnay [68] and the result is given in figure 4-14. Using the expression for half-power beamwidth,

$$\theta_{hp} = \frac{70\lambda}{D}, \qquad (4.53)$$

where θ_{hp} is in degrees, D is the major aperture dimension of the antenna, and λ is the wavelength. The power gain of an antenna is

$$G = \frac{4\pi}{\lambda^2} A = \frac{4\pi}{\lambda^2} \eta_r A_g, \qquad (4.54)$$

where λ is the wavelength, A is the effective area of the antenna, η_r is the aperture radiation efficiency and A_g is the geometrical aperture area. The expected reduction in measured power gain due to tracking inaccuracy is given as a function of power gain and of antenna diameter in figure 4-15.

In calculating total error in the measured power gain discussed in section 4.3.4 to follow, it is assumed that the tracking error is 5 seconds of arc.

G. Waveguide Feed Loss Uncertainty

The uncertainty in the difference between losses arising between the ground antenna output port and the receiver input port and losses arising between the standard gain antenna output port and the receiver input port contributes an error to the measured power gain of the ground antenna. It is assumed in section 4.3.4 that this difference is 0.01 dB, which in turn causes a 0.01 dB error in the measured power gain of the ground antenna.

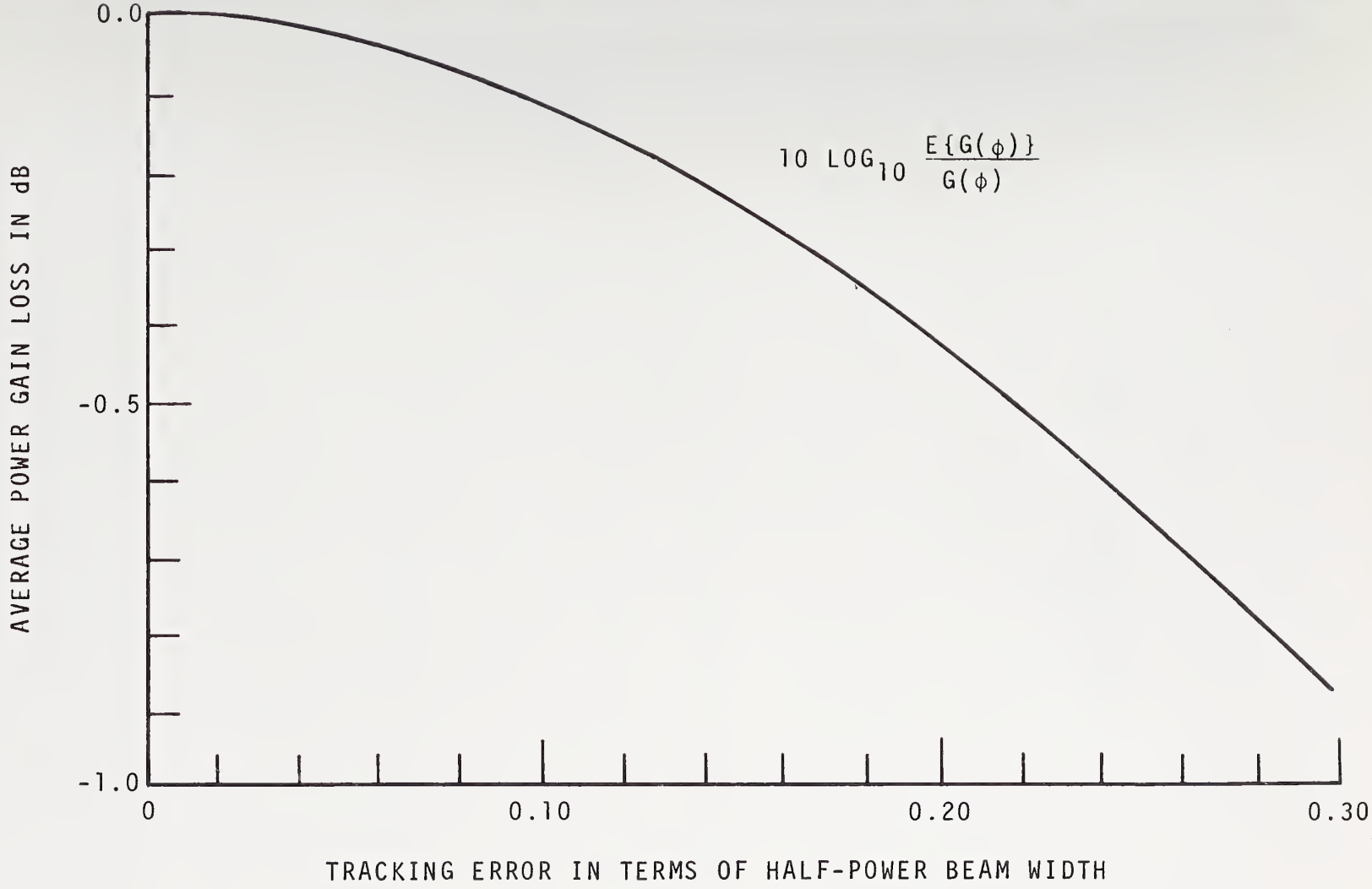

Figure 4-14 Average power gain loss as a function of ratio of tracking error to half power bandwidth

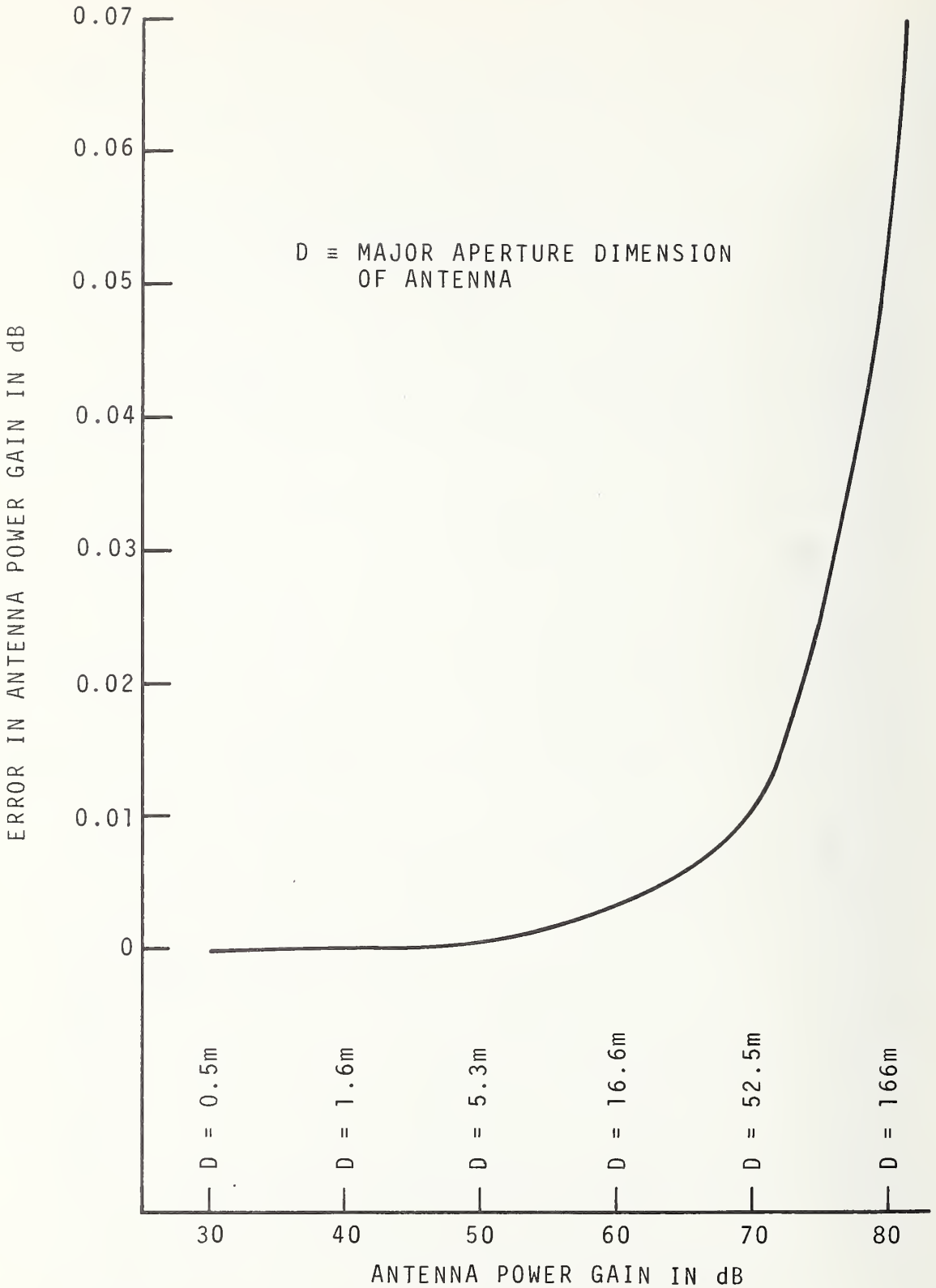

Figure 4-15 Error in the antenna power gain due to tracking inaccuracy (frequency = 7.25 GHz, tracking inaccuracy = 5 seconds of arc, rms).

H. Uncertainty in Power Ratio Measurement

One of the most significant errors in the calibration of the power gain of a ground antenna is due to the uncertainty in the power ratio measurements. This is especially true when the effective radiated power (ERP) from the satellite and/or the power gain of the antenna is small. Figure 4-16 shows the error in the power gain of an antenna due to the uncertainty in Y as a function of uncertainty in Y, and figure 4-17 shows the error in the power gain due to uncertainty in Z as a function of uncertainty in Z. The ratios Y and Z are defined in eqs. (4.41) and (4.42). It is clear from this figure that the ratio of the power measurement for a standard antenna receiving a signal to that without a signal should be performed with great care in order to minimize the relatively large Z related error.

I. Uncertainty Due to Receiver Gain Instability and Nonlinearity

Receiver gain instability and nonlinearity are often significant sources of error in the calibration of the power gain of a ground antenna. In order to minimize these measurement errors, extremely good receiver stability and linearity are required, especially during the power measurements when the standard gain antenna is connected.

The gains of the receiving system during the power measurement with the standard gain antenna are g_2 and g_4 in eq. (4.39). Figures 4-18 and 4-19 show uncertainty in the measured power gain of the ground antenna due to uncertainty in g_2 and g_4 as a function of uncertainty in g_2 and g_4 respectively.

To avoid the nonlinearity errors that result from widely different levels it may be desirable to reduce the signal level from the larger (ground) antenna to the same level as

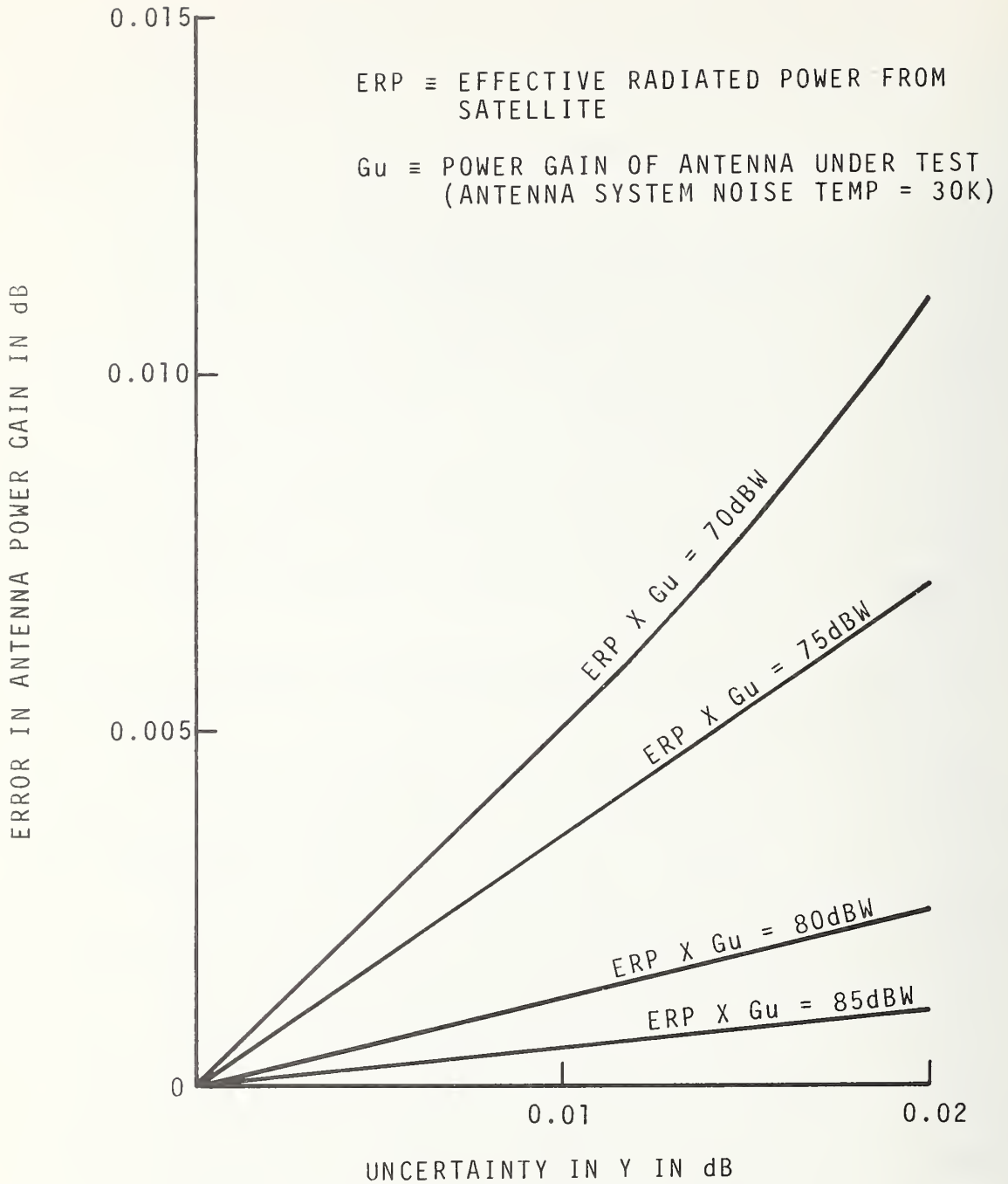

Figure 4-16 Error in the antenna power gain due to uncertainty in Y = P1/P3

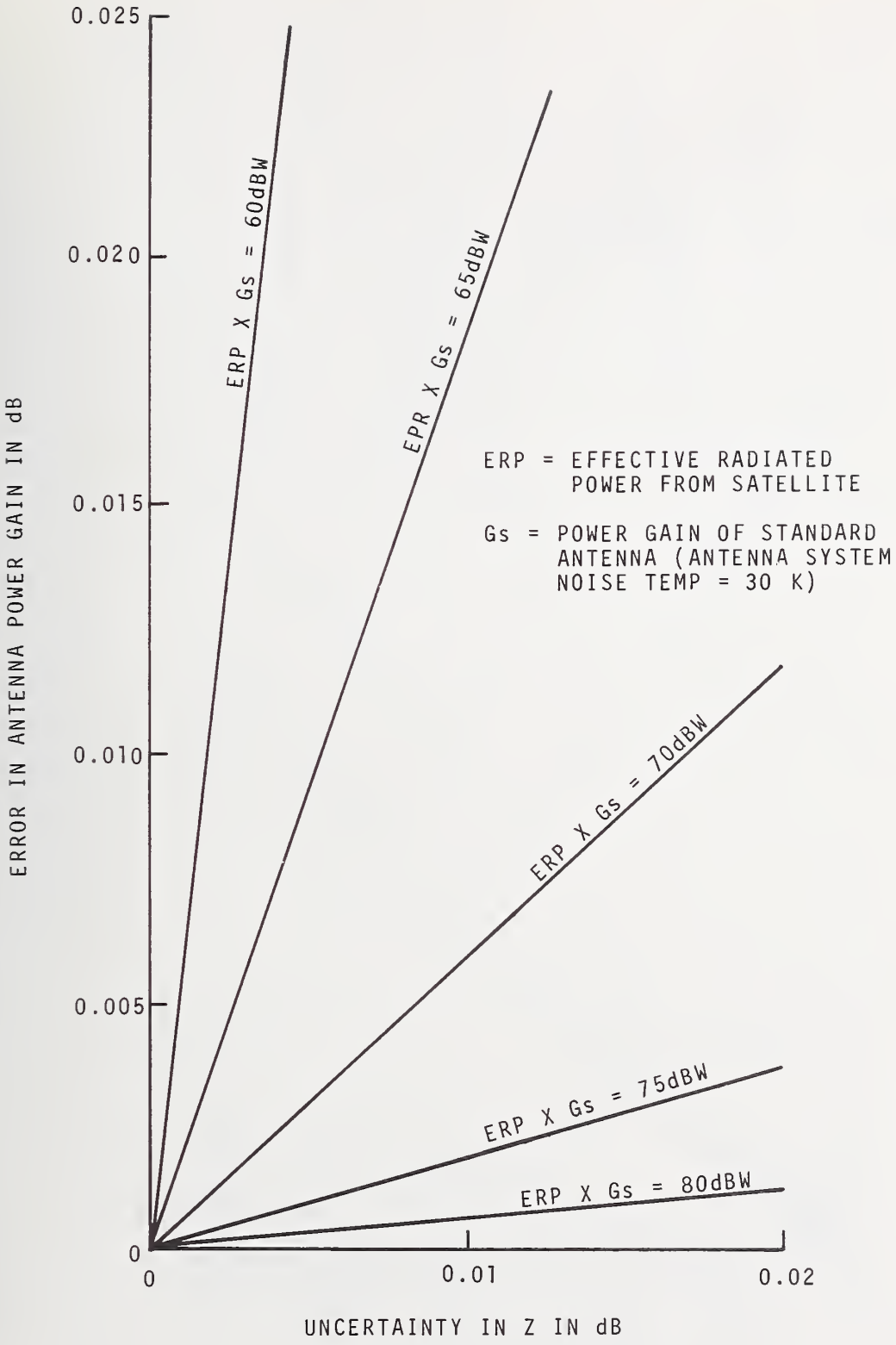

Figure 4-17 Error in the antenna power gain due to uncertainty in Z = P2/P4

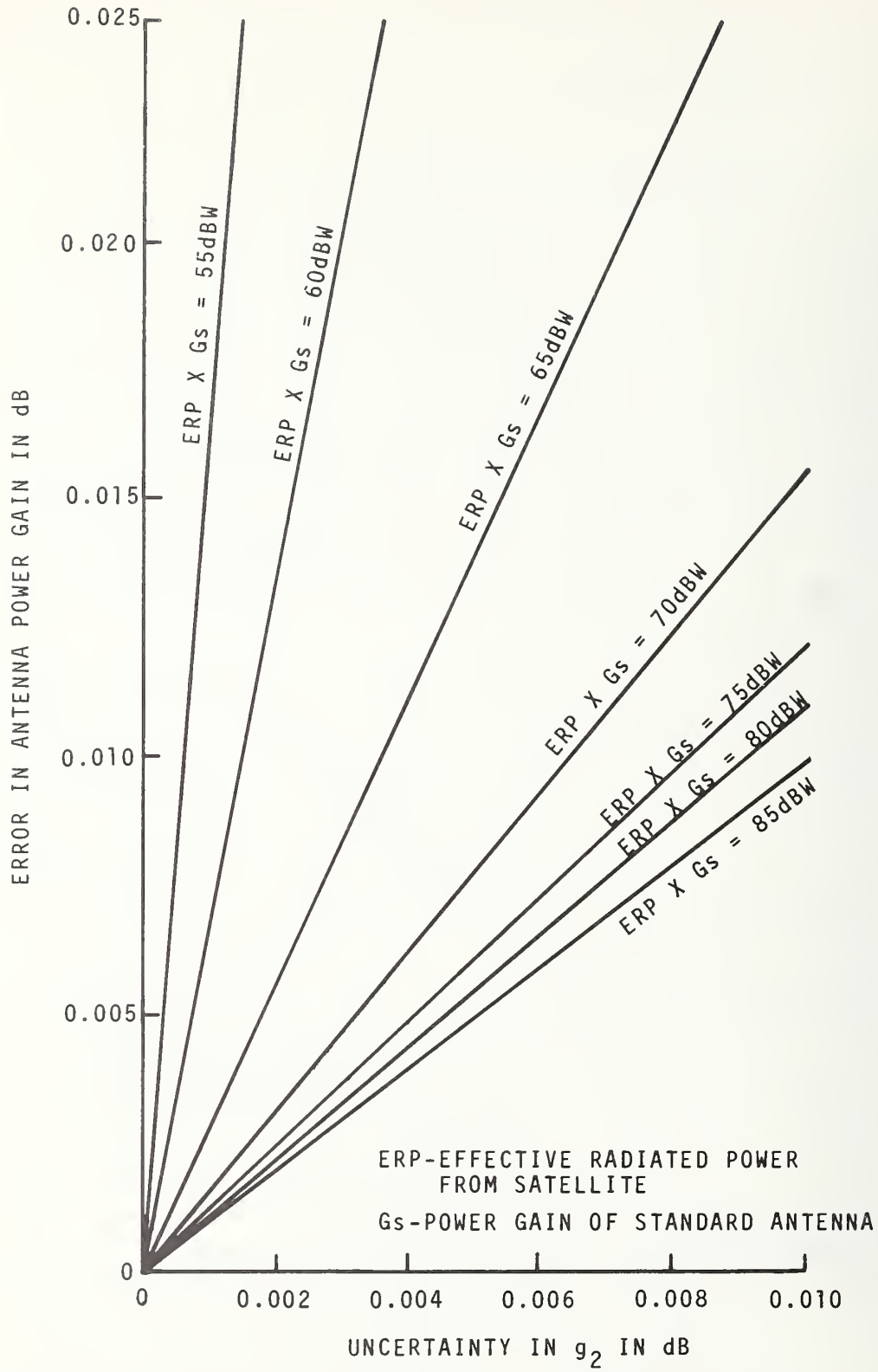

Figure 4-18 Error in the antenna power gain due to uncertainty in g_2

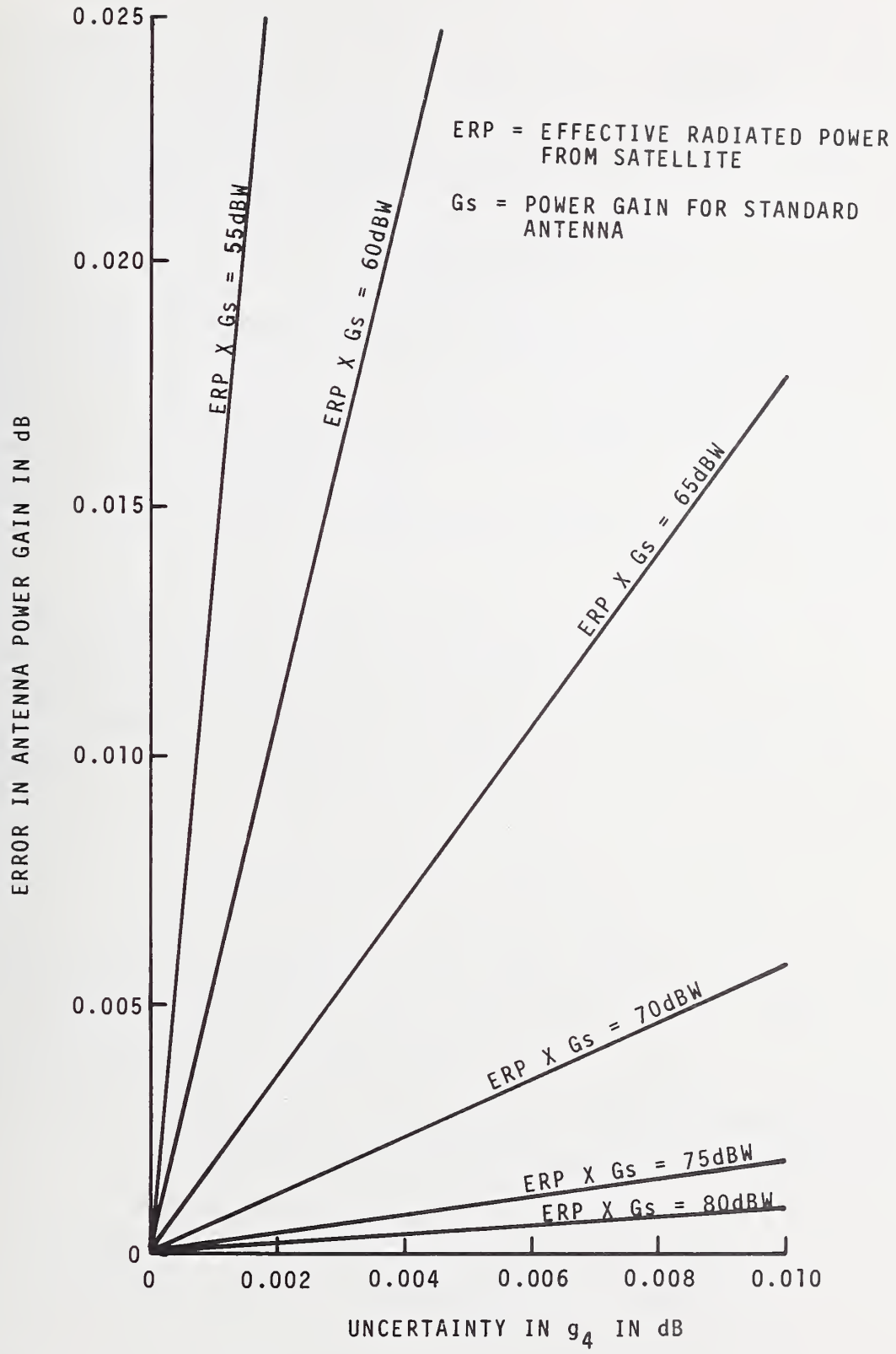

Figure 4-19 Error in the antenna power gain due to uncertainty in g_4

that from the smaller (standard gain) antenna. This is accomplished by the use of a calibrated directional coupler and/or a precision attenuator. This technique introduces an additional error due to the coupler and/or the attenuator. Moreover, since this technique degrades the signal-to-noise ratio of the receiving system as used with the large antenna, the error due to the power ratio measurements (Y) becomes large just as in the case of the smaller antenna. Therefore, the use of a coupler and/or attenuator may not reduce the total measurement error.

If receiver gain instability is regarded as a random phenomenon, the resulting error is also random and can be minimized by statistical averaging. However, the uncertainty due to receiver nonlinearity should still be included as a systematic error.

J. Uncertainty in Antenna System Noise Temperature

The noise temperature, T_n, represents the available power at the output port of a hypothetical lossless antenna. T_n is due to noise sources external to the antenna aperture and is given by

$$T_n = \frac{G_o}{4\pi\eta_r} \int_\Omega T(\theta,\phi) f(\theta,\phi) d\phi, \qquad (4.55)$$

where $T(\theta,\phi)$ is the temperature distribution on the sphere surrounding the antenna and $f(\theta,\phi)$ is the antenna power normalized to the on axis power gain G_o, and η_r is the antenna radiation efficiency. The external noise consists of sky noise (cosmic noise plus noise due to atmospheric absorption) and ground noise (usually around 290K).

The antenna noise temperature, i.e., the noise temperature appearing at the output port of the antenna feed, consists of both the (lossless) antenna noise temperature, T_n, and noise introduced by the antenna and waveguide feed losses. The antenna noise temperature, T_a, can be stated in terms of the following equation

$$T_a = T_n\alpha + (1-\alpha)T_o, \qquad (4.56)$$

where T_n is the (lossless) antenna noise temperature (K) referred to the lossless antenna output port, α is the ratio of the power entering the antenna aperture to the available power at the output port of the waveguide feed, and T_o is the ambient temperature.

It should be noted that the antenna noise temperature changes drastically with elevation angles (θ), particularly at the lower elevation angles between 0 and 10 degrees, and reaches almost 290K at zero elevation angles. However, at elevation angles larger than 40 degrees the antenna noise temperature is relatively constant and is about 30K.

The instability or changes in the antenna noise temperature while on- and off-satellite measurements are being made with any one antenna cause an error in the measured power gain of the ground antenna. It can be assumed that when the sky noise temperature is about 5 degrees or less, as is usually the case, the antenna noise temperature does not change much during the measurements. Therefore the error due to this source is assumed to be negligible.

K. Error Due to Change in Effective Input Noise Temperature, Bandwidth, and Ambient Temperature

The effective input noise temperature, the limiting bandwidth of the receiving system, and the ambient temperature at various points of the system are assumed to be stable

provided measurements are carried out rapidly. This rapid measurement process also minimizes the errors caused by changes in the receiver gain and ERP. Thus, errors due to changes in the effective input noise temperature, bandwidth, and ambient temperature are negligible.

4.3.4 Results and Concluding Remarks

The estimated errors incurred in the course of the gain comparison method used to calibrate power gain of a large ground antenna are summarized below.

In this estimate we assume that:

1) satellite ERP is 10 or 30 dBW;
2) antenna noise temperature of the ground antenna is 30K, and that of a standard gain antenna is 40K;
3) path loss is 200 dB;
4) bandwidth of the receiving system is 40 MHz;
5) gain of the receiving system is 100 dB;
6) differences in loss between the antenna output port and the receiver input port are 1 dB for the standard gain antenna and 2 dB for the large ground antenna;
7) the ambient temperature is 290K.

Only the errors not judged to be negligible have been listed here.

Using a 30 dB standard gain antenna, the linear sum of all errors as a function of power gain of a ground antenna is given in figure 4-20. As expected, although the error in the measured power gain of the standard gain antenna is quite small (0.08 dB), the uncertainty in the measurements of power ratio, Z, and that due to stabilities in gains

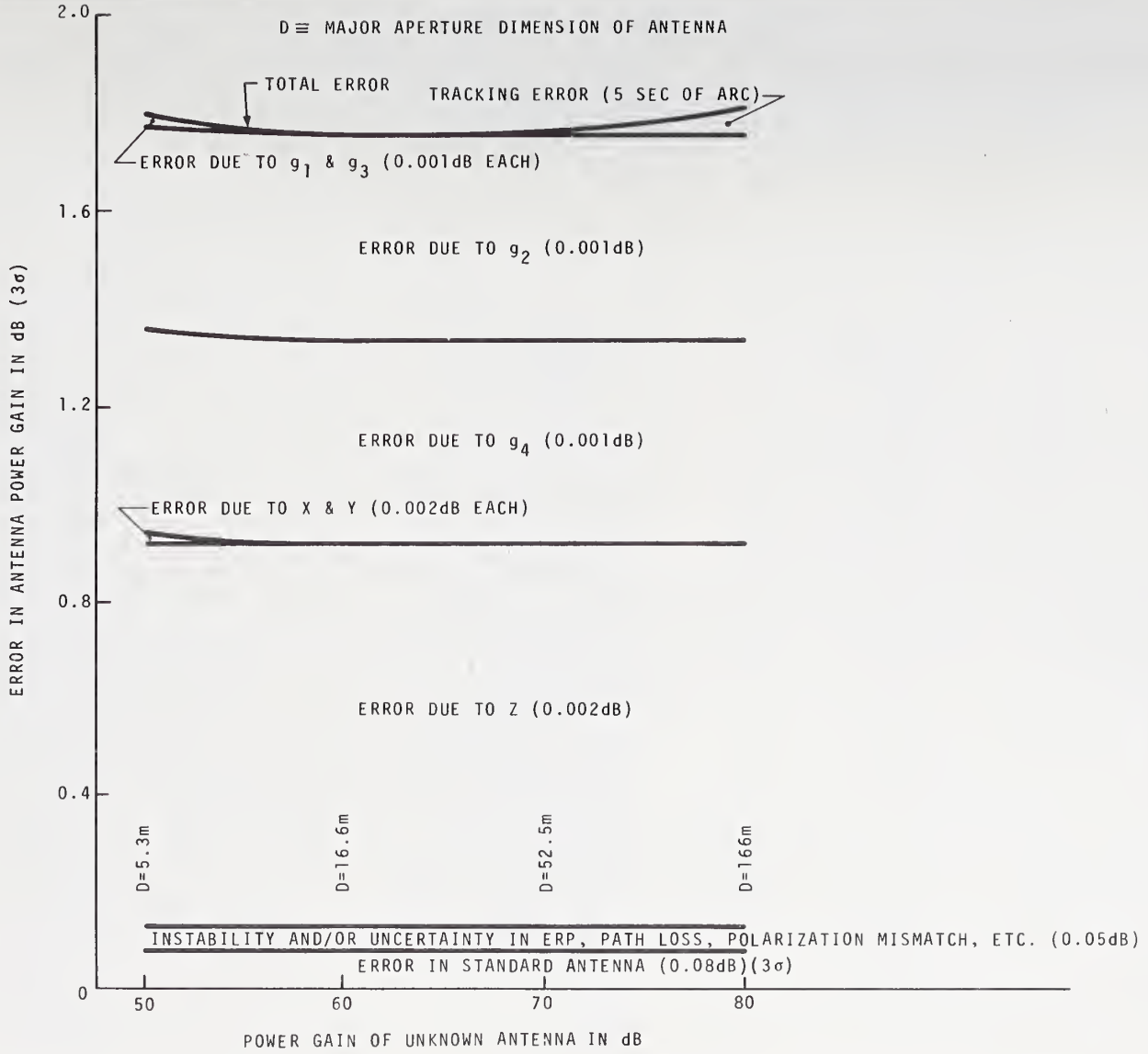

Figure 4-20. Linear error accumulation for the power gain of a large microwave antenna using the gain comparison method (frequency = 7.25 GHz, standard antenna gain = 30 dB nominal, effective radiated power = 10 dBW nominal).

g_2 and g_4 will contribute large errors because of the poor signal-to-noise ratio for a standard gain antenna.

It appears that this problem can be reduced by use of a standard gain antenna with higher gain. Figure 4-21 shows the linear accumulation of all errors as a function of the power gain of a ground antenna using a 40-dB standard gain antenna. The errors due to Z and instabilities in gains g_2 and g_4 are indeed reduced by use of a larger, in this case 50 dB, standard gain antenna, as shown in figure 4-22. Unfortunately, the power gain calibration of a 50-dB standard gain antenna is easier said than done: the near-field scanning or extrapolation ranges needed for accurate calibration of 50-dB antennas do not exist. Furthermore, the alignment accuracy and stability necessary for such an extrapolation range are at best very difficult to build in view of a length requirement of approximately 1.4 km. Therefore, larger standard gain antennas are impractical at least for the present.

The linear accumulation of errors in the measured power gain of a large (60 dB) antenna as a function of power gain of standard gain antennas is shown in figure 4-23. Figure 4-24 shows the same errors for a larger (70 dB) antenna.

Some of the contributing sources of error are independent and satisfy the condition for quadrature error addition. For example, errors due to the standard gain antenna, ERP, path loss, waveguide feed loss, polarization mismatch, and tracking inaccuracy are independent and can be added in quadrature. However, uncertainties in the measurements of X, Y and Z are not independent of each other. Similarly, the uncertainties due to nonlinearity and instability in g_1, g_2, g_3, and g_4 are not independent. These should be added linearly. Figure 4-25 shows the total quadrature error in the measured power gain of a ground antenna, calculated in the fashion just described as a function of power gain of the unknown antenna.

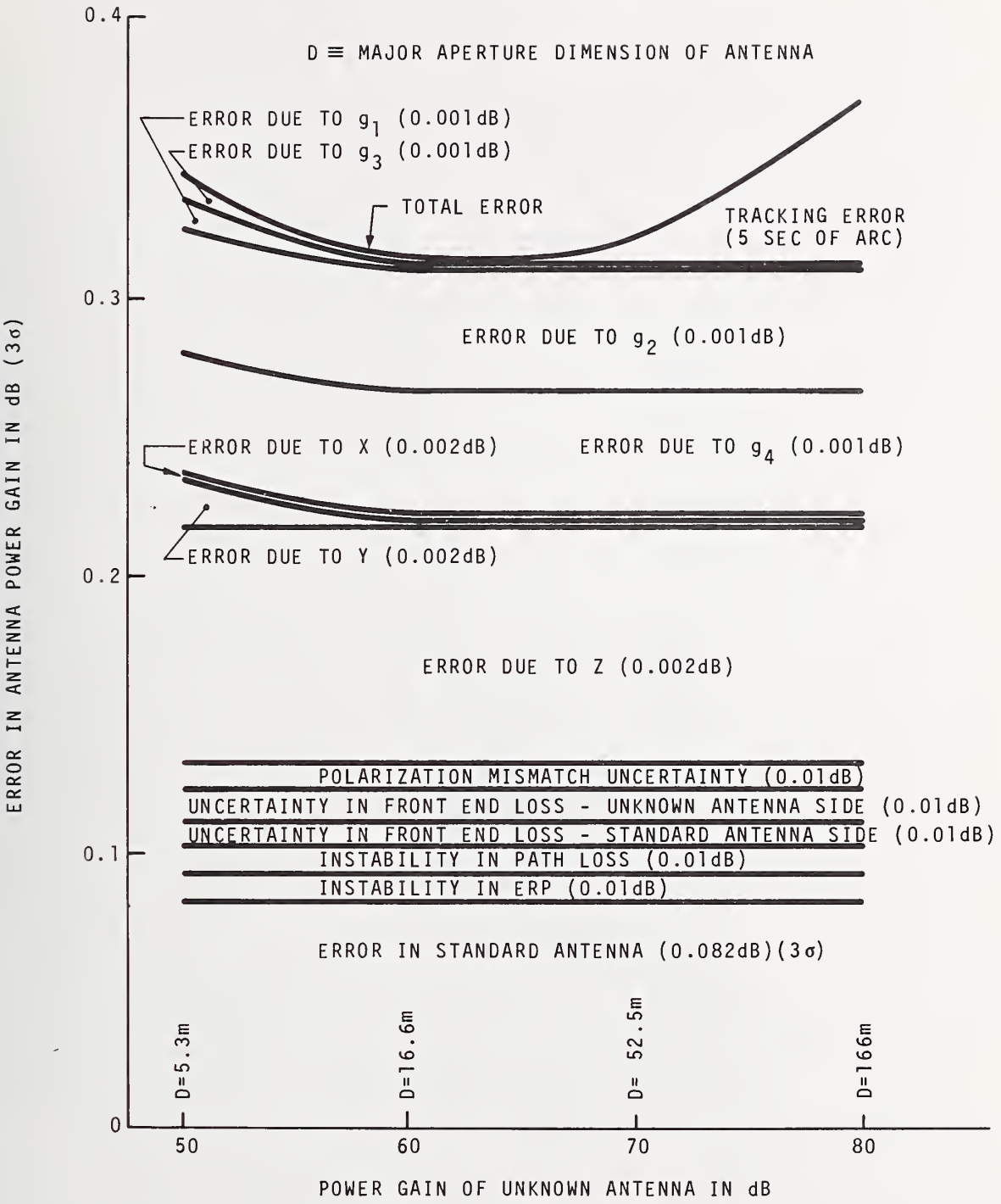

Figure 4-21. Linear error accumulation for the power gain of a large microwave antenna using the gain comparison method (frequency = 7.25 GHz, standard antenna gain = 40 dB nominal, effective radiated power = 10 dBW nominal).

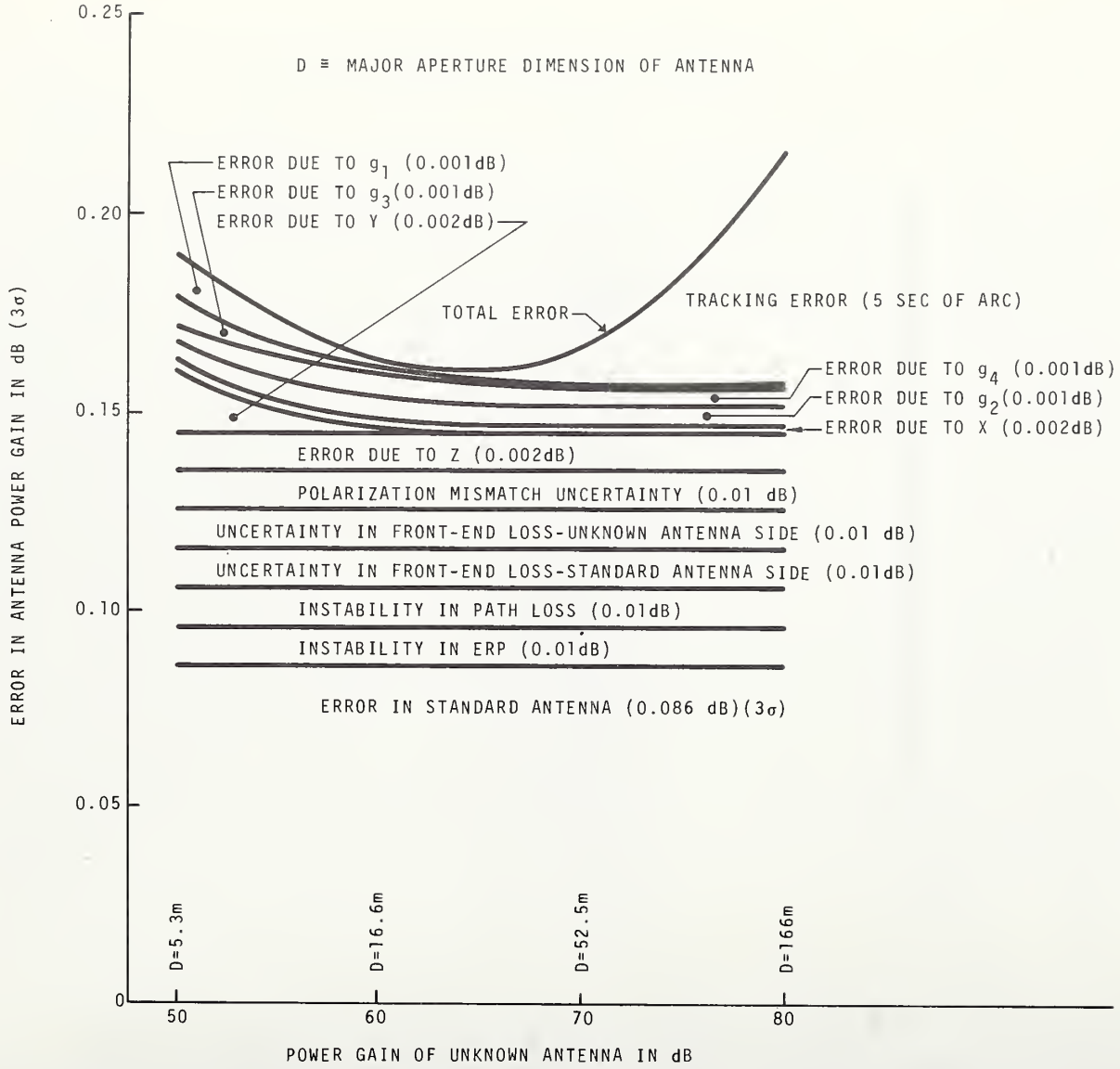

Figure 4-22. Linear error accumulation for the power gain of the large microwave antenna using the gain comparison method (frequency = 7.25 GHz, standard antenna gain = 50 dB nominal, effective radiated power = 10 dBW nominal).

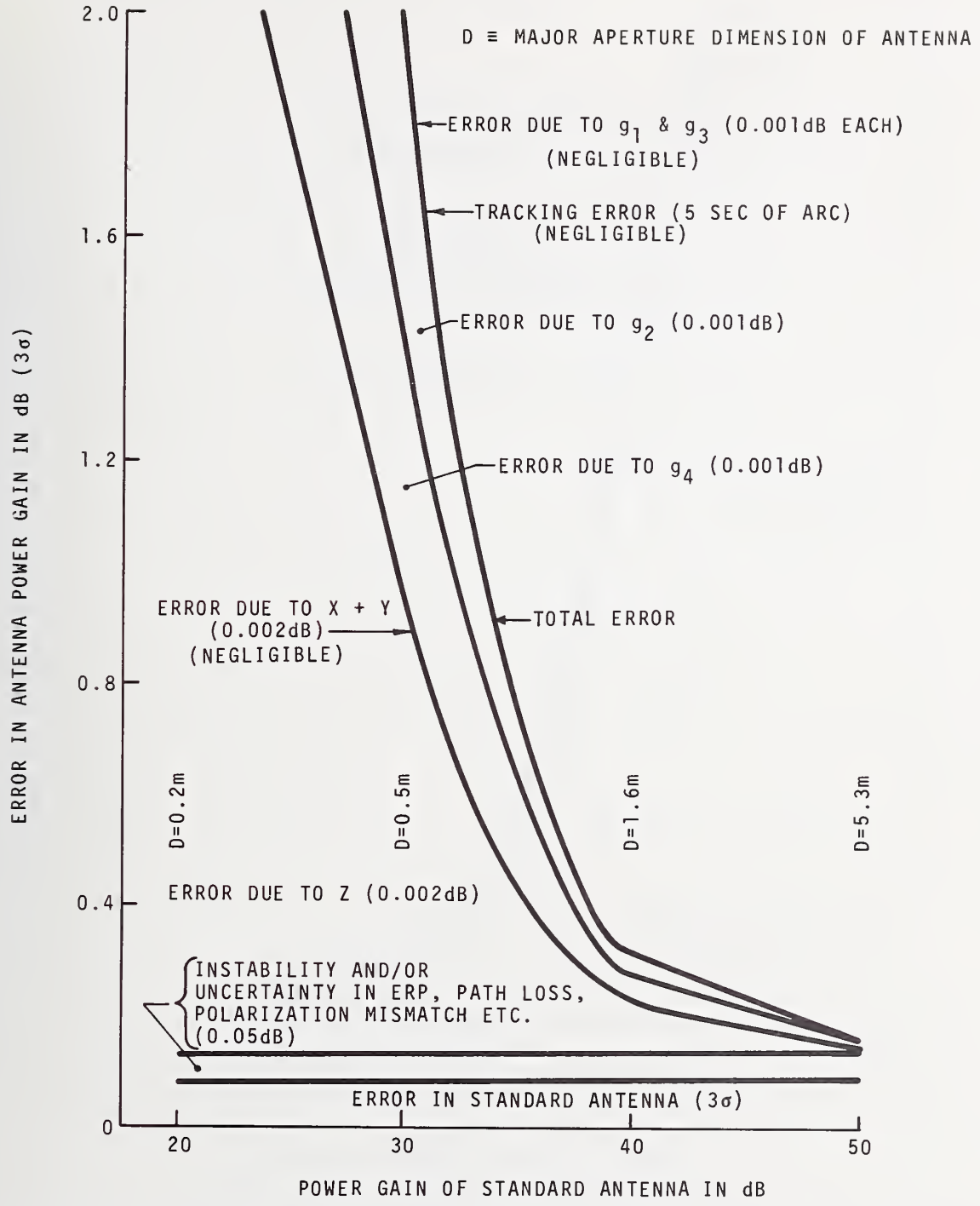

Figure 4-23. Linear error accumulation for the power gain of the large microwave antenna using the gain comparison method (frequency = 7.25 GHz, standard antenna gain = 60 dB nominal, effective radiated power = 10 dBW nominal).

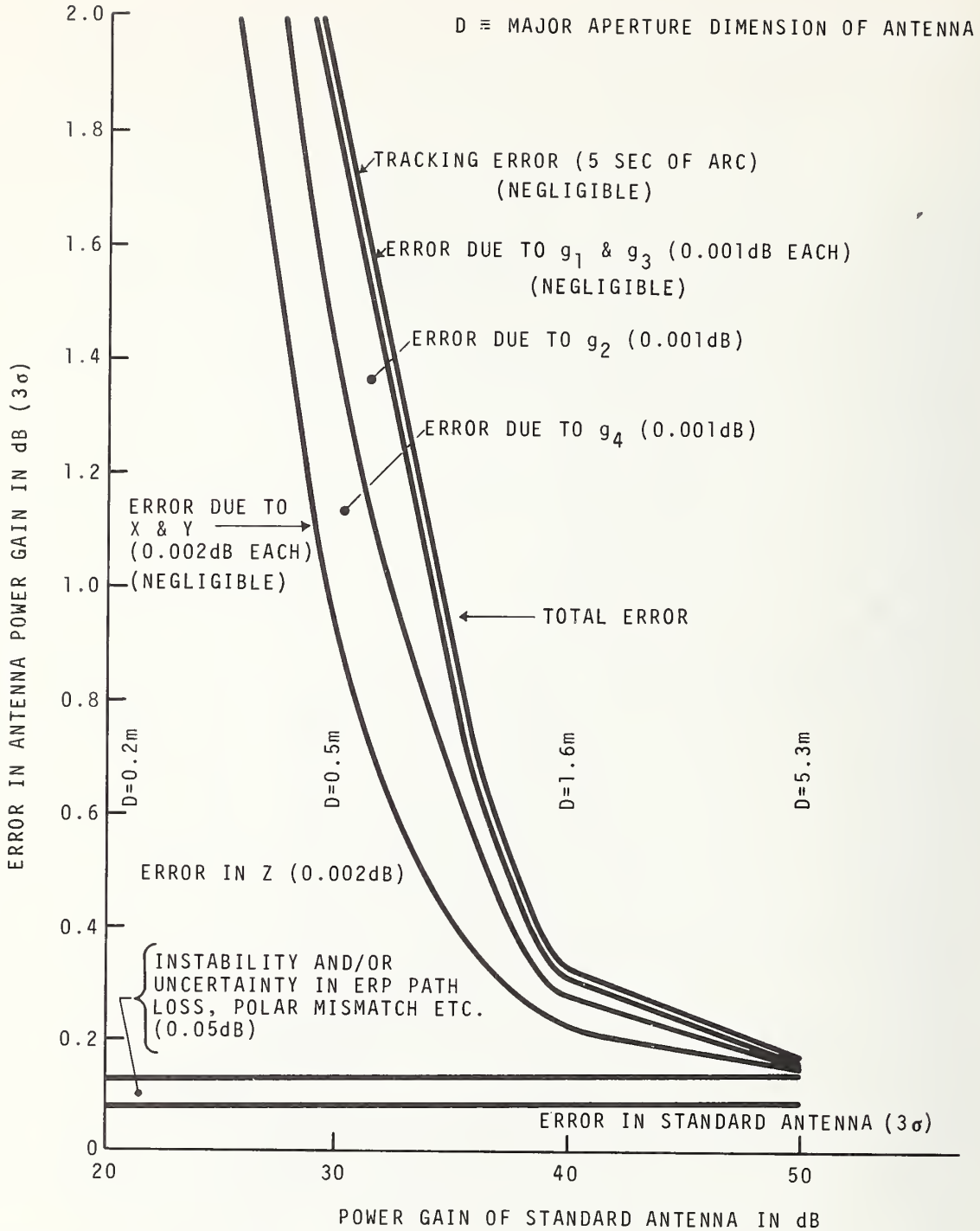

Figure 4-24. Linear error accumulation for the power gain of the large microwave antenna using the gain comparison method (frequency = 7.25 GHz, unknown antenna gain = 40 dB nominal, effective radiated power = 10 dBW nominal).

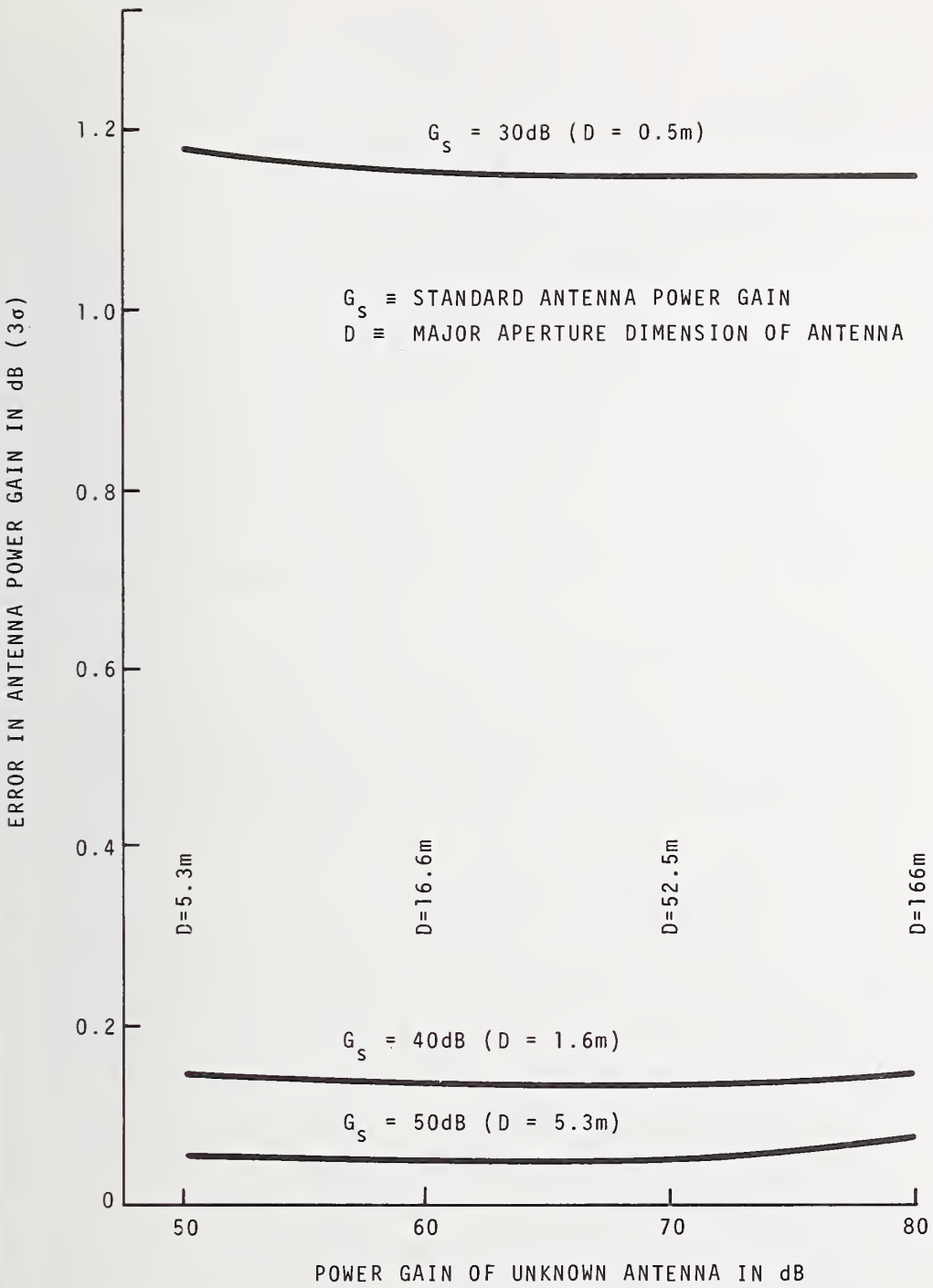

Figure 4-25. Quadrature error accumulation for the power gain of the large microwave antenna using the gain comparison method (frequency = 7.25 GHz, effective radiated power = 10 dBW nominal).

If a higher ERP is available, the error in the measured power gain of the ground antenna can be reduced. Therefore let us assume an ERP of 30 dBW, but assume that other parameters are the same as mentioned above. Then the results are shown in figures 4-26, 4-27, and 4-28 for 30, 40, and 50-dB standard gain antennas as a function of the power gain of a ground antenna. When a satellite with 30 dBW ERP is available, the use of a 50-dB (instead of 40-dB) standard gain antenna reduces the error in the power gain by only 0.01 dB. Figures 4-29 and 4-30 show the linear accumulation of the errors in measured power gain for 60 and 70 dB ground antennas as a function of standard antenna gain. Quadrature error in measured power gain based on the assumptions mentioned above is shown in figure 4-31 as a function of the ground antenna power gain.

In summary it seems possible to calibrate a 60 or 70-dB ground antenna to within a 0.18-dB linear error or a 0.06-dB quadrature error. These results assume a 40-dB standard gain antenna, the gain comparison method, and an ERP of 30 dBW.

4.4 Summary and Conclusions

The calibration of the power gain of large antennas to be used primarily for the purpose of calibrating Cas A has been described. First, a practical, generalized three-antenna method of determining the power gain of a relatively small standard gain antenna has been discussed. It has been found that using the extrapolation method the power gain of a 40-dB standard gain antenna can be calibrated to within a linear accumulation error of 0.08 dB for 3σ limits or quadratic accumulation error of 0.04 dB.

Although it is in principle possible to calibrate standard gain antennas with a power gain of 50 dB or higher, a 1.4 km-long extrapolation range is required for separation

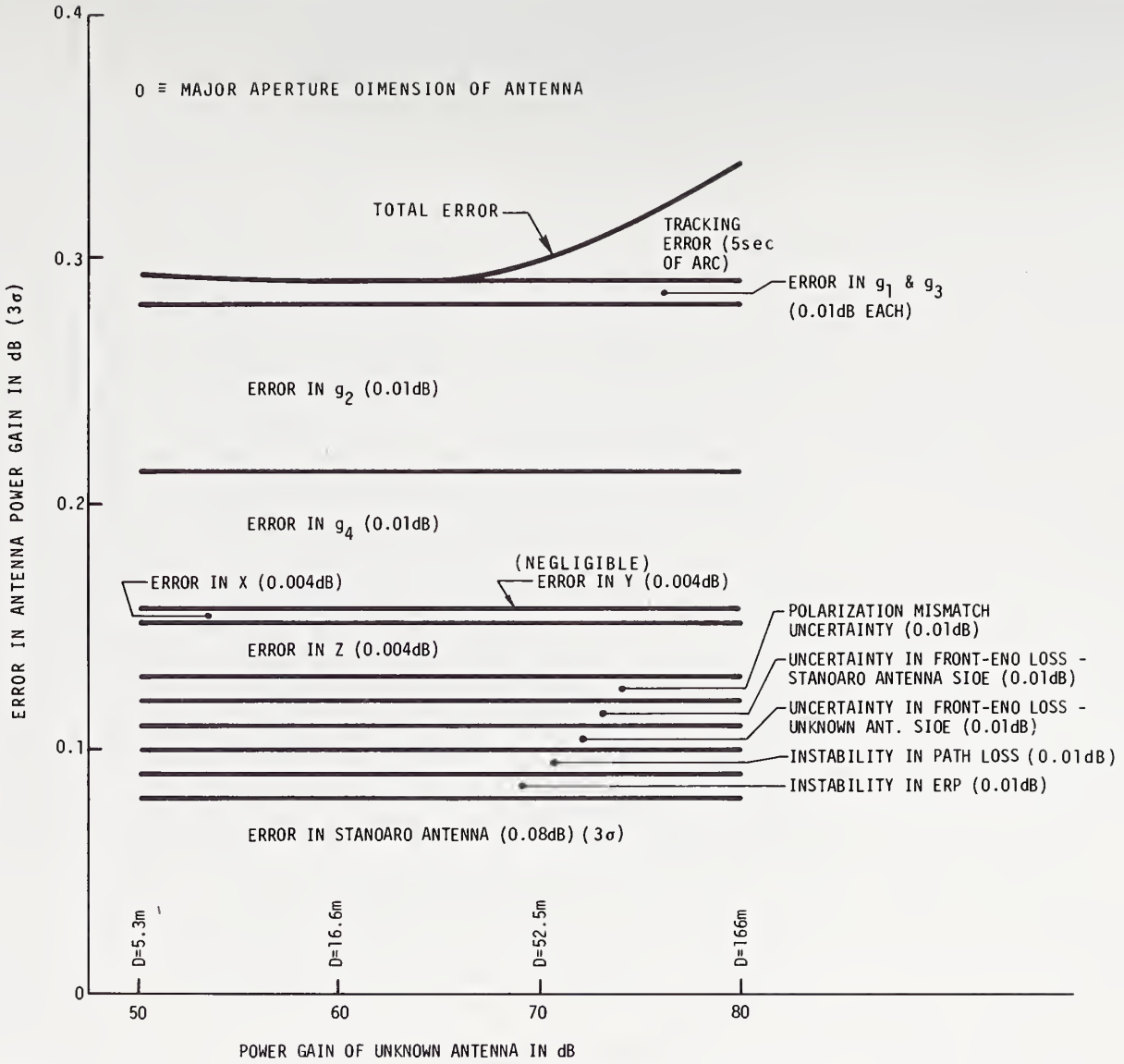

Figure 4-26. Linear error accumulation for the power gain of the large microwave antenna using the gain comparison method (frequency = 7.25 GHz, standard antenna gain = 30 dB nominal, effective radiated power = 30 dBW nominal).

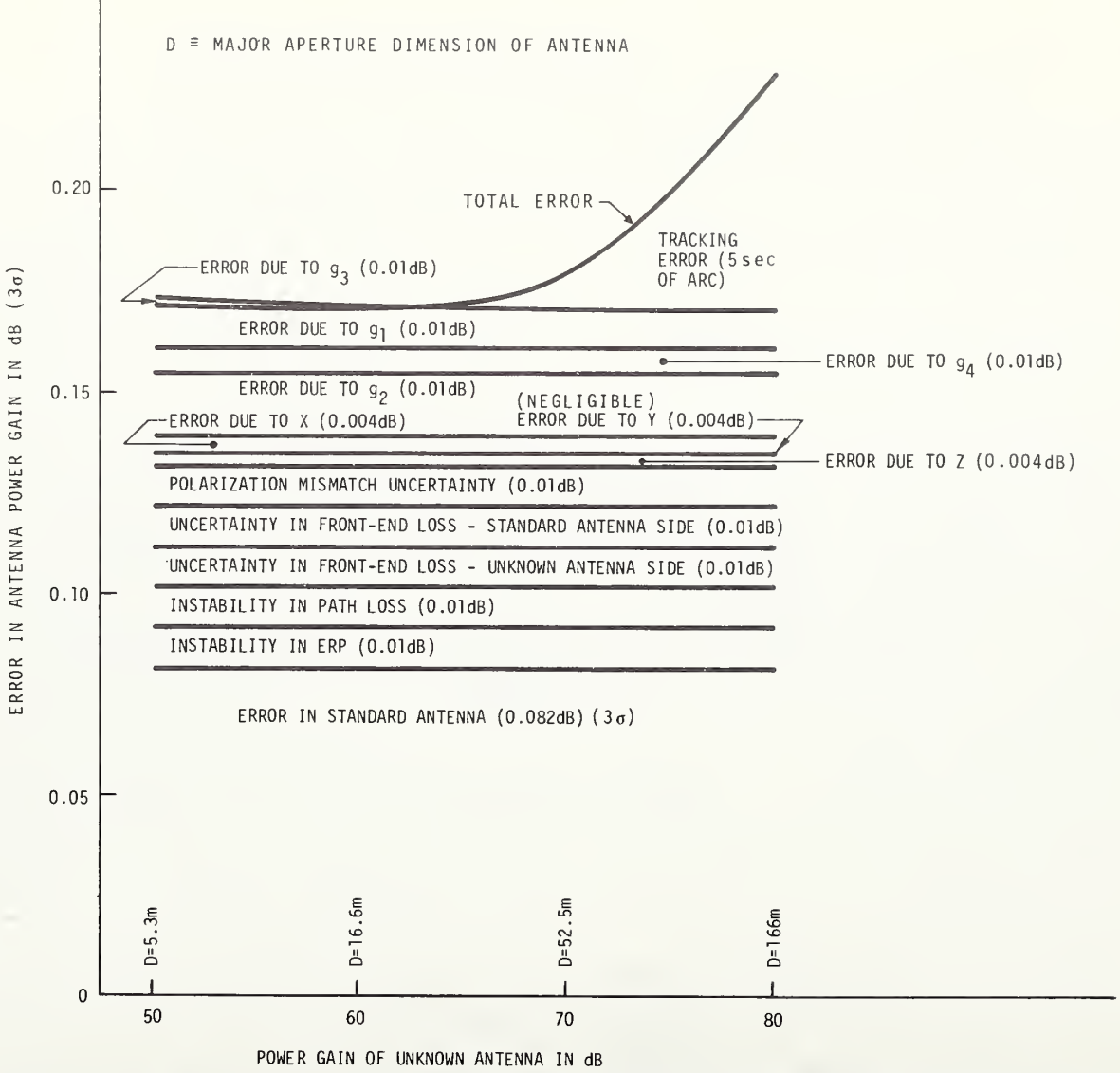

Figure 4-27. Linear error accumulation for the power gain of the large microwave antenna using the gain comparison method (frequency = 7.25 GHz, standard antenna gain = 40 dB nominal, effective radiated power = 30 dBW nominal).

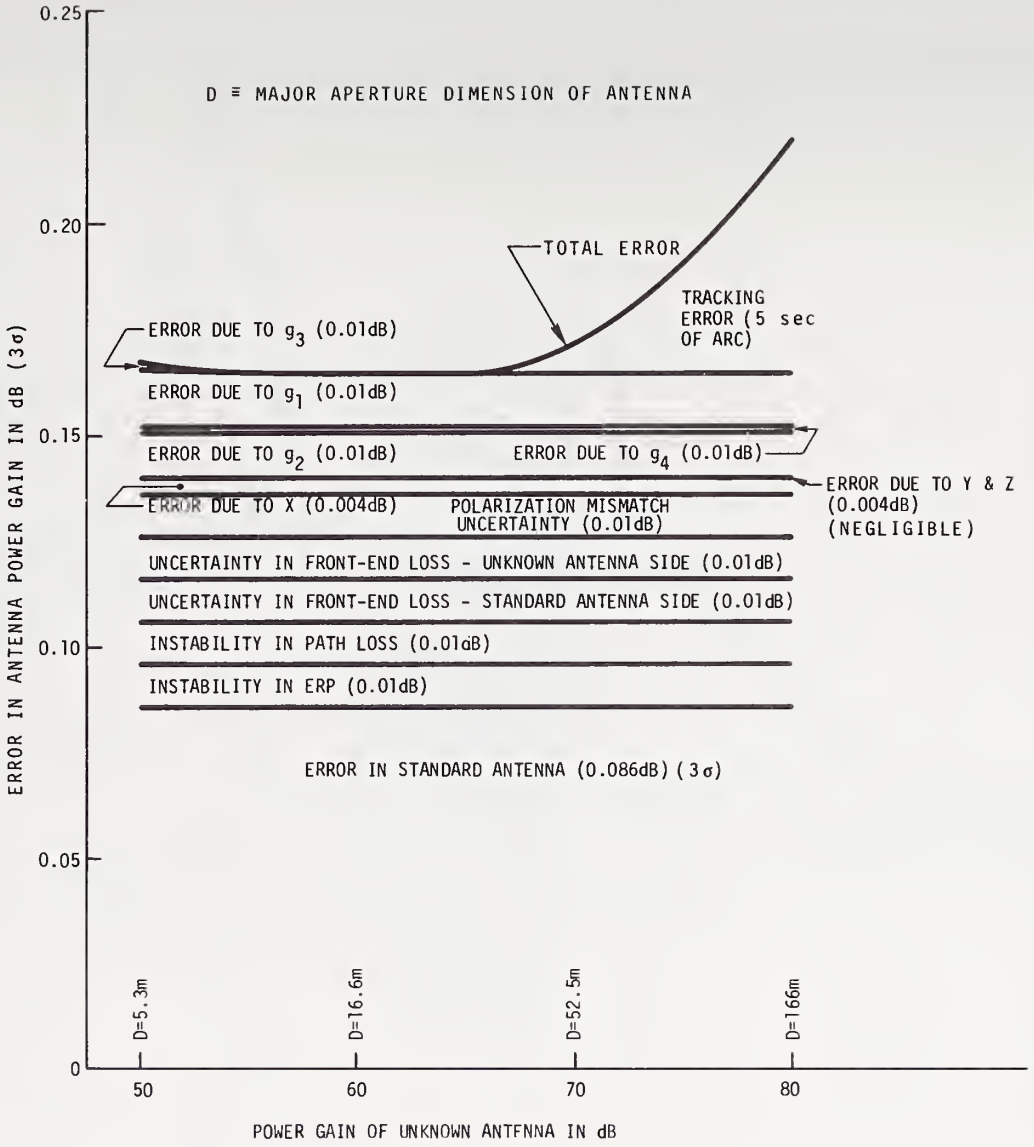

Figure 4-28. Linear error accumulation for the power gain of the large microwave antenna using the gain comparison method (frequency = 7.25 GHz, standard antenna gain = 50 dB nominal, effective radiated power = 30 dBW nominal).

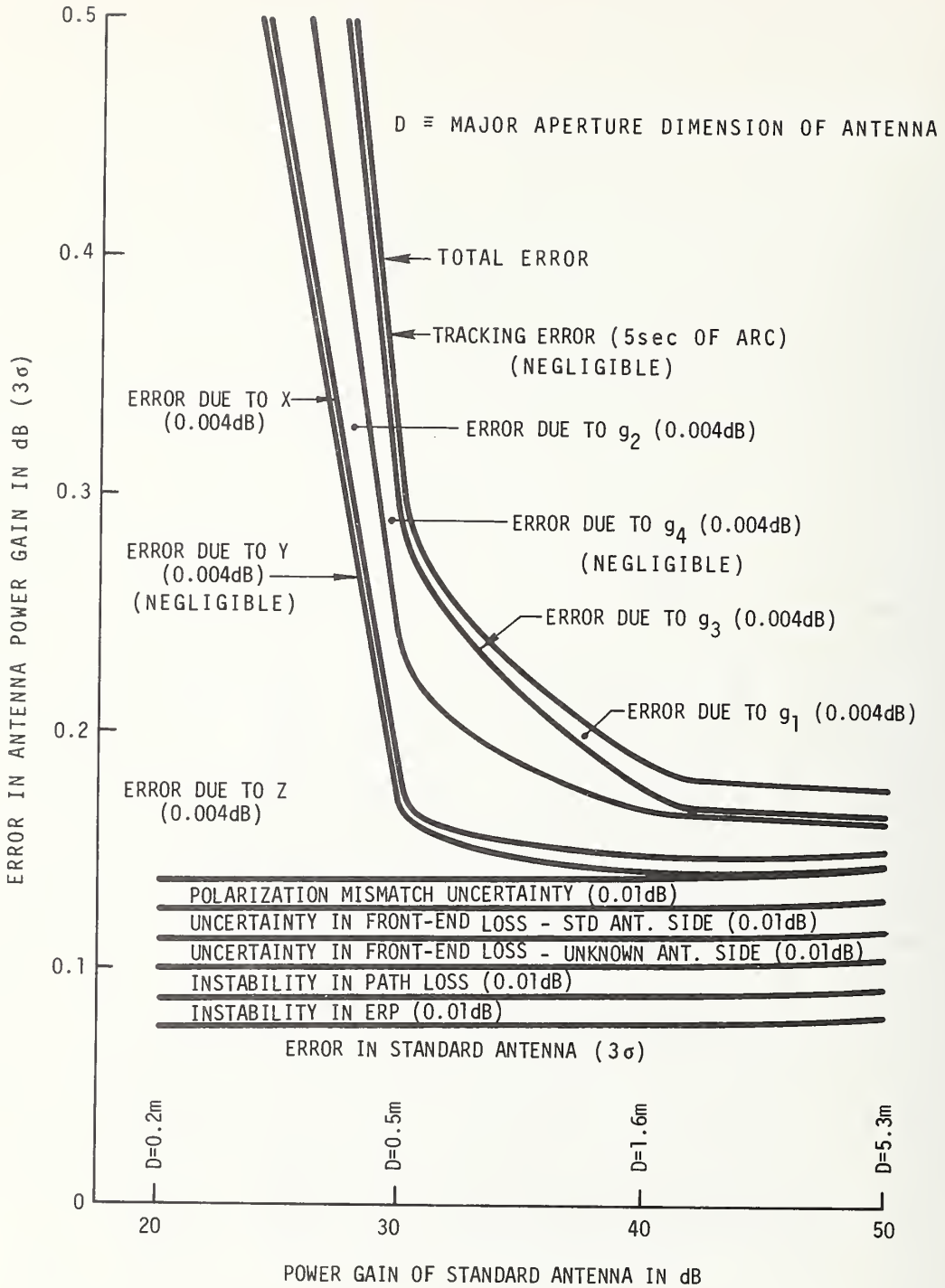

Figure 4-29. Linear error accumulation for the power gain of the large microwave antenna using the gain comparison method (frequency = 7.25 GHz, unknown antenna gain = 60 dB nominal, effective radiated power = 30 dBW nominal).

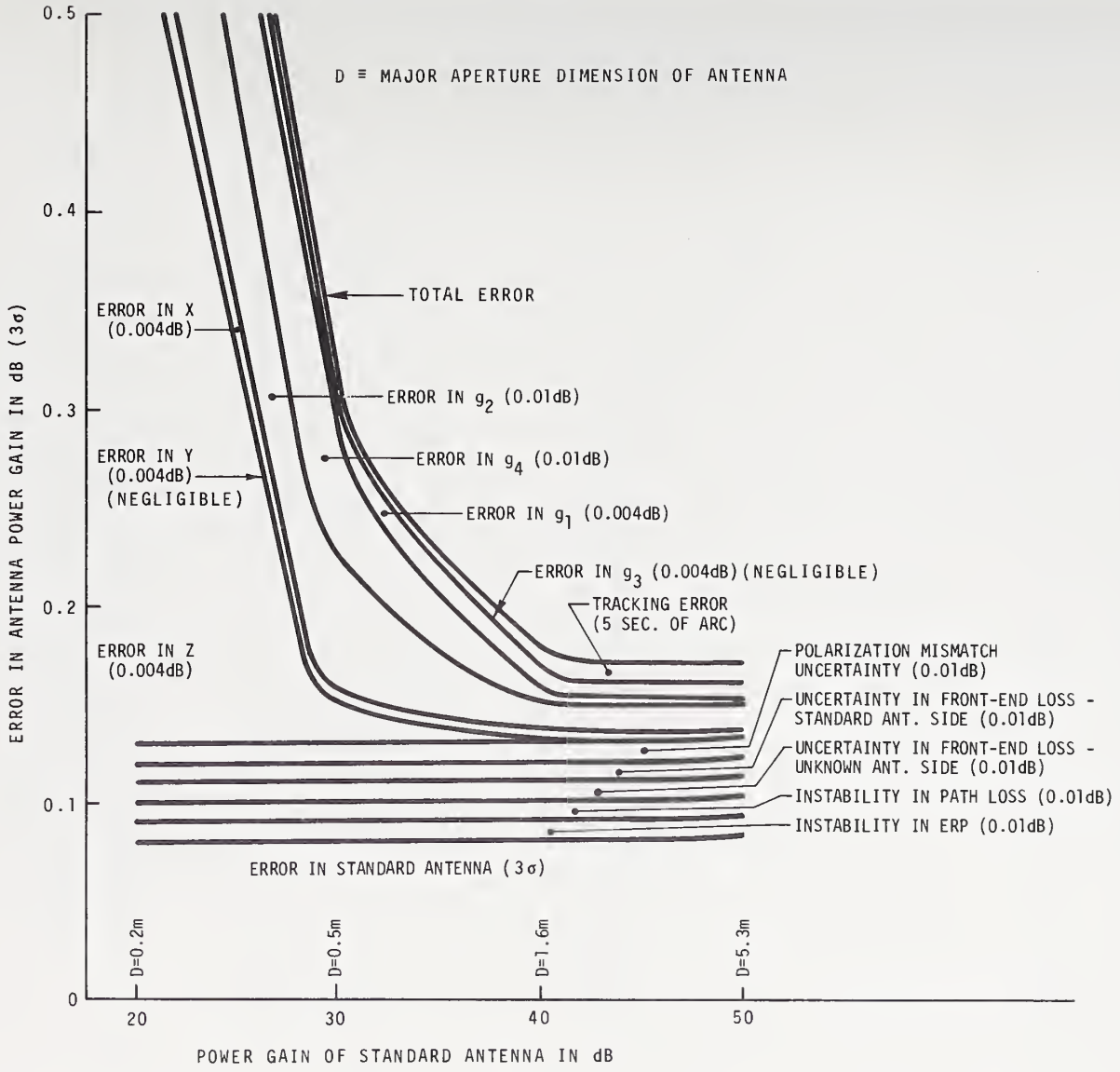

Figure 4-30. Linear error accumulation for the power gain of the large microwave antenna using the gain comparison method (frequency = 7.25 GHz, unknown antenna gain = 70 dB nominal, effective radiated power = 30 dBW nominal).

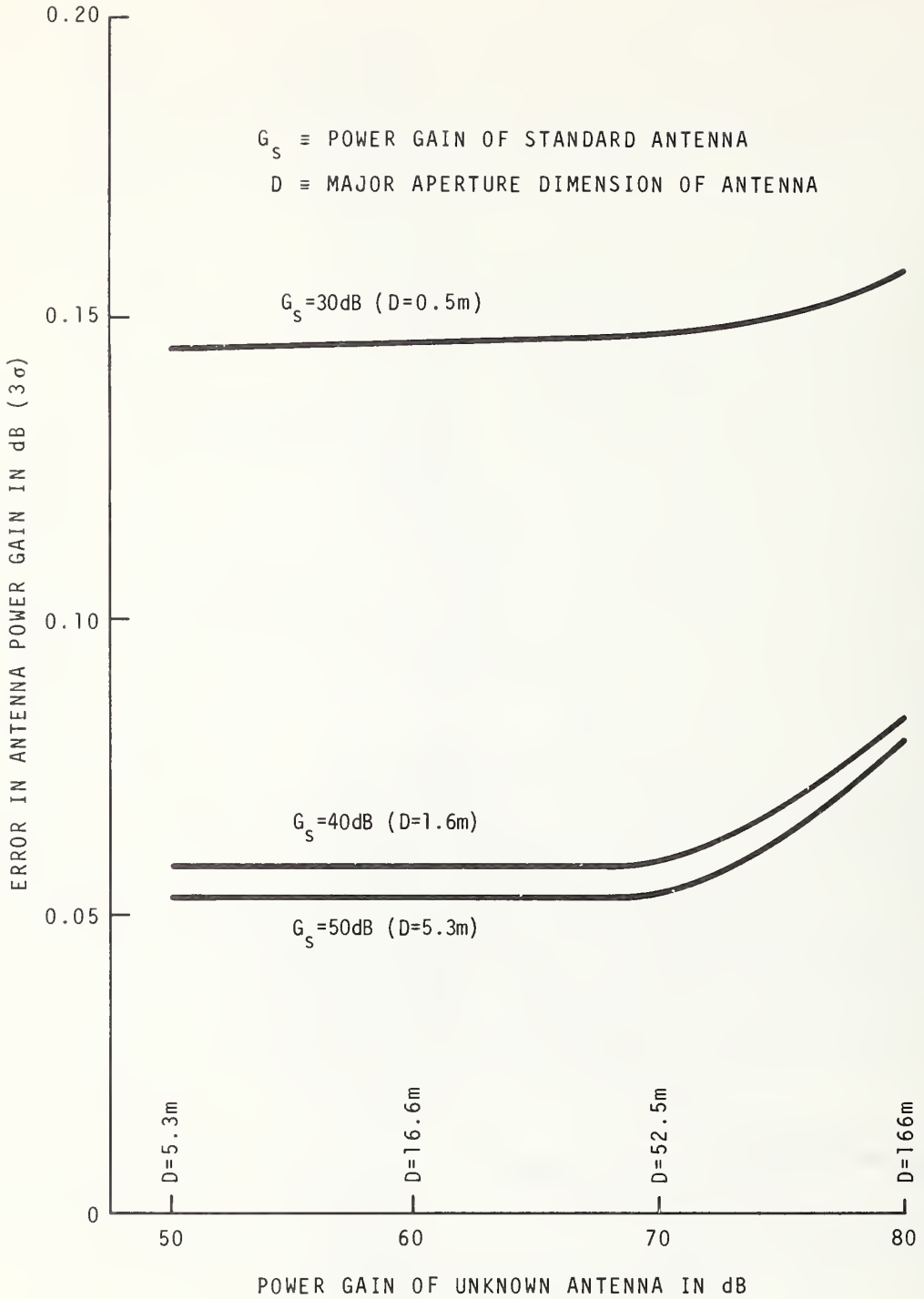

Figure 4-31. Quadrature error accumulation for the power gain of the large microwave antenna using the gain comparison method (frequency = 7.25 GHz, effective radiated power = 30 dBW nominal).

distance to be varied from 0.2 to 2 $\frac{D^2}{\lambda}$. In practice, it is almost impossible to construct and maintain such a long extrapolation range with sufficiently good stability and alignment.

The planar or possibly the spherical scanning technique promises better power gain calibration accuracy than the extrapolation method, particularly for larger standard gain antennas, if the necessary planar or spherical scanner is available. Although an error analysis has not yet been performed, it is estimated that the power gain of a 50-dB standard gain antenna with major aperture dimension of typically 5.3 m can be determined to within 0.1 dB by the planar near-field scanning technique.

It will be found from section 5 that a 60-dB ground antenna is required for calibrating Cas A. Therefore, it is generally necessary to use the gain comparison method to determine the power gain of a ground antenna which is intended for flux density measurements of Cas A. This procedure has established a lower bound on the error in the measured power gain of a typical, high-quality antenna, in which a 3σ random error estimate has been included along with various systematic errors. By use of a 40-dB standard gain antenna, it is possible to measure the power gain of a 60-dB ground antenna to within a linear accumulation error of 0.18 dB for 3σ limits or quadrature accumulation error of 0.06 dB for 3σ limits; this assumes use of the gain comparison method, and an ERP of 30 dBW. Therefore, 0.06 dB is a good estimate of the lower bound of the uncertainty within which a 60-dB ground antenna can be calibrated.

5. THE ACCURACY OF MEASURING THE FLUX DENSITY OF CAS A

In this report the term "practicable error" refers to calculations based upon the assumption that the measurement has been performed under careful but not quite state-of-the-art conditions; and the term "lower-bound error" refers to calculations based upon a best guess of the foreseeable state-of-the-art and ideal measurement conditions. In calculating practicable and lower-bound errors, the antenna gain error contributions are taken to be their linear and quadrature sums respectively. For example, the antenna-gain error contribution in Tables 5-1 and 5-2 are ± 0.18 dB (from figure 4-30) and 0.06 dB (from figure 4-31), which represent linear and quadrature error sums respectively in the calculation of the antenna gain errors. It should be pointed out that this procedure represents the particular viewpoint adopted in this report and not necessarily a standard procedure. A decision of how to sum error contributions depends heavily upon measurement conditions and the intended use of the error analysis.

Quadrature-sum estimates of the accuracy of measuring the flux density of Cas A are shown in figure 5-1 assuming that a noise-adding technique (appendix C) is used. The errors shown are obtained from computer printouts like the one in appendix B. For the estimate of practicable errors, the antenna gain was restricted to be less than 60-dB in order to avoid difficult, star-shape corrections. The contributions to the measurement errors at 7.25 GHz are listed in Tables 5-1 and 5-2. The best accuracy (lower-bound error) noted in the 2 to 16 GHz range in figure 5-1 is 1.4%. Therefore, the flux-density uncertainty of about ± 1% quoted in the recent literature is clearly not realistic.

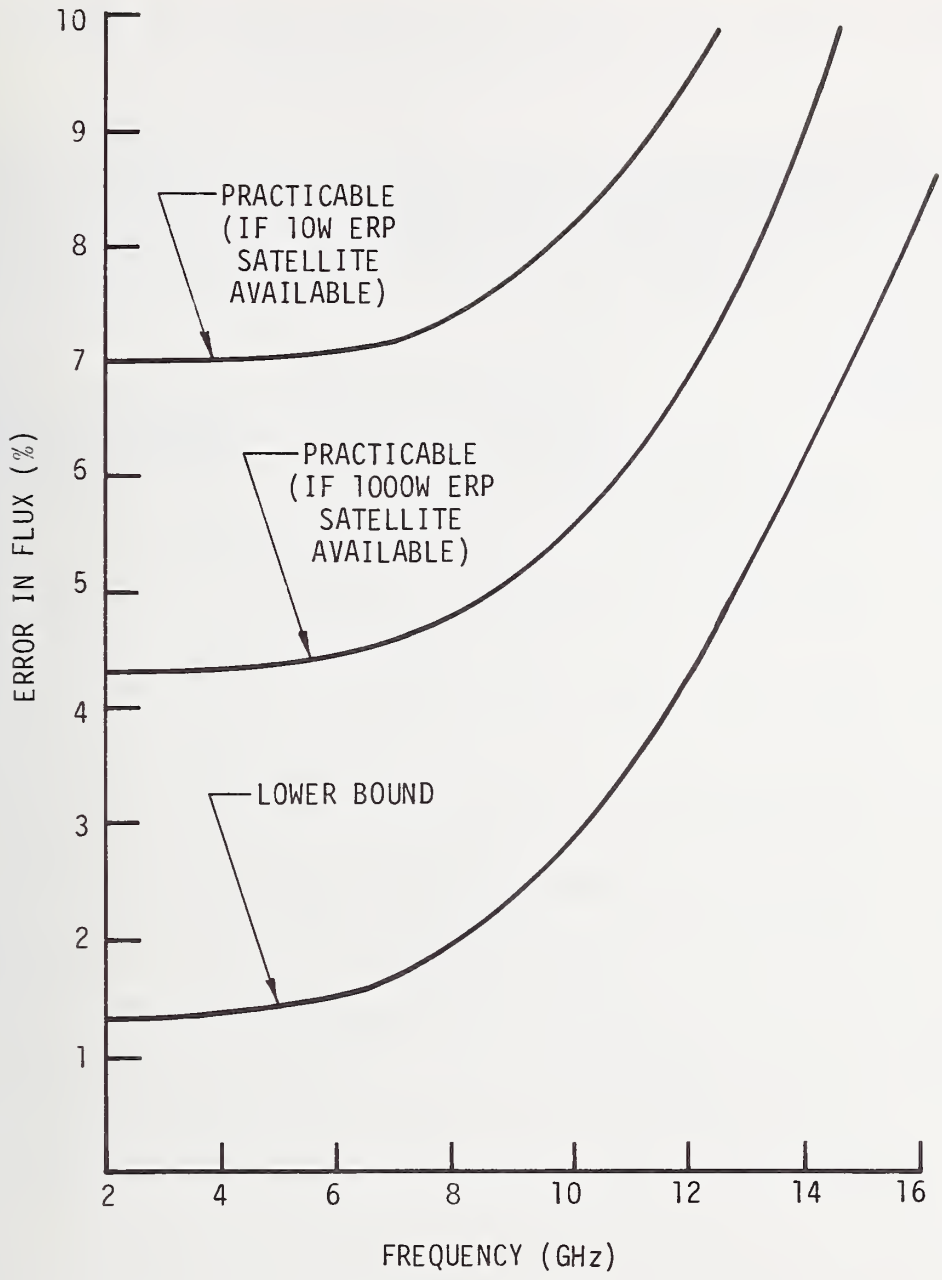

Figure 5-1 Practicable and lower bound errors in the measurement of the flux density of Cas A .

Table 5-1. The practicable error of measuring the flux density of Cas A at 7.25 GHz.

The following assumptions were used in calculating the errors: The system temperature referred to the output port of the antenna is 100 K; antenna beam efficiency is 55%; the HPBW (half power beamwidth) of the antenna is 70° divided by the diameter of the antenna expressed in free-space wavelengths (70° λ/D).

	Source of Error	Error Contribution to Measuring Flux
1.	Antenna gain (fig. 4-30) (59 ± 0.18 dB)	4.14%
2.	Temperature calibration standard (± 0.2%)	0.20%
3.	Temperature rise due to Cas A (22.2 ± 0.2 K)	0.90%
4.	Sky background (6 ± 0.3 K)	1.33%
5.	Atmospheric transmission (.98 ± 0.01)	1.02%
6.	Star shape correction, K_2 (.933 ± 0.007)	0.72%
7.	Antenna pointing (± 5% HPBW)	0.65%
	Quadrature sum	4.67%

Table 5-2. The lower bound error of measuring the flux density of Cas A at 7.25 GHz.

The following assumptions were used in calculating the errors: The system temperature referred to the output port of the antenna is 100 K; antenna beam efficiency is 55%; the HPBW of the antenna is 70° λ/D.

	Source of Error	Error Contribution to Measuring Flux
1.	Antenna gain (fig. 4-31) (59 ± 0.06 dB)	1.34%
2.	Temperature calibration standard (± 0.2%)	0.20%
3.	Temperature rise due to Cas A (22.2 ± 0.1 K)	0.45%
4.	Sky background (6 ± 0.2 K)	0.89%
5.	Atmospheric transmission (0.98 ± 0.001)	0.10%
6.	Star shape correction, K_2 (0.933 ± 0.0034)	0.36%
7.	Antenna pointing (± 2% HPBW)	0.10%
	Quadrature sum	1.73%

6. THE ACCURACY OF MEASURING G/T

The primary concern in this section is the accuracy of measuring G/T using Cas A. For comparison purposes, a few remarks will be addressed to the accuracy of determining G/T by separate measurements of gain and noise temperature.

6.1 The Measurement of G/T Using Cas A

The practicable accuracy of measuring G/T using Cas A is given in figure 6-1 in terms of quadrature error. The magnitude of this error depends on the magnitude of the G/T being measured. The measurement assumptions and the origin of the error contributions are tabulated in Table 6-1 for the frequency 7.25 GHz. The errors listed are estimates based on the assumption of reasonable, but not exceptional measurement conditions. The same information as given in figure 6-1, but using antenna diameter as the parameter, is shown in figure 6-2. The computer program and printout on which this figure is based are given in appendix B.

Estimates of the lower bound errors (best possible accuracy) are also shown in figure 6-2, and the origin of the error contributions are tabulated in Table 6-2. In this table a best guess of the foreseeable state-of-the-art under ideal measurement conditions is assumed, and in cases of doubt, the error has been underestimated.

6.2 Cas A Method of Measuring G/T Compared to the Gain/Noise Temperature Method

The practicable errors in the separate measurements of noise temperature, T_{ant}, and effective receiver input noise temperature, T_e, are independent of frequency for the frequency

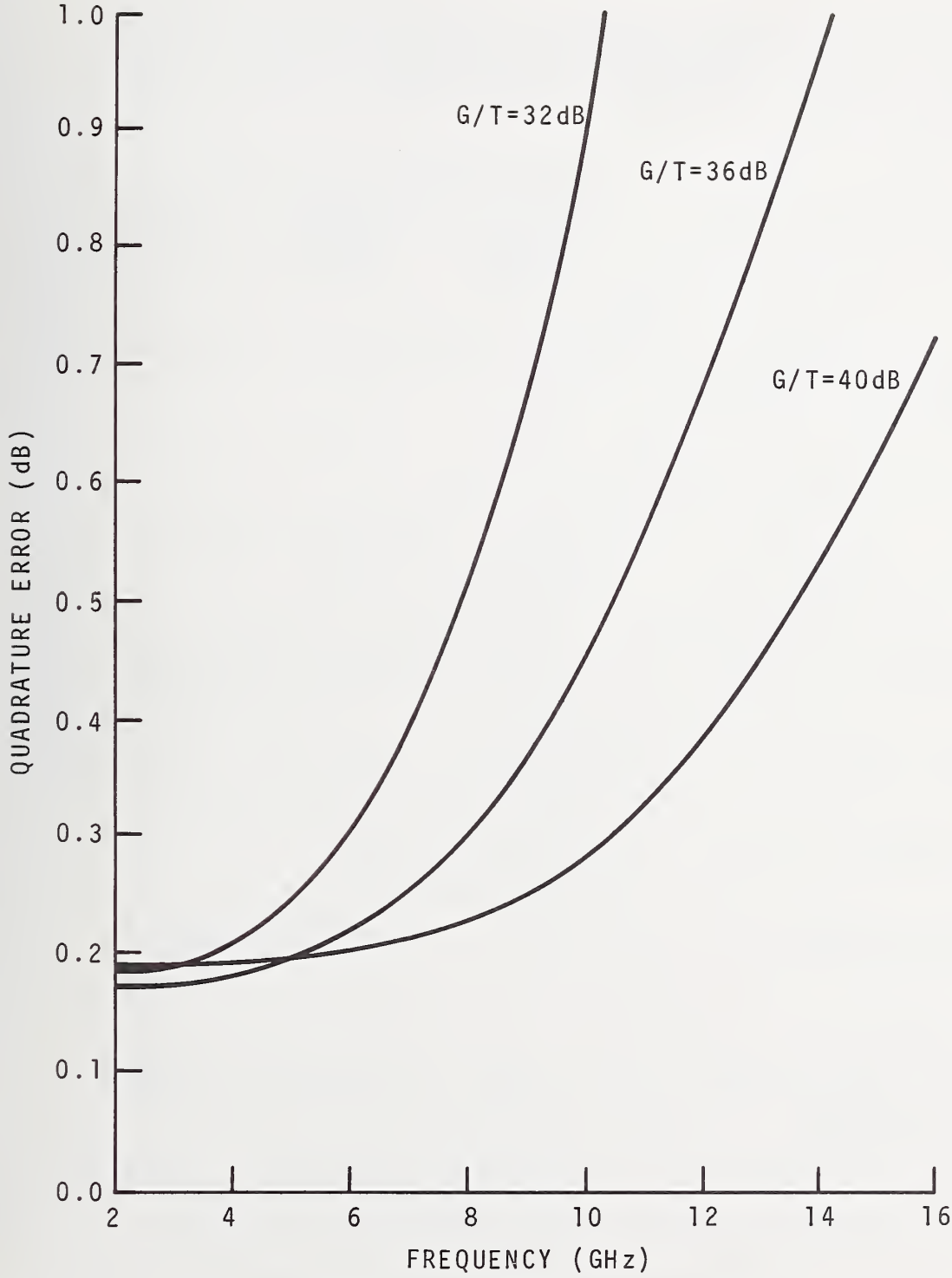

Figure 6-1 Practicable error in the measurement of G/T using Cas A.

Table 6-1. The practicable error of measuring G/T at 7.25 GHz using Cas A.

The following assumptions were used in calculating the errors: The system temperature referred to the output port of the antenna is 100 K; antenna beam efficiency is 55%; the HPBW of the antenna is 70° λ/D.

	Error Contribution to G/T in dB		
Antenna diameter =	11m(37')	18m(58')	28m(93')
G/T =	36 dB	40 dB	44 dB
G =	56 dB	60 dB	64 dB
Source of Error			
1. Flux Density of Cas A 700 fu ± 4.67%	0.194	0.194	0.194
2. Secular decay (6 mos.) 1.1 ± 0.15%/yr	0.004	0.004	0.004
3. Sky background 6 ± 0.3 K	0.101	0.043	0.019
4. Atmospheric transmission 0.98 ± 0.01	0.044	0.044	0.044
5. Star shape factor	(K_2=.965)	(K_2=.916)	(K_2=.807)
$K_2 \pm (1-K_2)0.1$	0.016	0.040	0.104
6. Bandwidth effect 1 ± 0.001	0.004	0.004	0.004
7. Antenna pointing ± 5% HPBW	0.028	0.028	0.028
8. Y-factor ± 0.01 dB	0.089	0.043	0.025
9. Resolution ± 0.01 dB	0.089	0.043	0.025
Quadrature Sum	0.248 dB	0.218 dB	0.230 dB

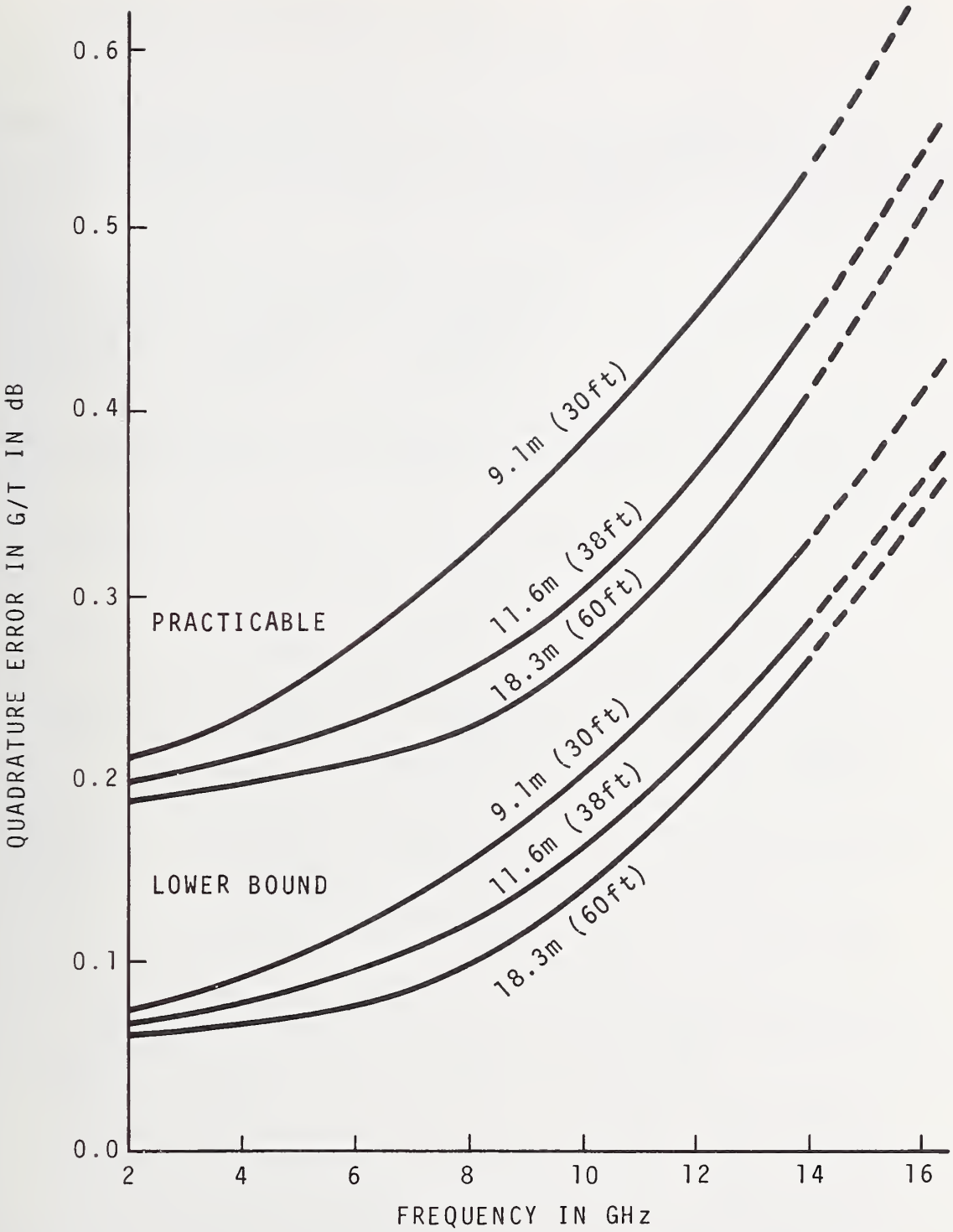

Figure 6-2 Practicable and lower bound errors in the measurement of G/T using Cas A.

Table 6-2. The lower bound error of measuring G/T at 7.25 GHz using Cas A.

The following assumptions were used in calculating the errors: The system temperature referred to the output port of the antenna is 100 K; antenna beam efficiency is 55%; the HPBW of the antenna is 70° λ/D.

	Error Contribution to G/T in dB		
Antenna diameter =	11m(37')	18m(58')	28m(93')
G/T =	36 dB	40 dB	44 dB
G =	56 dB	60 dB	64 dB
Source of Error			
1. Flux of Cas A 700 fu ± 1.73	0.075 dB	0.075 dB	0.075 dB
2. Secular decay (6 mos.) 1.1 ± 0.15%/yr	0.004	0.004	0.004
3. Sky background 6 ± 0.2 K	0.068	0.029	0.013
4. Atmospheric transmission 0.98 ± 0.001	0.004	0.004	0.004
5. Star shape factor	(K_2=.965)	(K_2=.916)	(K_2=.807)
K_2 ±(1-K_2)0.05	0.008	0.020	0.052
6. Bandwidth effect 1 ± 0.001	0.004	0.004	0.004
7. Antenna pointing ± 2% HPBW	0.005	0.005	0.005
8. Y-factor ± 0.003 dB	0.027	0.013	0.008
9. Resolution ± 0.005 dB	0.045	0.022	0.013
Quadrature Sum	0.114 dB	0.086 dB	0.094 dB

ranges considered here. The use of frequencies at which NBS calibration services are available has an advantage in practice. The practicable errors in measuring T_e and T_{ant} are noted in Tables 6-3 and 6-4. The error components of T_e are taken from reference [69] and for T_{ant} from reference [70]. Because the output port of the antenna may be defined at one of several reference points in the system, error contributions for two different values of T_e are shown in Tables 6-3 and 6-4.

For the best accuracy of the measurement of T_{sys}, there is some advantage in defining the antenna measurement plane as close to the preamplifier as possible. The practicable

Table 6-3. The practicable accuracy of measuring T_e. The basic measurement equation used to determine T_e is $T_e = (T_{hot} - Y\,T_{cold})/(Y - 1)$ where Y is the ratio of power at the receiver output port when T_{hot} then T_{cold} respectively are connected to the receiver input port. For the measurement of T_e we assume $T_{hot} = 300 \pm 0.1$K, and $T_{cold} = 80 \pm 0.2$K, that the reflection coefficient of these standards differs from that of the antenna such that $|\Gamma_{ant} - \Gamma_{std}| < 0.05$, and that the antenna to the receiver such that $|\Gamma_{ant} - \Gamma^*_{rec}| < 0.1$ [71].

Parameter uncertainty causing the error	Error Contribution to T_e in K	
	T_e = 30K	T_e = 70K
T_{hot}, ± 0.1K	0.05 K	0.07 K
T_{cold}, ± 0.2K	0.30	0.34
Y-factor, ± 0.01 dB	0.38	0.58
Receiver gain, ± 0.1%	0.17	0.25
Connector loss variation = 0.005 dB	0.38	0.42
Mismatch induced error	0.39	0.91
Quadrature sum	0.75 K	1.23 K

Table 6-4. The practicable error of measuring T_{ant}. It is assumed that a compensated radiometer with an effective input noise temperature of 100 K and a resolution of 0.005 dB is used to measure T_{ant}.

Source of the Error	Error Contribution to T_{ant} in K	
	T_{ant} = 70K	T_{ant} = 30K
T_{std} = 80 ± 0.2K	0.20K	0.20K
Extrapolation error (0.23% of temperature difference)	0.02	0.09
Resolution error	0.34	0.26
Quadrature sum	0.39K	0.34K

Table 6-5. The practicable accuracy of measuring G/T for frequencies near 7.25 GHz by separate measurement of antenna power Ggain G_{ant}, and system noise temperature, $T_{syst} = T_{ant} + T_e$. The basic measurement equation is $G/T = G_{ant}/T_{syst}$. It is assumed that a satellite with an ERP of 1000 W is available for the gain transfer calibration, and that T_{syst} = 100 K.

Source of Error	Error Contribution to G/T
G_{ant} (fig. 4-30)	0.18 dB
T_{ant} = 70 ± 0.39K	0.017
T_e = 30 ± 0.75K	0.033
Quadrature sum	0.184 dB

error components in a G/T determination by separate G and T measurements are tabulated in Table 6-5, where the practicable antenna gain error from figure 4-27 has been used. Table 6-5 can be compared with figures 6-1 and 6-2 to judge how an ideal G/T measurement using Cas A compares with an ideal measurement of G_{ant} divided by the ideal measurement of T_{sys}. For a 60-foot antenna and for frequencies near 7.25 GHz, the measurement error of G/T using Cas A differs in accuracy from the error in a measurement of G and T separately by less than 0.05 dB.

7. G/T MEASUREMENT REPEATABILITY

The use of Cas A to monitor ground station G/T changes, or to compare G/T ratios for separate but similar ground stations, requires only relative (not absolute) G/T determinations. The purpose of this section is to estimate to what repeatability these comparisons can be made for 60' antenna ground stations. The word "repeatability" as used here distinguishes between the usual G/T measurement precision (measurement scatter for a number of similar measurements performed over a short period) and how closely the averages of two sets of G/T measurements performed six months apart agree, assuming the G/T has not changed during this period. The repeatability estimated in this section will then be a limit beyond which two G/T measurements performed six months apart on a 60'-antenna ground station must differ if it is to be concluded that the ground station G/T has changed. This repeatability also gives an idea of how meaningfully relative G/T measurements between two similar 60'-antenna ground stations can be compared.

Table 7-1, which is an example of how the repeatability was estimated at 7 GHz for 33'- and 52'- antenna ground stations, gives a list of parameters that affect the repeatability. Similar estimates were performed to generate figure 7-1, which shows the repeatability for 33'- and 52'- antenna ground stations as a function of frequency. Although a similar graph for a 60'-antenna ground station was not generated, it can at least be inferred from figure 7-1 that the repeatability is better than 0.1 dB for frequencies less than 8 GHz. Therefore, for a 60'-antenna ground station with specifications similar to those in the example, G/T changes greater than 0.1 dB over periods less than or equal to six months can be positively identified.

Table 7-1. 7 GHz G/T measurement repeatability using Cas A.

The following assumptions were used in calculating the repeatability: the system temperature referred to the output of the antenna is 100 K; antenna beam efficiency is 55%; the HPBW of the antenna is 70° λ/D.

	Error Contribution to G/T in dB	
Antenna diameter =	16m(52')	10m(32')
G/T =	38.7 dB	34.8 dB
G =	58.7 dB	54.8 dB
Source of Error		
1. Secular decay (6 mos.) 1.1 ± 0.15%/yr	0.004 dB	0.004 dB
2. Sky background 6 ± 0.2K	0.035	0.083
3. Atmospheric transmission 0.98 ± 0.002	0.009	0.009
4. Antenna pointing ± 5% HPBW	0.028	0.028
5. Y-factor ± 0.01 dB	0.051	0.108
6. Resolution ± 0.01 dB	0.051	0.108
Quadrature sum	0.085 dB	0.176 dB

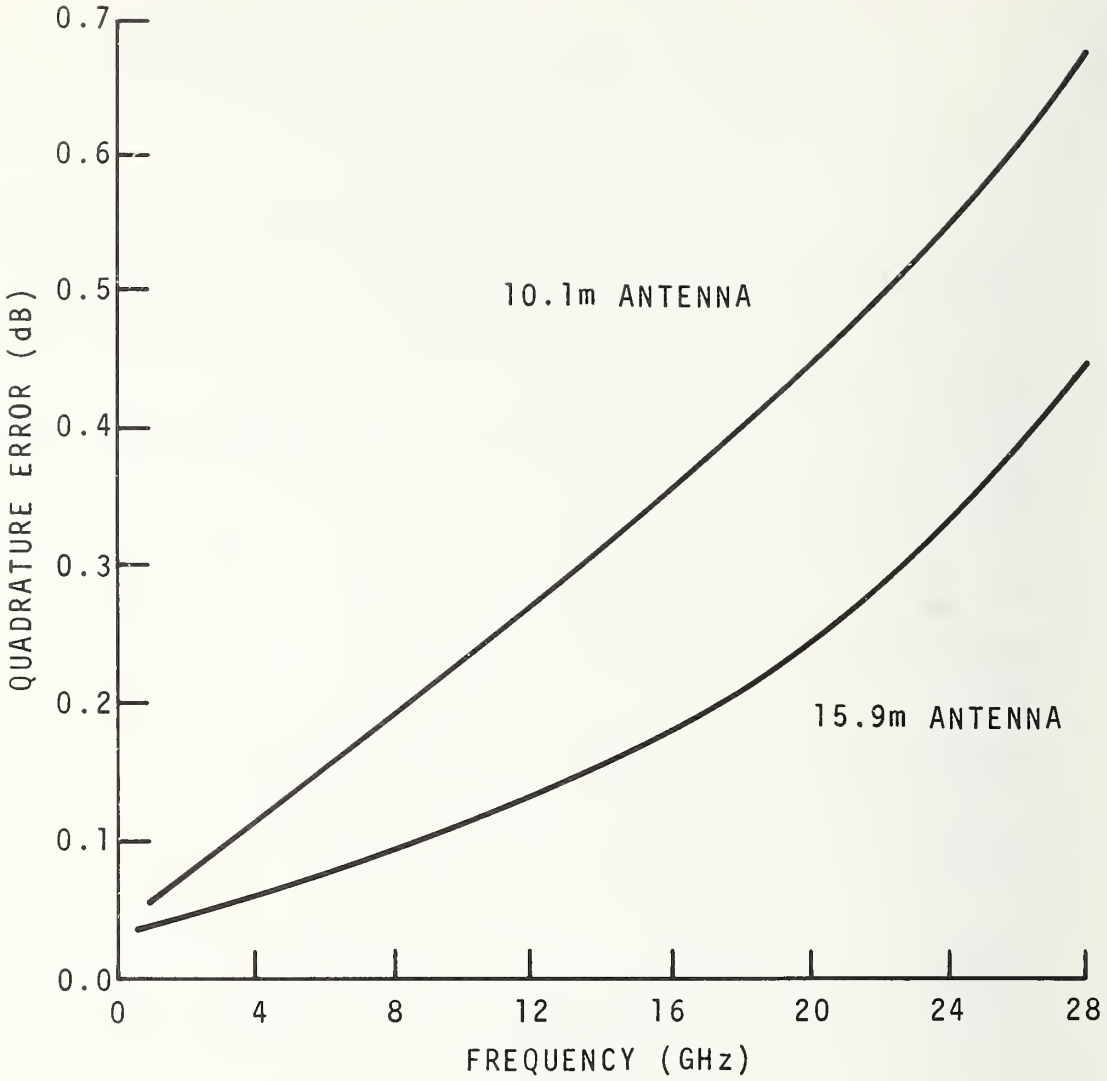

Figure 7-1 G/T measurement repeatability versus frequency.

8. CONCLUSIONS

As will be seen the use of Cas A to measure G/T is clearly the measurement technique that should be used in certain frequency and G/T ranges. Listed below are some of the prospects and problems concerning accurate G/T measurements.

8.1 The Accuracy of Measuring G/T

Several graphs and tables showing the lower-bound error (best possible accuracy) the practicable error of measuring G/T by the Cas A method have been presented and compared (section 6) with the accuracy of measuring G/T by a method in which antenna power gain and system noise temperature are measured separately from each other. We concluded (figure 6-2, Table 6-5) that for a 60'-antenna system operating at less than 8 GHz,

the practicable error (Cas A method) = ± 0.25 dB

the practicable error (gain-noise temperature method) = ± 0.18 dB

the lower bound error (Cas A method) = ± 0.10 dB

the lower bound error (gain-noise temperature method) = ± 0.07 dB

the repeatability (section 7) (Cas A Method) = ± 0.10 dB.

For this case, the potential accuracy of the gain-temperature method is a little better than the Cas A method, but we seriously doubt whether this advantage is often realized. This is because the gain-noise temperature method, as it is usually implemented, is a very difficult measurement: the difficulty is that the worst possible measurement plane, namely, the antenna output reference plane, is used for measuring system noise temperature. At this plane mismatch

errors are difficult to control, and noise temperatures to be measured have small magnitudes. Sometimes these measurements are further degraded when the temperature contributions of the diplexer and/or the antenna lead are calculated from data obtained in separate loss measurements. Better noise temperature measurements at a different measurement plane would alleviate these objections.

As seen in figure 6-2, lower-bound error for the 60'-antenna system is roughly one-third of the practicable error. Although we can visualize some of the practicable error contributions being reduced to their lower bound values, some errors not easily accounted for, making it unlikely that the total error can be reduced much below the practicable curve. Examples of possible causes of such errors are antenna gain and pointing hysteresis, harsh climatic conditions, antenna surface warping due to wind or temperature gradients, oxidizing, and antenna stress relief. To a certain extent, these time-dependent effects can be monitored within the repeatability, ± 0.1 dB (section 7), of the G/T measurement.

For half-power beamdwidths of 8.6' and larger, the antenna power gain pattern is sufficiently constant across the Cas A profile to permit using the flux density in calculating the antenna temperature with Cas A in the main beam. For smaller beamwidths, however, the antenna response must be calculated from a brightness contour map like figure 2-10 instead of using the flux density. (Restricting the beamwidth to twice the star width, or 8.6', is to a certain extent arbitrary, but to be more exact requires a convolution of the star map with the antenna power gain pattern.) Therefore, the use of Cas A is restricted to 8.6' HPBW (or greater) antennas, thereby setting an upper limit to the G/T (41 dB for a 100 K system noise temperature and a 0.55 antenna aperture efficiency)

that can be measured using Cas A. It can be seen from figure 6-1, that for less than 8 GHz, G/T ratios greater than 36 dB up to 41 dB maximum have about the minimum G/T error. This G/T range corresponds to (100K noise temperature, 0.55 antenna aperture efficiency) antenna diameter from 37' to 65' for systems operating at 7.25 GHz. Therefore, G/T ratios can be measured most accurately (for systems operating at 7.25 GHz) for antenna diameters from 37' to 65'.

8.2 The Accuracy of the Cas A Flux Densities Cited in the Literature

The most recent literature [29] quotes the uncertainty in Cas A flux density as about ± 1%. This uncertainty is comparable to some of the most accurate electromagnetic measurements made by the Electromagnetics Division at NBS; in particular it is better than the best noise temperature and antenna power gain measurements ever made at NBS. Because a flux density measurement intrinsically contains both a noise measurement, and an antenna power gain measurement under difficult field operations, the 1% value quoted above seems unrealistic.

There are many difficulties with obtaining an accurate flux density value for Cas A, namely: (1) accounting for flux density decay from the time of last measurement; (2) correcting for the difference between the measurement frequency and the frequencies at which Cas A data is available; (3) the star-shape correction -- there are hints that different portions of the star have different spectral indices (figure 2-11); (4) corrections for cosmic backgrounds -- especially when a background map is not available at the measurement frequency or when the antenna to be measured must be pointed to a location near Cas A because of the satellite location; (5) accounting for atmospheric effects -- diffraction, diffusive attenuation, apparent solid-angle, correction,

absorption, reradiation, temperature and humidity corrections, and (6) availability of equipment or personnel capable of the best measurement techniques.

Because there are many problems related to using published Cas A data for G/T measurements, a substantial effort is required to determine by a study of the published papers which of the experimenters have properly minimized their errors and have properly accounted for the various sources of uncertainty in their error estimates.

8.3 Proposed Future Effort

Several areas in which future effort seems to be needed have been uncovered during this study. These are discussed below.

8.3.1 Evaluation of the Literature

Some of the published radio astronomy papers are much too optimistic in estimating the accuracy of Cas A flux density measurements. More reliable flux density values can possibly be obtained by reanalyzing the various experimental results where presented in the literature so that the resulting accuracies conform to more realistic error appraisals.

8.3.2 Stars Other than Cas A for G/T Measurements

The use of Cas A looks very promising for the measurements of G/T. Still, other stars, the sun and the moon should also be examined to determine their utility. Their advantages as regards G/T, if any, should be tabulated. Cas A is not visible from some southern hemisphere ground stations. For certain measurements on small antennas, the moon and/or sun should be useful, and for larger antennas, smaller and weaker stars look interestingly useful.

8.3.3 Independent Methods for Measurement of G/T

It would be worthwhile to measure the G/T of a ground station by two independent methods. This approach almost always uncovers unsuspected errors and greatly increases the confidence placed in a particular method. The two methods discussed in this report (i.e., the Cas A method and the gain-noise temperature method) when used on one ground station, would be suitable for the purpose.

8.3.4 Definition of and Alternatives to G/T

There is a real need for a figure-of-merit performance parameter for a ground station, be it G/T or a substitute parameter. G/T is a useful figure-of-merit of a ground station, but the difficulties in its accurate determination must be recognized. It therefore seems worthwhile 1) to examine the details of the definition of G/T in order to determine whether an improved definition (from a measurement accuracy point of view) can be generated, and 2) to examine other possible figures-of-merit with regard to their suitability as substitutes for G/T that are amenable to more accurate measurement.

8.3.5 Uncertainties in Antenna Gain Measurements

The error budgets of flux density and G/T measurements are dominated by the uncertainty in measuring the power gain of standard gain antennas. This error source is therefore a key to improved G/T measurements. In the antenna analysis of this report we assumed the use of the extrapolation technique because it is currently the best implemented technique at NBS. The planar-near-field calibration technique and the spherical-near-field technique look promising especially for large

antennas for improving gain accuracy. The planar technique has been developed, and a near-field planar scanning range that can accommodate 40-dB standard gain antennas at 7.25 GHz has recently been constructed at NBS. The spherical technique is in its early stages of development; no spherical range has ever been built, and there is therefore no experimental experience with it. Further development and analysis of these techniques would be very valuable in further reducing the major error source in G/T measurements.

8.3.6 Radio Star Method of Measuring G and T

It would be useful to examine the separate measurements of G and T by use of radio stars. Although the measurements proposed are independent, the topics are related. Some of the theory for such measurements is contained in appendix C. This theory should be extended to measurements of G and T by techniques that do not require breaking into the antenna system. If this were done, the resulting technique would have the same measurement convenience as the Cas A method of measuring G/T. This becomes possible if one chooses the measurement reference plane to be at the aperture of the feed horn in the antenna instead of at the output of the antenna.

Acknowledgment

The authors appreciate the extensive and critical technical review given this report by Dr. H. M. Altschuler. His criticism was very helpful.

REFERENCES

[1] Miller, C.K.S., Daywitt, W.C., and Arthur, M.G., "Noise Standards, Measurements, and Receiver Noise Definitions," Proc. IEEE, 55, No. 6, 865-877 (June 1967).

[2] "IEEE Standard Definitions of Terms for Antennas," IEEE Std. 145-1973, 18 pages (Aug. 2, 1973).

[3] "Electrical and Mechanical Characteristics of Antennas for Satellite Earth Stations," Electronic Industries Association, EIA RS-411, 77 pages (Aug. 1973).

[4] "Satellite Communications Reference Handbook," Defense Communications Agency, National Technical Information Service Document AD 7461 65 (July 1972).

[5] Kreutel, R.W., Jr. and Pacholder, A.O., "The Measurement of Gain and Noise Temperature of a Satellite Communications Earth Station," Microwave Journal, 12, No. 10, 61-66 (Oct. 1969).

[6] Kraus, John D., "Radio Astronomy," (McGraw-Hill Book Co., New York, 1966).

[7] Ryle, M. and Smith, F.G., "A New Intense Source of Radio-Frequency Radiation in the Constellation of Cassiopeia," Nature, 162, No. 4116, 462-463 (Sept. 1948).

[8] Baade, W. and Minkowski, R., "On the Identification of Radio Sources," Astrophysical Journal, 119, No. 1, 215-231 (Jan. 1954).

[9] Minkowski, R., "Radio Astronomy" (I.A.U. Symposium No. 4, 1955) Cambridge, England, 114 (1957).

[10] Minkowski, R., "Optical Observations of Nonthermal Galactic Radio Sources," Paris Symposium on Radio Astronomy; International Astronomical Union & URSI, No. 61, Pt. III, 315-322 (July 30-Aug. 6, 1958).

[11] Minkowski, R., "Nebulae and Interstellar Matter" (Univ. of Chicago Press, 1968).

[12] Brown, R.H., Jennison, R. and Das Gupta, M., "Apparent Angular Sizes of Discrete Radio Source-Observations at Jordell Bank, Manchester," Nature, 170, 1061 (1952).

[13] Smith, F.G., "Apparent Angular Sizes of Discrete Radio Sources," Nature, 170, No. 4338, 1061-1065 (Dec. 20, 1952).

[14] Rosenberg, Ivan, "Distribution of Brightness and Polarization in Cassiopeia A at 5.0 GHz," Mon. Not. R. Astr. Soc., 151, No. 1, 109-122 (1970).

[15] Bergh, S. vanden and Dodd, W.W., Preprint, 1970.

[16] Pauliny-Toth, I.I.K. and Kellermann, K.I., "Measurements of the Flux Density and Spectra of Discrete Radio Sources at Centimeter Wavelengths. II. The Observations at 5 GHz (6 cm)," Astronomical Journal, 73, No. 10, Pt. 1, 953-969 (Dec. 1968).

[17] Dmitrenko, D.A., Tseitlin, N.M., Vinogradova, L.V., and Gitterman, K.F., Radiofizika, 13, 823 (1970).

[18] Medd, W.J., "Absolute Flux Density Measurements at Centimeter Wavelengths," Astrophysical Journal, 171, No. 1, 41-50 (Jan. 1, 1972).

[19] Dent, W.A. and Haddock, F.T., "The Extension of Non-Thermal Radio-Source Spectra at 8000 Mc/s," Astrophysical Journal, 144, No. 2, 568-586 (May 1966).

[20] Stankevich, K.S., "Precision Measurements of the Spectrum of the Discrete Source Cassiopeia-A in the Centimeter Region," Soviet Astronomy - AJ, 6, No. 4, 480-482 (Jan.-Feb. 1963).

[21] Lastochkin, V.P., Plankin, E.S., and Stankevich, K.S., "Precision Measurement of the Flux of Radio Emission from the Discrete Source Cassiopeia-A at λ = 3.2 cm," Radiophysics and Quantum Electronics, 6, No. 3, 382-383 (1963).

[22] Baars, J.W.M., Mezger, P.G., and Wendker, H., "The Spectra of the Strongest Non-Thermal Radio Sources in the Centimeter-Wavelength Range," Astrophysical Journal, 142, No. 1, 122-134 (July 1, 1965).

[23] Shklovsky, I.S., "Supernovae" (John Wiley and Sons Ltd., New York, 1968).

[24] Brosche, Peter, "Supernova Gesucht!," Stern und Weltraum (in German), 6, 198-202 (1967).

[25] Högborm, J.A. and Shakeshaft, J.R., Nature, 189, 561 (1961).

[26] Scott, P.F., Shakeshaft, J.R., and Smith, M.A., "Decrease of Flux Density of the Radio Source Cassiopeia A at 81.5 MHz," Nature, 223, No. 5211, 1139-1140 (Sept. 13, 1969).

[27] Mayer, C.H., McCullough, T.P., Sloanaker, R.M., and Haddock, F.T., "Secular Variation of the λ 9.4-cm Radio Emission from Discrete Sources," Astrophysical Journal, 141, No. 3, 867-872 (1965).

[28] Findlay, J.W., "The Flux Density of Cassioepia A at 1440 MHz and its Rate of Decrease," Astrophysical Journal, 174, No. 2, Pt. 1, 527-528 (June 15, 1972).

[29] Barrs, J.W.M. and Hartsuijker, A.P., "The Decrease of Flux Density of Cassiopeia A and the Absolute Spectra of Cassiopeia A, Cygnus A and Taurus A," Astronomy and Astrophysics (a European Journal), 17, No. 2, 172-181 (1972).

[30] Pauliny-Toth, I.I.K. and Shakeshaft, J.R., "A Survey of the Background Radiation at a Frequency of 404 Mc/s," Royal Astronomical Society Monthly Notices, 124, No. 1, 61-77 (May 1962).

[31] Gardner, F.F. and Davies, R.D., "The Polarization of Radio Sources," Aust. J. Phys., 19, 441 (1966).

[32] Baars, Jacob W.M., "The Measurement of Large Antennas with Cosmic Radio Sources," IEEE Trans. Antennas & Propagation, AP-21, No. 4, 461-474 (July 1973).

[33] Allen, Ronald John, "Observations of Several Discrete Radio Sources at 3.64 and 1.94 Centimeters," Mass. Inst. Tech., Doctor's Thesis, 162 pages (Jan. 1967).

[34] Mayer, C.H. and Hollinger, J.P., "Polarized Brightness Distribution Over Cassiopeia A, the Crab Nebula, and Cygnus A at 1.55-cm Wavelength," Astrophysical Journal, 151, Pt. 1, 53-63 (Jan. 1968).

[35] Boland, J.W., Hollinger, J.P. Mayer, C.H. and McCullough, T.P., "Polarization of Cygnus A, Taurus A, and Cassiopeia A at 2.07 Centimeters," Astrophysical Journal, 144, No. 1, 437-439 (April 1966).

[36] Ryle, M., Elsmore, B. and Neville, Ann C., "High-Resolution Observations of the Radio Sources in Cygnus and Cassiopeia," Nature 205, No. 4978, 1259-1262 (March 27, 1965).

[37] Dicke, R.H., Peebles, P.J.E., Roll, P.G., and Wilkinson, D.T., "Cosmic Black-Body Radiation," Astrophysical Journal, 142, No. 1, 414-419 (July 1, 1965).

[38] Penzias, A.A. and Wilson, R.W., "A Measurement of Excess Antenna Temperature at 4080 Mc/s," Astrophysical Journal, 142, No. 1, 419 (1965).

[39] Roll, P.G. and Wilkinson, David T., "Cosmic Background Radiation at 3.2 cm -- Support for Cosmic Black-Body Radiation," Physical Review Letters, 16, No. 10, 405-407 (March 7, 1966).

[40] Ewen, H.I. and Purcell, E.M., "Observation of a Line in the Galactic Radio Spectrum," Nature, 168, No. 4270, 356 (Sept. 1, 1951).

[41] Wilson, A.W. and Penzias, A.A., "The Flux Density of Six Radio Sources at 4.08 GHz," Astrophysical Journal, 146, No. 1, 286-287 (Oct. 1966).

[42] Lynds, C.R., "Observations of H II Regions at 1400 Mc," Publ. National Radio Astronomy Observatory, 1, No. 3, 43-62 (May 1961).

[43] RaghavaRao, R., Medd, W.J., Higgs, L.A. and Broten, N.W., "Survey of 9.4 cm Radio Emission in Cassiopeia and Cepheus," Royal Astronomical Society Monthly Notices, 129, No. 2 159-168 (plus 5 plates)(1965).

[44] Howell, T.F. and Shakeshaft, J.R., "Attenuation of Radio Waves by the Troposphere Over the Frequency Range 0.4-10 GHz," J. Atmospheric and Terrestrial Physics, 29, No. 7, 1559-1571 (July 1967).

[45] Yokoi, H.M. and Yamada, T. Satoh, "Atmospheric Attenuation and Scintillation of Microwaves from Outer Space," Pub. Astrn. Soc. of Japan, 22, No. 4, 511 (1970).

[46] Snider, J.B. and Westwater, Ed R., "Atmospheric Attenuation at 15, 31, and 53 GHz," ESSA Tech. Report ERL 156-WPL 11, 84 pages (Dec. 1969).

[47] "Influence of the Non-Ionized Regions of the Atmosphere on the Propagation of Waves," CCIR Plenary Assembly Report No. 234-1 (1966).

[48] Kuz'min, A.D. and Salomonovich, A.E., "Radioastronomical Methods of Antenna Measurements" (Academic Press, New York, 182 pages, 1966).

[49] "U.S. Standard Atmosphere, 1962" (Washington, D.C., for sale by the Superintendent of Documents, U.S. Government Printing Office, Washington 25, D.C.).

[50] Dicke, Robert H., Beringer, Robert, Kyhl, Robert, and Vane, A.B., "Atmospheric Absorption Measurements with a Microwave Radiometer," Physical Rev., 70, Nos. 5 & 6, 340-348 (Sept. 1 & 15, 1946).

[51] Schelkunoff, S.A., "Electromagnetic Waves" (Van Nostrand, New York, 1943).

[52] Slayton, W.T., NRL Rpt. No. 4433, Naval Res. Lab., Washington, D.C. (1954).

[53] Braun, E.H., "Gain of Electromagnetic Horns, Proc. I.R.E., 41, No. 1, 109-115 (Jan. 1953).

[54] Chu, T.S. and Semplak, R.A., "Gain of Electromagnetic Horns," Bell System Technical Journal, 44, No. 1, 527-537 (March 1965).

[55] Treytlin and Kinher, "Measurements of Directive Gain of Horn Antennas at a Short Distance," Radio Eng. and Electronics Phys., 10, 10-16 (Jan. 1965).

[56] Kerns, D.M., "New Method of Gain Measurement Using Two Identical Antennas," Electronics Letters, 6, 348-349 (May 1970).

[57] Baird, R.C., Newell, A.C., Wacker, P.F., and Kerns, D.M., "Recent Experimental Results in Near-Field Antenna Measurements," Electronics Letters, 6, 349-351 (May 1970).

[58] Newell, A.C. and Kerns, D.M., "Determination of Both Polarisation and Power Gain of Antennas by a Generalised 3-Antenna Measurement Method," Electronics Letters, 7, No. 3, 68-70 (Feb. 11, 1971).

[59] Newell, A.C., Baird, R.C., and Wacker, P. F., "Accurate Measurement of Antenna Gain and Polarization at Reduced Distances by an Extrapolation Technique," IEEE Trans. on Antennas and Propagation, AP-21, No. 4, 418-423 (July 1973).

[60] Wacker, Paul F., "Theory and Numerical Techniques for Accurate Extrapolation of Near-Zone Antenna and Scattering Measurement," Unpublished NBS Report, 40 pages (April 1972).

[61] Kerns, D.M., "Correction of Near-Field Antenna Measurements Made with an Arbitrary but Known Measuring Antenna," Electronics Letters, 6, No. 11, 346-347 (May 28, 1970).

[62] Kerns, David M., "Plane-Wave Scattering Matrix and Generalized Reciprocity Relations for Antennas and Scatterers," Unpublished NBS Report, 57 pages (June 1972).

[63] Kerns, D.M., Private Communications.

[64] Wacker, Paul F., "Theory and Numerical Techniques for Accurate Extrapolation of Near-Zone Antenna and Scattering Measurements," Unpublished NBS Report, 40 pages (April 1972).

[65] Larson, Wilbur and Campbell, Eugene, "Microwave Attenuation Measurement System (Series Substitution)," NBS Tech. Note 647 (Feb. 1974).

[66] Hiroshi, Yokoi, Yamada, Matsuichi, and Satch, Toshio, "Atmospheric Attenuation and Scintillation of Microwaves from Outer Space," Publ. of Astronomical Society of Japan, 22, No. 4, 511-524 (1970).

[67] Hartop, Bob, "Design Curves Speed Antenna Polarization-Loss Calculations," MicroWaves, 3, No. 8, 24-27.

[68] Zolnay, Stephen L., "Performance Characteristics of Communication Systems Employing Near-Synchronous (IDCSP) Satellites," Ohio State University, Technical Report 2358-6, 371 pages (June 21, 1968).

[69] Wait, D.F. and Nemoto, T., "Measurement of the Noise Temperature of a Mismatched Noise Source," IEEE Trans. on Microwave Theory and Techniques, MTT-16, No. 9, 670-675 (Sept. 1968).

[70] Wait, D.F., "The Precision Measurement of Noise Temperature of Mismatched Noise Generators," IEEE Trans. on Microwave Theory and Techniques, MTT-18, 715-724 (Oct. 1970).

[71] Engen, Glenn F., "Mismatch Considerations in Evaluating Amplifier Noise Performance, IEEE Trans. on Instrumentation and Measurement, IM-22, No. 3, 274 (Sept. 1973).

[72] Mattes, J.E., "Verification of the Figure of Merit of Earth Stations for Satellite Communications," Proc. IREE, 61, No. 4, 77-84 (April 1973).

[73] Wait, David F., "Thermal Noise from a Passive Linear Multiport," IEEE Trans. Microwave Theory and Techniques, MTT-16, No. 9, 687-691 (Sept. 1968).

APPENDIX A: COMMENTS ON THE INTRODUCTORY SECTIONS

Section 1.1

1. The system as defined in section 1.1 is time varying, and care must be taken to insure that the state of the system at the time its G/T is measured is adequately specified. At least the following parameters should be specified or implied when reporting a value for G/T: the epoch and time of day when the measurements were taken; the longitude and latitude of the antenna site; the measurement frequency or frequencies; the antenna polarization; and, if the antenna is steerable, its pointing angles.

2. The on-axis power gain of the antenna is the maximum of the antenna power pattern which is assumed to be measured in the far field of the antenna with all attenuation effects of the atmosphere removed, i.e., the gain assuming no atmosphere.

3. It should be recognized that the power gain of an antenna is a transmitting concept and can be used for a receiving antenna only if the antenna is reciprocal. However, a quantity can be defined for a non-reciprocal receiving antenna that is analogous to the power gain of a transmitting antenna. This point needs to be expanded in a later phase of the G/T project, and the results should properly be included in any formal definition of G/T.

4. It should be noted that the system noise temperatures defined in section 1.1 are combinations of real noise temperatures and effective input noise temperatures.

5. The IEEE defines G/T [2] as the ratio of antenna gain to antenna noise temperature. In contrast, the G/T ratios discussed in section 1.1 are antenna gain to system noise temperature ratios, and are consequently more appropriate measurands of ground station performance.

Section 1.2

It is implicitly assumed throughout these introductory sections that the noise radiated by the satellite is insignificant compared to the noise associated with the ground station which includes the cosmic and terrestrial noise. It should be expressly noted that the system noise temperature T includes only the latter noise contributions and not the satellite noise.

If the ground station noise does not predominate over the radiated satellite noise, then n of section 1.2 includes the satellite noise and the following expression [72] for the carrier-to-noise ratio must be used:

$$\frac{C}{n} = \frac{(G/T)(ERP)L}{k + (G/T)n_s L}$$

where n_s is referred to the satellite and corresponds to the satellite noise. The other parameters are defined in section 1.2.

Section 1.4

1. A number of assumptions were made in section 1.4 to simplify the presentation. These assumptions include: the radio star is treated as a point source of unpolarized radiation; the atmospheric attenuation of the power from the radio star is zero; and the radio star is positioned in the center of the antenna main beam during the first part of the measurement.

2. The brightness temperature of the radio star is that thermodynamic temperature to which a black body of the same angular extent and position as the star must be raised in order for its flux density to equal that of the radio star.

APPENDIX B: COMPUTER PRINTOUT AND PROGRAMS

The error contributions to the total error in the measurement of the Cas A flux density and a ground station G/T have been completed for various sets of parameters. The computer printouts for G/T are included here in appendix B.1, some computed errors of which have been used in section 5. Appendix B.2 gives the basic program for the G/T error computations, and since this program is only slightly more comprehensive than the program for the flux density error computations, the latter has been omitted.

B.1 A Printout for the Practicable Accuracy of G/T

This printout lists the input variables and assumptions first. The errors contributed to measured values of G/T by the nine error sources listed are tabulated in the last four columns. The meaning of the information in the first three columns (three deep) is as follows:

Heading	Meaning
G/T(DB)	The value of G/T assumed in the calculation.
Y(DB)	The Y-factor of eq. (1.9) expressed in decibels.
G(D)	The power gain of the antenna.
FLUX(FU)	The magnitude of the flux density of Cas A that has been assumed for the calculation expressed in flux units: 1 F.U. = 10^{-26} Watts/m^2/Hz.
+-LINE	The linear accumulation of the nine error contributions to the error in measuring the flux density.
K2	The star-shape correction factor computed assuming Cas A has a disk intensity distribution [22].
HPBW	The half-power beamwidth of the antenna expressed in minutes.
+-QUAD	The quadratic (root mean square) accumulation of the nine error contributions.
T(STAR)	The noise temperature rise at the output of the antenna caused by Cas A.
DIAM	The diameter of the antenna.

The meaning of the last four columns is:

Heading	Meaning
E-G	Error contribution from the antenna gain.
E-DT	Error contribution from the output noise temperature difference.
E-T(STAR)	Error contribution from inability to completely resolve star measurement.
E-Sky	Error contribution from cosmic radio background.
E-K1	Error contribution from atmospheric transmission.
E-K2	Error contribution from star-shape correction.
E-Polzn	Error contribution from polarization mismatch between star and antenna.
E-BW	Error contribution for receiver bandwidth.
E-Point	Error contribution from imperfect antenna tracking of star.

Table 6-1 is based on this printout.

MEASUREMENT OF G/T USING CAS A

	QUANTITY	UNIT	VALUE	UNCERTAINTY
1	FLUX AT 1 GHZ(1974)	F.U.	3185	LISTED
2	SPECTRAL INDEX		-.765	+- 0
3	SECULAR DECAY	%/YR	1.1	+- .15
4	SKY BACKGROUND	K	6	+- .3
5	K1(ATM TRANS)		.98	+- .01
6	K2(STAR SHAPE)		LISTED	+-(K2-1)*(.1)
7	STAR POLARIZATION	%	1	+- .01
8	K3(BANDWIDTH EFFECTS)		1	+- .001
9	ANT POINTING	% HPBW	*	+- 5
10	Y-FACTOR	DB	*	+- .01
11	GAIN INSTABILITY	DB	*	+- 0
12	MEASUREMENT RESOLUTION	DB	*	+- .01

ASSUMPTIONS; T(SYST)= 100 K
DATE OF MEASUREMENT IS 1974.6
HPBW OF CAS A= 4.3 MIN
ANT BEAM EFFICIENCY= 55 %
ANT POLARIZATION RATIO= 0

FREQ= 7.25 GHZ
FLUX= 700 F.U.
FLUX UNCERTAINTY= 4.67 %

G/T(DB)	+-LIN +-QUAD	Y(DB) K2 T(STAR)	G(DB) HPBW DIAM	[ERROR CONTRIBUTIONS TO G/T IN DB] E-FLUX E-K1 E-POINT	E-INDEX E-K2 E-Y	E-DECAY E-POLZN E-GAIN	E-SKY E-BW E-RESOL
22	+- 5.723	.02	42	.194	0	.004	1.587
	+- 3.164	.999	67.4 '	.044	.001	0	.004
		.52	7.3 FT	.028	1.93	0	1.93
24	+- 3.879	.04	44	.194	0	.004	1.158
	+- 2.091	.998	53.6 '	.044	.001	0	.004
		.82	9.2 FT	.028	1.223	0	1.223
26	+- 2.64	.06	46	.194	0	.004	.812
	+- 1.38	.997	42.6 '	.044	.002	0	.004
		1.31	11.6 FT	.028	.776	0	.776
28	+- 1.817	.09	48	.194	0	.004	.551
	+- .913	.994	33.8 '	.044	.002	0	.004
		2.06	14.6 FT	.028	.494	0	.494
30	+- 1.277	.14	50	.194	0	.004	.366
	+- .612	.991	26.8 '	.044	.004	0	.004
		3.26	18.4 FT	.028	.317	0	.317

FREQ= 7.25 GHZ
FLUX= 700 F.U.
FLUX UNCERTAINTY= 4.67 %

G/T(DB)	+-LIN +-QUAD	Y(DB) K2 T(STAR)	G(DB) HPBW DIAM	[ERROR CONTRIBUTIONS TO G/T IN DB] E-FLUX E-K1 E-POINT	 E-INDEX E-K2 E-Y	 E-DECAY E-POLZN E-GAIN	 E-SKY E-BW E-RESOL
32	+- .929	.22	52	.194	0	.004	.239
	+- .426	.986	21.3 '	.044	.006	0	.004
		5.14	23.2 FT	.028	.204	0	.204
34	+- .707	.34	54	.194	0	.004	.155
	+- .317	.978	16.9 '	.044	.01	0	.004
		8.08	29.2 FT	.028	.134	0	.134
36	+- .569	.52	56	.194	0	.004	.101
	+- .258	.965	13.5 '	.044	.016	0	.004
		12.65	36.7 FT	.028	.089	0	.089
38	+- .486	.78	58	.194	0	.004	.065
	+- .229	.946	10.7 '	.044	.025	0	.004
		19.64	46.2 FT	.028	.061	0	.061
40	+- .443	1.14	60	.194	0	.004	.043
	+- .218	.916	8.5 '	.044	.04	0	.004
		30.14	58.2 FT	.028	.043	0	.043
42	+- .431	1.63	62	.194	0	.004	.028
	+- .217	.871	6.7 '	.044	.064	0	.004
		45.44	73.3 FT	.028	.032	0	.032
44	+- .448	2.22	64	.194	0	.004	.019
	+- .23	.807	5.4 '	.044	.104	0	.004
		66.66	92.3 FT	.028	.025	0	.025

FREQ= 2 GHZ
FLUX= 1874 F.U.
FLUX UNCERTAINTY= 4.32 %

G/T(DB)+-LIN +-QUAD	Y(DB) K2 T(STAR)	G(DB) HPBW DIAM	[ERROR CONTRIBUTIONS TO G/T IN DB] E-FLUX E-K1 E-POINT	 E-INDEX E-K2 E-Y	 E-DECAY E-POLZN E-GAIN	 E-SKY E-BW E-RESOL
22 +- .46	.73	42	.18	0	.004	.07
+- .22	.999	67.4 '	.044	.001	0	.004
	18.33	26.6 FT	.028	.065	0	.065
24 +- .395	1.11	44	.18	0	.004	.044
+- .203	.998	53.6 '	.044	.001	0	.004
	29.02	33.4 FT	.028	.044	0	.044
26 +- .354	1.64	46	.18	0	.004	.028
+- .195	.997	42.6 '	.044	.002	0	.004
	45.94	42.1 FT	.028	.032	0	.032
28 +- .328	2.37	48	.18	0	.004	.018
+- .191	.994	33.8 '	.044	.002	0	.004
	72.66	53 FT	.028	.024	0	.024
30 +- .313	3.32	50	.18	0	.004	.011
+- .19	.991	26.8 '	.044	.004	0	.004
	114.78	66.7 FT	.028	.019	0	.019
32 +- .305	4.49	52	.18	0	.004	.007
+- .189	.986	21.3 '	.044	.006	0	.004
	180.97	84 FT	.028	.016	0	.016
34 +- .302	5.85	54	.18	0	.004	.005
+- .189	.978	16.9 '	.044	.01	0	.004
	284.48	105.8 FT	.028	.014	0	.014
36 +- .303	7.36	56	.18	0	.004	.003
+- .189	.965	13.5 '	.044	.016	0	.004
	445.08	133.1 FT	.028	.012	0	.012
38 +- .31	8.98	58	.18	0	.004	.002
+- .19	.946	10.7 '	.044	.025	0	.004
	691.17	167.6 FT	.028	.011	0	.011
40 +- .323	10.65	60	.18	0	.004	.001
+- .192	.916	8.5 '	.044	.04	0	.004
	1060.91	211 FT	.028	.011	0	.011
42 +- .347	12.3	62	.18	0	.004	.001
+- .199	.871	6.7 '	.044	.064	0	.004
	1599.42	265.7 FT	.028	.011	0	.011
44 +- .386	13.88	64	.18	0	.004	.001
+- .215	.807	5.4 '	.044	.104	0	.004
	2346.09	334.5 FT	.028	.01	0	.01

FREQ= 4 GHZ
FLUX= 1103 F.U.
FLUX UNCERTAINTY= 4.33 %

G/T(DB)	+-LIN +-QUAD	Y(DB) K2 T(STAR)	G(DB) HPBW DIAM	[ERROR CONTRIBUTIONS TO G/T IN DB] E-FLUX E-K1 E-POINT	E-INDEX E-K2 E-Y	E-DECAY E-POLZN E-GAIN	E-SKY E-BW E-RESOL
22	+- 1.458	.12	42	.18	0	.004	.435
	+- .717	.999	67.4 '	.044	.001	0	.004
		2.7	13.3 FT	.028	.381	0	.381
24	+- 1.035	.18	44	.18	0	.004	.285
	+- .486	.998	53.6 '	.044	.001	0	.004
		4.27	16.7 FT	.028	.244	0	.244
26	+- .763	.28	46	.18	0	.004	.185
	+- .345	.997	42.6 '	.044	.002	0	.004
		6.76	21.1 FT	.028	.158	0	.158
28	+- .589	.44	48	.18	0	.004	.119
	+- .266	.994	33.8 '	.044	.002	0	.004
		10.69	26.5 FT	.028	.104	0	.104
30	+- .479	.68	50	.18	0	.004	.076
	+- .225	.991	26.8 '	.044	.004	0	.004
		16.89	33.4 FT	.028	.069	0	.069
32	+- .411	1.03	52	.18	0	.004	.048
	+- .205	.986	21.3 '	.044	.006	0	.004
		26.62	42 FT	.028	.048	0	.048
34	+- .369	1.52	54	.18	0	.004	.031
	+- .197	.978	16.9 '	.044	.01	0	.004
		41.85	52.9 FT	.028	.034	0	.034
36	+- .347	2.19	56	.18	0	.004	.02
	+- .193	.965	13.5 '	.044	.016	0	.004
		65.48	66.6 FT	.028	.025	0	.025
38	+- .338	3.05	58	.18	0	.004	.013
	+- .192	.946	10.7 '	.044	.025	0	.004
		101.68	83.8 FT	.028	.02	0	.02
40	+- .342	4.08	60	.18	0	.004	.008
	+- .194	.916	8.5 '	.044	.04	0	.004
		156.07	105.5 FT	.028	.016	0	.016
42	+- .359	5.25	62	.18	0	.004	.006
	+- .2	.871	6.7 '	.044	.064	0	.004
		235.3	132.8 FT	.028	.014	0	.014
44	+- .395	6.48	64	.18	0	.004	.004
	+- .216	.807	5.4 '	.044	.104	0	.004
		345.14	167.2 FT	.028	.013	0	.013

FREQ= 6 GHZ
FLUX= 809 F.U.
FLUX UNCERTAINTY= 4.45 %

G/T(DB) +-LIN +-QUAD	Y(DB) K2 T(STAR)	G(DB) HPBW DIAM	[ERROR CONTRIBUTIONS TO G/T IN DB] E-FLUX E-K1 E-POINT	 E-INDEX E-K2 E-Y	 E-DECAY E-POLZN E-GAIN	 E-SKY E-BW E-RESOL
22 +- 3.667	.04	42	.185	0	.004	1.105
+- 1.973	.999	67.4 '	.044	.001	0	.004
	.88	8.9 FT	.028	1.148	0	1.148
24 +- 2.494	.06	44	.185	0	.004	.77
+- 1.301	.998	53.6 '	.044	.001	0	.004
	1.39	11.1 FT	.028	.729	0	.729
26 +- 1.716	.09	46	.185	0	.004	.521
+- .859	.997	42.6 '	.044	.002	0	.004
	2.2	14 FT	.028	.464	0	.464
28 +- 1.207	.15	48	.185	0	.004	.344
+- .576	.994	33.8 '	.044	.002	0	.004
	3.48	17.7 FT	.028	.297	0	.297
30 +- .877	.23	50	.185	0	.004	.225
+- .401	.991	26.8 '	.044	.004	0	.004
	5.5	22.2 FT	.028	.192	0	.192
32 +- .667	.36	52	.185	0	.004	.145
+- .299	.986	21.3 '	.044	.006	0	.004
	8.68	28 FT	.028	.125	0	.125
34 +- .536	.56	54	.185	0	.004	.093
+- .244	.978	16.9 '	.044	.01	0	.004
	13.64	35.3 FT	.028	.083	0	.083
36 +- .455	.84	56	.185	0	.004	.06
+- .218	.965	13.5 '	.044	.016	0	.004
	21.34	44.4 FT	.028	.057	0	.057
38 +- .41	1.24	58	.185	0	.004	.039
+- .206	.946	10.7 '	.044	.025	0	.004
	33.14	55.9 FT	.028	.04	0	.04
40 +- .39	1.79	60	.185	0	.004	.025
+- .202	.916	8.5 '	.044	.04	0	.004
	50.87	70.3 FT	.028	.03	0	.03
42 +- .393	2.47	62	.185	0	.004	.017
+- .206	.871	6.7 '	.044	.064	0	.004
	76.69	88.6 FT	.028	.023	0	.023
44 +- .419	3.27	64	.185	0	.004	.012
+- .221	.807	5.4 '	.044	.104	0	.004
	112.49	111.5 FT	.028	.019	0	.019

FREQ= 8 GHZ
FLUX= 649 F.U.
FLUX UNCERTAINTY= 4.79 %

G/T(DB)	+-LIN +-QUAD	Y(DB) K2 T(STAR)	G(DB) HPBW DIAM	[ERROR CONTRIBUTIONS TO G/T IN DB] E-FLUX E-K1 E-POINT	 E-INDEX E-K2 E-Y	 E-DECAY E-POLZN E-GAIN	 E-SKY E-BW E-RESOL
22	+- 7.212	.02	42	.199	0	.004	1.87
	+- 4.044	.999	67.4 '	.044	.001	0	.004
		.4	6.6 FT	.028	2.531	0	2.531
24	+- 4.888	.03	44	.199	0	.004	1.404
	+- 2.673	.998	53.6 '	.044	.001	0	.004
		.63	8.4 FT	.028	1.602	0	1.602
26	+- 3.319	.04	46	.199	0	.004	1.007
	+- 1.766	.997	42.6 '	.044	.002	0	.004
		.99	10.5 FT	.028	1.016	0	1.016
28	+- 2.269	.07	48	.199	0	.004	.696
	+- 1.167	.994	33.8 '	.044	.002	0	.004
		1.57	13.3 FT	.028	.646	0	.646
30	+- 1.576	.11	50	.199	0	.004	.468
	+- .776	.991	26.8 '	.044	.004	0	.004
		2.48	16.7 FT	.028	.413	0	.413
32	+- 1.125	.17	52	.199	0	.004	.309
	+- .528	.986	21.3 '	.044	.006	0	.004
		3.92	21 FT	.028	.265	0	.265
34	+- .836	.26	54	.199	0	.004	.202
	+- .377	.978	16.9 '	.044	.01	0	.004
		6.16	26.4 FT	.028	.172	0	.172
36	+- .654	.4	56	.199	0	.004	.131
	+- .292	.965	13.5 '	.044	.016	0	.004
		9.63	33.3 FT	.028	.114	0	.114
38	+- .543	.61	58	.199	0	.004	.085
	+- .249	.946	10.7 '	.044	.025	0	.004
		14.96	41.9 FT	.028	.077	0	.077
40	+- .482	.9	60	.199	0	.004	.056
	+- .229	.916	8.5 '	.044	.04	0	.004
		22.96	52.8 FT	.028	.054	0	.054
42	+- .458	1.29	62	.199	0	.004	.037
	+- .225	.871	6.7 '	.044	.064	0	.004
		34.62	66.4 FT	.028	.039	0	.039
44	+- .468	1.78	64	.199	0	.004	.026
	+- .235	.807	5.4 '	.044	.104	0	.004
		50.77	83.6 FT	.028	.03	0	.03

FREQ= 10 GHZ
FLUX= 547 F.U.
FLUX UNCERTAINTY= 5.49 %

G/T(DB)	+-LIN +-QUAD	Y(DB) K2 T(STAR)	G(DB) HPBW DIAM	(ERROR CONTRIBUTIONS TO G/T IN DB) E-FLUX E-K1 E-POINT	 E-INDEX E-K2 E-Y	 E-DECAY E-POLZN E-GAIN	 E-SKY E-BW E-RESOL
22	+- 12.206	.01	42	.226	0	.004	2.535
	+- 7.094	.999	67.4 '	.044	.001	0	.004
		.21	5.3 FT	.028	4.682	0	4.682
24	+- 8.268	.01	44	.226	0	.004	2.039
	+- 4.663	.998	53.6 '	.044	.001	0	.004
		.34	6.7 FT	.028	2.961	0	2.961
26	+- 5.614	.02	46	.226	0	.004	1.558
	+- 3.083	.997	42.6 '	.044	.002	0	.004
		.54	8.4 FT	.028	1.874	0	1.874
28	+- 3.821	.04	48	.226	0	.004	1.134
	+- 2.041	.994	33.8 '	.044	.002	0	.004
		.85	10.6 FT	.028	1.189	0	1.189
30	+- 2.617	.06	50	.226	0	.004	.794
	+- 1.352	.991	26.8 '	.044	.004	0	.004
		1.34	13.3 FT	.028	.756	0	.756
32	+- 1.819	.09	52	.226	0	.004	.54
	+- .901	.986	21.3 '	.044	.006	0	.004
		2.11	16.8 FT	.028	.483	0	.483
34	+- 1.298	.14	54	.226	0	.004	.36
	+- .614	.978	16.9 '	.044	.01	0	.004
		3.32	21.2 FT	.028	.311	0	.311
36	+- .964	.22	56	.226	0	.004	.237
	+- .438	.965	13.5 '	.044	.016	0	.004
		5.2	26.6 FT	.028	.202	0	.202
38	+- .755	.34	58	.226	0	.004	.156
	+- .338	.946	10.7 '	.044	.025	0	.004
		8.07	33.5 FT	.028	.134	0	.134
40	+- .631	.51	60	.226	0	.004	.103
	+- .287	.916	8.5 '	.044	.04	0	.004
		12.39	42.2 FT	.028	.091	0	.091
42	+- .566	.74	62	.226	0	.004	.069
	+- .266	.871	6.7 '	.044	.064	0	.004
		18.68	53.1 FT	.028	.064	0	.064
44	+- .551	1.05	64	.226	0	.004	.047
	+- .267	.807	5.4 '	.044	.104	0	.004
		27.4	66.9 FT	.028	.047	0	.047

FREQ= 12 GHZ
FLUX= 476 F.U.
FLUX UNCERTAINTY= 6.7 %

G/T(DB) +-LIN +-QUAD	Y(DB) K2 T(STAR)	G(DB) HPBW DIAM	[ERROR CONTRIBUTIONS TO G/T IN DB] E-FLUX E-K1 E-POINT	E-INDEX E-K2 E-Y	E-DECAY E-POLZN E-GAIN	E-SKY E-BW E-RESOL
22 +- 18.88	.01	42	.273	0	.004	3.035
+- 11.37	.999	67.4 '	.044	.001	0	.004
	.13	4.4 FT	.028	7.746	0	7.746
24 +- 12.726	.01	44	.273	0	.004	2.581
+- 7.393	.998	53.6 '	.044	.001	0	.004
	.2	5.6 FT	.028	4.895	0	4.895
26 +- 8.635	.01	46	.273	0	.004	2.088
+- 4.859	.997	42.6 '	.044	.002	0	.004
	.32	7 FT	.028	3.096	0	3.096
28 +- 5.882	.02	48	.273	0	.004	1.604
+- 3.216	.994	33.8 '	.044	.002	0	.004
	.51	8.8 FT	.028	1.961	0	1.961
30 +- 4.022	.04	50	.273	0	.004	1.174
+- 2.135	.991	26.8 '	.044	.004	0	.004
	.81	11.1 FT	.028	1.245	0	1.245
32 +- 2.773	.06	52	.273	0	.004	.826
+- 1.421	.986	21.3 '	.044	.006	0	.004
	1.28	14 FT	.028	.793	0	.793
34 +- 1.945	.09	54	.273	0	.004	.565
+- .956	.978	16.9 '	.044	.01	0	.004
	2.01	17.6 FT	.028	.508	0	.508
36 +- 1.405	.13	56	.273	0	.004	.379
+- .661	.965	13.5 '	.044	.016	0	.004
	3.14	22.2 FT	.028	.329	0	.329
38 +- 1.06	.21	58	.273	0	.004	.252
+- .483	.946	10.7 '	.044	.025	0	.004
	4.88	27.9 FT	.028	.215	0	.215
40 +- .848	.31	60	.273	0	.004	.167
+- .385	.916	8.5 '	.044	.04	0	.004
	7.48	35.2 FT	.028	.144	0	.144
42 +- .727	.46	62	.273	0	.004	.112
+- .337	.871	6.7 '	.044	.064	0	.004
	11.28	44.3 FT	.028	.099	0	.099
44 +- .676	.67	64	.273	0	.004	.077
+- .322	.807	5.4 '	.044	.104	0	.004
	16.55	55.7 FT	.028	.07	0	.07

FREQ= 14 GHZ
FLUX= 423 F.U.
FLUX UNCERTAINTY= 8.8 %

G/T(DB)+-LIN +-QUAD	Y(DB) K2 T(STAR)	G(DB) HPBW DIAM	[ERROR CONTRIBUTIONS TO G/T IN DB] E-FLUX E-K1 E-POINT	 E-INDEX E-K2 E-Y	 E-DECAY E-POLZN E-GAIN	 E-SKY E-BW E-RESOL
22 +- 27.538	0	42	.351	0	.004	3.389
+- 17.113	.999	67.4 '	.044	.001	0	.004
	.08	3.8 FT	.028	11.858	0	11.858
24 +- 18.418	.01	44	.351	0	.004	3.004
+- 11.017	.998	53.6 '	.044	.001	0	.004
	.13	4.8 FT	.028	7.49	0	7.49
26 +- 12.453	.01	46	.351	0	.004	2.547
+- 7.175	.997	42.6 '	.044	.002	0	.004
	.21	6 FT	.028	4.737	0	4.737
28 +- 8.484	.01	48	.351	0	.004	2.053
+- 4.724	.994	33.8 '	.044	.002	0	.004
	.33	7.6 FT	.028	2.998	0	2.998
30 +- 5.811	.02	50	.351	0	.004	1.572
+- 3.135	.991	26.8 '	.044	.004	0	.004
	.53	9.5 FT	.028	1.902	0	1.902
32 +- 4.007	.04	52	.351	0	.004	1.149
+- 2.091	.986	21.3 '	.044	.006	0	.004
	.83	12 FT	.028	1.21	0	1.21
34 +- 2.797	.06	54	.351	0	.004	.809
+- 1.406	.978	16.9 '	.044	.01	0	.004
	1.31	15.1 FT	.028	.773	0	.773
36 +- 1.998	.09	56	.351	0	.004	.554
+- .964	.965	13.5 '	.044	.016	0	.004
	2.05	19 FT	.028	.498	0	.498
38 +- 1.479	.14	58	.351	0	.004	.374
+- .69	.946	10.7 '	.044	.025	0	.004
	3.18	23.9 FT	.028	.324	0	.324
40 +- 1.152	.21	60	.351	0	.004	.251
+- .532	.916	8.5 '	.044	.04	0	.004
	4.89	30.1 FT	.028	.215	0	.215
42 +- .957	.31	62	.351	0	.004	.17
+- .449	.871	6.7 '	.044	.064	0	.004
	7.37	38 FT	.028	.146	0	.146
44 +- .858	.45	64	.351	0	.004	.117
+- .414	.807	5.4 '	.044	.104	0	.004
	10.81	47.8 FT	.028	.103	0	.103

FREQ= 16 GHZ
FLUX= 382 F.U.
FLUX UNCERTAINTY= 11.87 %

G/T(DB)	+-LIN +-QUAD	Y(DB) K2 T(STAR)	G(DB) HPBW DIAM	[ERROR CONTRIBUTIONS TO G/T IN DB] E-FLUX E-K1 E-POINT	 E-INDEX E-K2 E-Y	 E-DECAY E-POLZN E-GAIN	 E-SKY E-BW E-RESOL
22	+- 38.479	0	42	.461	0	.004	3.636
	+- 24.53	.999	67.4 '	.044	.001	0	.004
		.06	3.3 FT	.028	17.151	0	17.151
24	+- 25.531	0	44	.461	0	.004	3.32
	+- 15.684	.998	53.6 '	.044	.001	0	.004
		.09	4.2 FT	.028	10.834	0	10.834
26	+- 17.158	.01	46	.461	0	.004	2.919
	+- 10.125	.997	42.6 '	.044	.002	0	.004
		.15	5.3 FT	.028	6.848	0	6.848
28	+- 11.662	.01	48	.461	0	.004	2.452
	+- 6.617	.994	33.8 '	.044	.002	0	.004
		.23	6.6 FT	.028	4.333	0	4.333
30	+- 7.996	.02	50	.461	0	.004	1.958
	+- 4.374	.991	26.8 '	.044	.004	0	.004
		.37	8.3 FT	.028	2.747	0	2.747
32	+- 5.526	.02	52	.461	0	.004	1.487
	+- 2.919	.986	21.3 '	.044	.006	0	.004
		.58	10.5 FT	.028	1.746	0	1.746
34	+- 3.86	.04	54	.461	0	.004	1.081
	+- 1.966	.978	16.9 '	.044	.01	0	.004
		.91	13.2 FT	.028	1.114	0	1.114
36	+- 2.747	.06	56	.461	0	.004	.759
	+- 1.347	.965	13.5 '	.044	.016	0	.004
		1.42	16.6 FT	.028	.716	0	.716
38	+- 2.016	.09	58	.461	0	.004	.521
	+- .958	.946	10.7 '	.044	.025	0	.004
		2.2	21 FT	.028	.464	0	.464
40	+- 1.548	.14	60	.461	0	.004	.354
	+- .728	.916	8.5 '	.044	.04	0	.004
		3.38	26.4 FT	.028	.306	0	.306
42	+- 1.26	.22	62	.461	0	.004	.242
	+- .602	.871	6.7 '	.044	.064	0	.004
		5.09	33.2 FT	.028	.206	0	.206
44	+- 1.101	.31	64	.461	0	.004	.168
	+- .544	.807	5.4 '	.044	.104	0	.004
		7.47	41.8 FT	.028	.144	0	.144

B.2 The BASIC Program for the Computation of the Errors in the Measurement of G/T Using Cas A

In this section the computer program which was used to produce the printout in section B.1 is given. The remarks in this printout starting with step 5851 identify many of the parameters used.

```
100  PRINT "DW26.2 (74 JAN 12) NBS 6514"
102  REM     SWITCH 0; BYPASS R-PRINTOUT OF INPUT DATA
103  REM    MODIFIED TO ALLOW VARIABLE FLUX ACCURACY PER 29.2 P6442
106  DIM E[12]
108  DIM D[4]
110  DIM S[12,1]
112  DEF  FNA(X)= INT (1000* ABS (X/.23026)+.5)/1000
114  DEF  FNB(X)= INT (1000* LOG X/ LOG (10)+.5)/100
120  READ Q5,G5,G6,G7,Y1,Y2,T
122  READ N
125  READ A1,A2,A3,A5,A6
130  FOR I=1 TO 4
135    READ D[I]
140  NEXT I
150  FOR I=1 TO 12
155    READ S[I, 0],S[I,1]
160  NEXT I
162  CALL 11, 0,V2
164  IF V2=1 GOTO  510
172  PRINT
173  PRINT
175  FOR I=1 TO 70
176    PRINT "#";
177  NEXT I
178  PRINT
179  PRINT
180  PRINT ,"MEASUREMENT OF G/T USING CAS A"
185  PRINT
190  PRINT "      QUANTITY"; TAB A1;"UNIT";
195  PRINT  TAB A2;"VALUE"; TAB A3;"UNCERTAINTY"
200  PRINT
205  LET M9=M9+10
207  LET I=1
210  PRINT " 1    FLUX AT";Q5;"GHZ(";Y1;")"; TAB A1;"F.U.";
215  PRINT  TAB A2;S[1, 0]; TAB A3;"LISTED"
220  GOSUB  2015
230  PRINT "SPECTRAL INDEX";
240  GOSUB  2000
250  PRINT "SECULAR DECAY"; TAB A1;"%/YR";
260  GOSUB  2000
270  PRINT "SKY BACKGROUND"; TAB A1;"K";
280  GOSUB  2000
284  PRINT "K1(ATM TRANS)";
286  GOSUB  2000
290  PRINT "K2(STAR SHAPE)"; TAB A2;"LISTED";
295  PRINT  TAB A3;"+-(K2-1)*(";S[I,1];")"
300  GOSUB  2015
330  PRINT "STAR POLARIZATION"; TAB A1;"%";
340  GOSUB  2000
350  PRINT "K3(BANDWIDTH EFFECTS)";
360  GOSUB  2000
370  PRINT "ANT POINTING"; TAB A1;"% HPBW"; TAB A2;"  *";
380  GOSUB  2010
```

```
390  PRINT "Y-FACTOR"; TAB A1;"DB"; TAB A2;"  *";
400  GOSUB  2010
410  PRINT "GAIN INSTABILITY"; TAB A1;"DB"; TAB A2;"  *";
420  GOSUB  2010
430  PRINT "MEASUREMENT RESOLUTION"; TAB A1;"DB"; TAB A2;"  *";
440  GOSUB  2010
450  PRINT
460  PRINT "  ASSUMPTIONS;","T(SYST)=";T;"K"
470  PRINT ,"DATE OF MEASUREMENT IS";Y2
480  PRINT ,"HPBW OF CAS A=";S[6, 0];"MIN"
485  PRINT ,"ANT BEAM EFFICIENCY=";100*N;"%"
490  PRINT ,"ANT POLARIZATION RATIO=";P
500  PRINT
502  FOR I=1 TO 70
504    PRINT "#";
506  NEXT I
507  LET M9=M9+20
510  PRINT
580  READ Q2,F
600  GOSUB  3000
770  FOR G2=G5 TO G6 STEP G7
778    LET S[1,1]=F*S[1, 0]/100
780    LET G1=10↑(G2/10)
790    LET G=G1*T
800    GOSUB  5900
805    LET Y=1+R4*G1
810    LET Q4=S[1,1]*1E-26
820    GOSUB  5984
830    LET E[1]=1-R4/R6
840    LET Q4= 0
850    LET Q7=S[2,1]
860    GOSUB  5984
870    LET E[2]=1-R4/R6
880    LET Q7= 0
890    LET R2=K2*S[5, 0]*((1-(S[3, 0]-S[3,1])/100)↑(Y2-Y1))
900    GOSUB  5984
920    LET E[3]=1-R4/R6
925    GOSUB  5900
930    LET E[4]=1-R4/(R4+S[4,1]/G)
950    LET E[5]=S[5,1]/S[5, 0]
960    LET E[6]=(1-K2)*S[6,1]/K2
1000    LET E[8]=S[8,1]/S[8, 0]
1010    LET X9=(2.784*S[9,1]/100)
1020    LET E[9]=1-( SIN (X9)/X9)↑2
1050    FOR I=10 TO 12
1060      LET E[I]=(S[I,1]*.23026*Y)/(Y-1)
1070    NEXT I
1100    LET X1= 0
1110    LET X2= 0
1120    FOR I=1 TO 12
1130      LET X1=X1+E[I]
1140      LET X2=X2+E[I]↑2
1150    NEXT I
```

```
1200    PRINT G2;"+-"; FNA(X1);
1210    PRINT  TAB A5; FNB(Y);
1220    PRINT  TAB A6; FNB(G);
1230    FOR I=1 TO 4
1240      PRINT  TAB D[I]; FNA(E[I]);
1250    NEXT I
1255    PRINT
1260    PRINT "    +-"; FNA( SQR (X2));
1270    PRINT  TAB A5; INT (1000*K2+.5)/1000;
1275    PRINT  TAB A6; INT (10*X3+.5)/10;"'";
1280    FOR I=1 TO 4
1290      PRINT  TAB D[I]; FNA(E[I+4]);
1300    NEXT I
1310    PRINT
1350    PRINT  TAB A5; INT (100*G*R4+.5)/100;
1360    PRINT  TAB A6; INT (3.13* SQR (G/N)/Q2+.5)/10;"FT";
1380    FOR I=1 TO 4
1390      PRINT  TAB D[I]; FNA(E[I+8]);
1400    NEXT I
1410    PRINT
1420    PRINT
1430    LET M9=M9+4
1440    LET M8=64
1445    IF M9<M8-5 GOTO  1500
1450    FOR I=M9 TO M8+8
1460      PRINT
1470    NEXT I
1480    LET M9=3
1490    GOSUB  3000
1500  NEXT G2
1600  FOR I=M9 TO M8+8
1610    PRINT
1620  NEXT I
1625  LET M9=3
1630  GOTO  510
2000  REM       INPUT DATA PRINT SUBROUTINE
2005  PRINT  TAB A2;S[I, 0];
2010  PRINT  TAB A3;"+-";S[I,1]
2015  REM
2020  IF I=12 GOTO  2050
2030  LET I=I+1
2040  PRINT I;"  ";
2050  RETURN
3000  PRINT
3002  PRINT
3003  LET G=1
3004  GOSUB  5900
3005  PRINT "FREQ=";Q2;"GHZ"
3007  PRINT "FLUX="; INT (Q3*(Q2/Q5)↑Q6*10↑(26)+.5);"F.U."
3009  PRINT "FLUX UNCERTAINTY=";F;"%"
3010  PRINT
3020  PRINT  TAB D[1];"[ERROR CONTRIBUTIONS TO G/T IN DB]"
3030  PRINT "G/T(DB)+-LIN";
```

```
3040  PRINT  TAB A5;"Y(DB)"; TAB A6;"G(DB)";
3050  PRINT  TAB D[1];"E-FLUX"; TAB D[2];"E-INDEX";
3060  PRINT  TAB D[3];"E-DECAY"; TAB D[4];"E-SKY"
3070  PRINT "       +-QUAD"; TAB A5;"K2";
3080  PRINT  TAB A6;"HPBW"; TAB D[1];"E-K1";
3090  PRINT  TAB D[2];"E-K2"; TAB D[3];"E-POLZN";
3100  PRINT  TAB D[4];"E-BW"
3110  PRINT  TAB A5;"T(STAR)"; TAB A6;"DIAM";
3120  PRINT  TAB D[1];"E-POINT"; TAB D[2];"E-Y";
3130  PRINT  TAB D[3];"E-GAIN"; TAB D[4];"E-RESOL"
3140  PRINT
3150  PRINT
3160  LET M9=M9+10
3170  RETURN
4926  LET K2=(1- EXP (-X*X))/(X*X)
5850  REM         ***** G/T COEFFICIENT SUBROUTINE ****
5851  REM              Q2 = FREQ
5852  REM              Q3 = STAR FLUX
5853  REM              Q4 =  "      "  ERROR
5854  REM              Q5 = FLUX FREQUENCY
5855  REM              Q6 = SPECTRAL INDEX
5856  REM              Q7 =   "          "   ERROR
5857  REM              R1 = ATMOSPHERIC TRANSMISSION
5858  REM              R2 = FINITE STAR CORRECTION AND STAR DECAY FACTOR
5860  REM              R4 = DT(STAR)/G
5861  REM              R6 =   "     "   (MAX) BUT NO ATM OR FINITE STAR ERR
5862  REM              R5 = ERROR IN FREQ
5863  REM              K  = C↑2/8 PI K
5864  REM              K2=K2(STAR SHAPE)
5867  REM            F=% ERROR IN FLUX
5870  REM            G=G
5872  REM            G1=G/T
5874  REM            G2=G/T(DB)
5875  REM              N=BEAM EFFICIENCY
5876  REM             X3=ANT HPBW IN MIN
5877  REM             Y1=YR FLUX MEASURED
5878  REM             Y2=YR G/T MEASURED
5900  LET Q3=S[1, 0]*10↑(-26)
5905  LET Q4= 0
5910  LET Q6=S[2, 0]
5915  LET Q7= 0
5920  LET R1=S[5, 0]
5922  LET X3=11448/ SQR (G/N)
5924  LET X=S[6, 0]/(1.2012*X3)
5926  LET K2=(1- EXP (-X*X))/X↑2
5930  LET R2=K2*S[5, 0]*(1-S[3, 0]/100)↑(Y2-Y1)
5975  LET K=2.99793E+8↑2*1E-18/(8*3.14159*1.38046E-23)
5980  LET R4=R1*R2*K*Q3*(Q2/Q5)↑Q6/Q2↑2
5982  RETURN
5984  REM         *** R6 IS THE MAXIMUM DT(STAR)/G ****
5990  LET R6=R1*R2*K*(Q3+Q4)*((Q2-R5)/Q5)↑(Q6+Q7)/(Q2-R5)↑2
5995  RETURN
7000  DATA  1
```

```
7010  REM       *** G/T(DB); START ,STOP,STEP ***
7015  DATA   22, 44, 2
7020  DATA   1974, 1974.6
7030  DATA   100
7035  DATA   .55
7040  DATA   30, 37, 47
7050  REM       A5,A6,D[1],D[2],D[3],D[4]
7055  DATA   15, 24, 35, 44, 53, 62
8001  DATA   3185, 30,-.765, 0
8003  DATA   1.1, .15, 6, .3
8005  DATA   .98, .01, 4.3, .1
8007  DATA   1, .01, 1, .001
8009  DATA   0, 5, 0, .01
8011  DATA   0, 0, 0, .01
8100  REM     FREQUENCY,FLUX ERROR PAIRS
8110  DATA   7.25, 4.67, 2, 4.32, 4, 4.33, 6, 4.45, 8, 4.79
8120  DATA   10, 5.49, 12, 6.7, 14, 8.8, 16, 11.87
```

APPENDIX C: DETERMINATION OF ANTENNA AND RECEIVER PARAMETERS BY NOISE-ADDING TECHNIQUES

Parameters such as antenna gain (when measured with the Cas A method), antenna noise temperature, system noise temperature, and gain to noise temperature ratio, are sometimes obtained by use of a noise-adding circuit such as that shown in figure C-1. The noise-adding circuit consists of a directional coupler with the sidearm terminated with a variable noise source. The purpose of this section is to discuss such a noise adding measurement system and its possible applications.

The output from port 2 of the directional coupler expressed in terms of noise temperature is given by [73]

$$T_{b2} = \alpha_{21}T_1 + \alpha_{23}T_3 + A_2T_{amb}, \qquad (C.1)$$

where α_{21} and α_{23} are the available power ratios for the directional coupler and depend on Γ_1 and Γ_3, A_2T_{amb} is the thermal energy originating within the three port. The parameters $\alpha_{ij}(i = 1,2,3;\ i \neq j = 1,2,3)$ represent ratios of the power available from port i to the available power of a signal source attached to port j. If T_1 is changed and T_3 is simultaneously adjusted so that T_{b2} remains unchanged, then

$$\Delta T_1 = -(\alpha_{23}/\alpha_{21})\Delta T_3. \qquad (C.2)$$

That is, a (plus) one kelvin change in $(\alpha_{23}/\alpha_{21})T_3$ affects the available noise temperature at port 2 in exactly the same way as a (minus) one kelvin change in T_1.

Two noise sources of known temperatures (say room-temperature and liquid nitrogen) successively placed at port 1 calibrate $(\alpha_{23}/\alpha_{21})\Delta T_3$ provided T_{b2} is held constant by adjusting

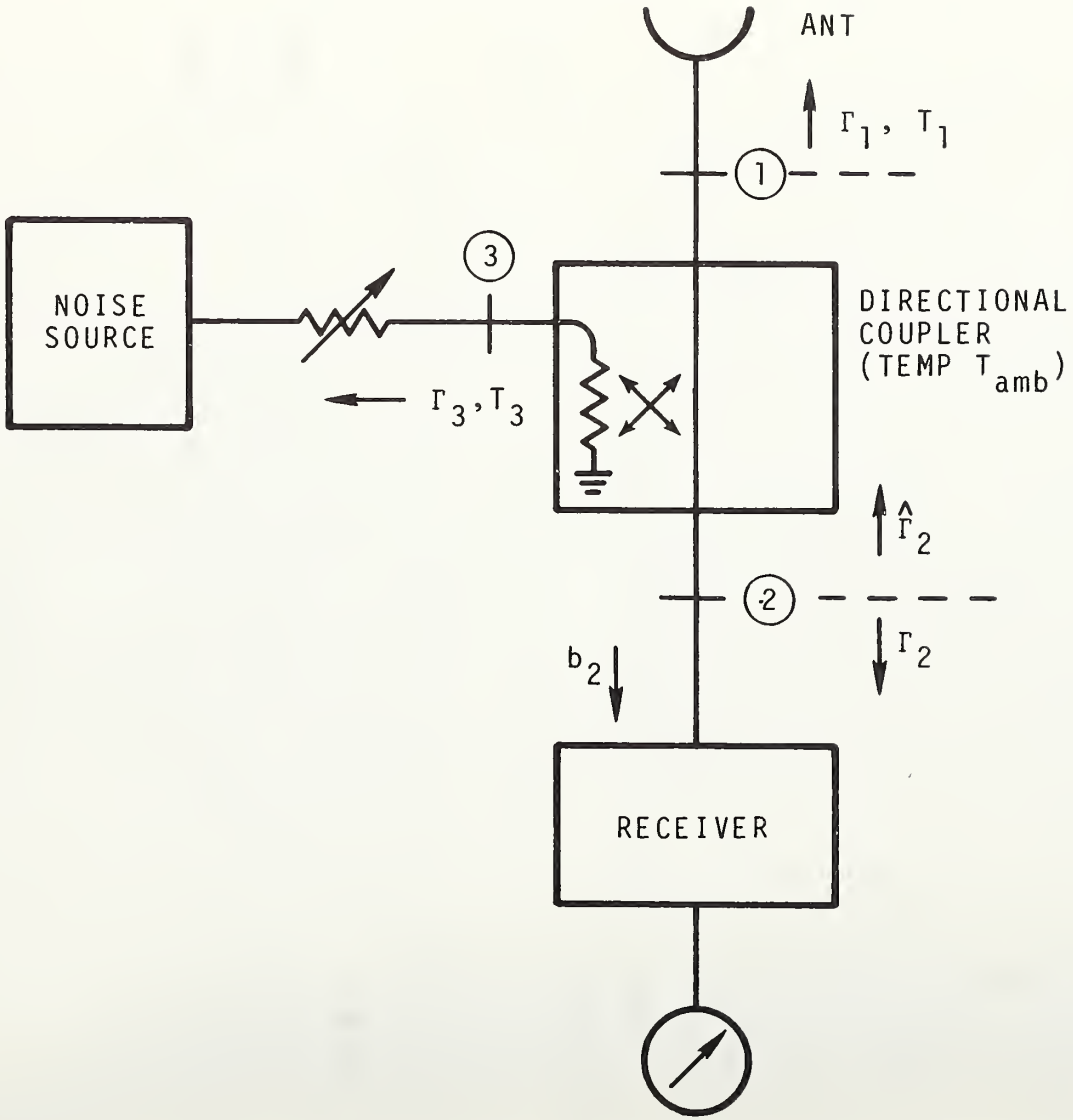

Figure C-1 Block diagram of the noise adding technique.

the attenuator on the sidearm. Once the system is calibrated, any change ΔT_1 can be calculated from eq. (C.2) once the corresponding ΔT_3 has been determined.

The calibration parameter α_{23}/α_{21} is a function of Γ_1 and Γ_3, and of the scattering parameters of the directional coupler [73]. It follows that once this parameter has been determined, care must be exercised to maintain Γ_1 and Γ_3 close to their original values in the course of subsequent measurements.

C.1 The Measurement of Antenna Parameters

The antenna parameters of interest are antenna gain and noise temperature.

Antenna gain can be deduced from the measured change in noise temperature, $(\Delta T_1)^{star}$, referred to the antenna output port, when a radio star drifts across the antenna beam;

$$G = (\Delta T_1)^{star}/\xi. \tag{C.3}$$

Here ξ is defined by $\xi = (\lambda^2/8\pi)k_1k_2S$, where S is the star flux density at measurement wavelength λ incident from outside the earth's atmosphere; k_1 and k_2 are correction factors for atmospheric effects and for the finite extent of the star in relation to the antenna power-gain pattern. For example, ξ is of the order of 10^{-4}K for Cas A at 4 GHz.

Antenna temperature can be deduced from the change in measured noise temperature $(\Delta T_1)^{ant\ -\ std}$ when the antenna is removed from port 1 and replaced by a cold standard noise source T_{std};

$$T_{ant} = T_{std} + (\Delta T_1)^{ant\ -std}. \tag{C.4}$$

Then a ratio method as will be seen below (the Y-factor method) can be used to determine system noise temperature and G/T.

C.2 The Measurement of System Noise Temperature and G/T

In order to determine the system noise temperature, T, the ratio Y_1 of the power at the receiver output port is measured for a known change ΔT_1, determined in a separate measurement based on eq. (C.2). T equals the sum of the antenna temperature, T_{ant}, and the receiver effective input noise temperature, T_e.

$$Y_1 \equiv (\Delta T_1 + T)/T. \tag{C.5}$$

Inverting eq. (C.5) to obtain T results in

$$T = \Delta T_1/(Y_1 - 1). \tag{C.6}$$

If T_{ant} is known from separate measurements and eq. (C.4), then T_e equals T minus T_{ant}.

To obtain G/T, the same star-drift measurement described in connection with eq. (C.3) can be used, except that in this case the ratio Y of the total power at the system output port is measured. It can be seen that

$$Y \equiv (\Delta T_1^{star} + T)/T, \tag{C.7}$$

and with eq. (C.3) in mind, that

$$G/T = (Y - 1)/\xi. \tag{C.8}$$

FORM NBS-114A (1-71)

U.S. DEPT. OF COMM. BIBLIOGRAPHIC DATA SHEET	1. PUBLICATION OR REPORT NO. NBSIR 74-382	2. Gov't Accession No.	3. Recipient's Accession No.

4. TITLE AND SUBTITLE

A STUDY OF THE MEASUREMENT OF G/T USING CASSIOPEIA A

5. Publication Date: June 1974

6. Performing Organization Code

7. AUTHOR(S)
D. F. Wait, W. C. Daywitt, C. K. S. Miller, M. Kanda

8. Performing Organization

9. PERFORMING ORGANIZATION NAME AND ADDRESS

NATIONAL BUREAU OF STANDARDS
DEPARTMENT OF COMMERCE
WASHINGTON, D.C. 20234

10. Project/Task/Work Unit No. 2766482

11. Contract/Grant No. P.O. No. SCC-411-73

12. Sponsoring Organization Name and Address

Advanced Concepts Office
United States Army Communications Command
Fort Huachuca, Arizona 85613

13. Type of Report & Period Covered

14. Sponsoring Agency Code

15. SUPPLEMENTARY NOTES

16. ABSTRACT (A 200-word or less factual summary of most significant information. If document includes a significant bibliography or literature survey, mention it here.)

This report describes a study intended to estimate the best possible accuracy of measuring the ratio G/T (system gain to system noise temperature) of a satellite communication ground station using the radio star Cassiopeia A (Cas A). The concept of G/T and its measurement using a radio star is briefly discussed. Results of an extensive literature search are presented, summarizing the properties of Cas A and its vicinity described by radio astronomers in order to utilize this information to assess the accuracy of a G/T measurement. Consideration is given to atmospheric effects upon a G/T measurement using Cas A based on information available in the literature. A detailed analysis of errors for gain measurements of large ground antennas, which includes the calibration of a standard gain antenna and the transfer of the calibration of this standard to a large antenna, is provided to validate radio star flux data since this analysis is not available in the literature. The results of these efforts are utilized to show that the best possible accuracy of a G/T measurement for a ground station having a 60 ft. diameter antenna and both practical and reasonable specifications is in the neighborhood of ± 0.25 dB.

17. KEY WORDS (Alphabetical order, separated by semicolons)

ccuracy; antenna; calibration; cassiopeia a; g/t; star flux.

18. AVAILABILITY STATEMENT

☒ UNLIMITED.

☐ FOR OFFICIAL DISTRIBUTION. DO NOT RELEASE TO NTIS.

19. SECURITY CLASS (THIS REPORT)	21. NO. OF PAGES
UNCLASSIFIED	
20. SECURITY CLASS (THIS PAGE)	22. Price
UNCLASSIFIED	

USCOMM-DC 66244-P71

☆ U.S. GOVERNMENT PRINTING OFFICE 1974 - 677-234/1214 REG. 8


AMERICAN REVOLUTION
BICENTENNIAL 1776-1976